NASA-CR-174705

DOE/NASA-0303-1
NASA CR-174705

NASA-CR-174705
19840020892

CREEP-RUPTURE BEHAVIOR OF CANDIDATE STIRLING ENGINE IRON SUPERALLOYS IN HIGH-PRESSURE HYDROGEN

VOLUME II - HYDROGEN CREEP-RUPTURE BEHAVIOR

S. Bhattacharyya, W. Peterman and C. Hales
IIT RESEARCH INSTITUTE
10 West 35th Street
Chicago, Illinois 60616

JUNE 1984

Prepared for

NATIONAL AERONAUTICS AND SPACE ADMINISTRATION
Lewis Research Center
Under Contract DEN 3-303

for

U.S. DEPARTMENT OF ENERGY
Office of Transportation Programs

8 1 1 RN/NASA-CR-174705
DISPLAY 08/2/1
84N28961*# ISSUE 19 PAGE 2992 CATEGORY 26 RPT#: NASA-CR-174705 NAS 1.26:174705 IITRI-M06116-15 CNT#: DEN3-303 DE-AI01-77CS-51040 84/06/00 105 PAGES UNCLASSIFIED DOCUMENT

UTTL: Creep-rupture behavior of candidate Stirling engine iron supperalloys in high-pressure hydrogen. Volume 2: Hydrogen creep-rupture behavior
TLSP: Final Report

AUTH: A/BHATTACHARYYA, S.; B/PETERMAN, W.; C/HALES, C.

CORP: IIT Research Inst., Chicago, Ill. AVAIL.NTIS SAP: HC A06/MF A01

MAJS: /*COBALT ALLOYS/*CREEP PROPERTIES/*HIGH PRESSURE/*HYDROGEN/*IRON ALLOYS/*PISTON ENGINES/*RUPTURING/*STIRLING CYCLE

MINS: / ANNEALING/ FRACTOGRAPHY/ FRACTURE MECHANICS/ PROBLEM SOLVING/ SERVICE LIFE/ STRESS ANALYSIS

ABA: M.A.C.

ABS: The creep rupture behavior of nine iron base and one cobalt base candidate Stirling engine alloys is evaluated. Rupture life, minimum creep rate, and time to 1% strain data are analyzed. The 3500 h rupture life stress and stress to obtain 1% strain in 3500 h are also estimated.

ENTER:

DOE/NASA-0303-1
NASA CR-174705

CREEP-RUPTURE BEHAVIOR OF CANDIDATE STIRLING ENGINE IRON SUPERALLOYS IN HIGH-PRESSURE HYDROGEN

VOLUME II: HYDROGEN CREEP-RUPTURE BEHAVIOR

S. Bhattacharyya, W. Peterman, and C. Hales
IIT Research Institute
10 West 35 Street
Chicago, Illinois 60616

June 1984

Prepared for

National Aeronautics and Space Administration
Lewis Research Center
Under Contract DEN3-303

for

U.S. Department of Energy
Office of Transportation Programs
Under Interagency Agreement
DE-A-101-77CS51040

N84-28961#

1. Report No. NASA CR-174705	2. Government Accession No.	3. Recipient's Catalog No.
4. Title and Subtitle Creep-Rupture Behavior of Candidate Stirling Engine Iron Superalloys in High-Pressure Hydrogen, Volume II: Hydrogen Creep-Rupture Behavior		5. Report Date June 1984
		6. Performing Organization Code
7. Author(s) S. Bhattacharyya, W. Peterman, and C. Hales		8. Performing Organization Report No. IITRI-M06116-15
9. Performing Organization Name and Address IIT Research Institute 10 West 35 Street Chicago, Illinois 60616		10. Work Unit No.
		11. Contract or Grant No. DEN3-303
12. Sponsoring Agency Name and Address U.S. Department of Energy Office of Transportation Programs Washington, DC 20545		13. Type of Report and Period Covered Contractor Report
		14. Sponsoring Agency Code

15. Supplementary Notes

Final Report, prepared under Interagency Agreement DE-A-101-77CS51040
Program Manager, R. H. Titran, MS 49-1, NASA-Lewis Research Center, Cleveland, Ohio, 44135

16. Abstract

The creep-rupture behavior of nine iron-base and one cobalt-base candidate Stirling engine alloys was evaluated at 650° to 925°C in 15 MPa H_2 and air. The test alloys included six wrought alloys for tube application (CG-27, N-155, 19-9DL, 12RN72, INCOLOY Alloy 800H, and A-286) and four cast alloys for cylinders and regenerator housing (SA-F11, HS-31, CRM-6D, and XF-818). Two heats of CRM-6D and XF-818 were tested in two different heat treated conditions--CRM-6D (aged vs. braze-cycled) and XF-818 (as-cast vs. braze-cycled), and SA-F11 and HS-31 with braze-cycle treatment only.

Rupture life, minimum creep rate, and time to 1% strain data were analyzed using Orowan-Sherby-Dorn temperature-compensated technique, and the 3500-h rupture life stress and stress to obtain 1% strain in 3500 h were estimated. The analysis indicated that tube alloys CG-27, N-155, and 19-9DL meet the design stress level of 28 MPa for 3500-h rupture life at 870°C in 15 MPa H_2, and cast alloys HS-31 (braze-cycled), CRM-6D (aged), and SA-F11 (braze-cycled) also adequately meet the design stress of 119 MPa for 3500-h rupture life at 775°C in 15 MPa H_2 for MOD 1A Stirling engine design criteria.

The hydrogen environment had no significant adverse effect, compared to air, on 3500-h rupture life stress and stress to obtain 1% creep strain in 3500-h or on minimum creep rates, and in a few cases, a positive effect was noted. However, ductility was adversely affected in hydrogen environment, more for the tube alloys than for the cast materials.

17. Key Words (Suggested by Author(s))		18. Distribution Statement
Iron superalloys	Stirling engine	Unclassified - unlimited
Creep-rupture	Hydrogen	Star Category - 26
Minimum creep rate	Activation energy	DOE Category - UC 96
Stress exponent	Ductility	

19. Security Classif. (of this report)	20. Security Classif. (of this page)	21. No. of Pages	22. Price*
Unclassified	Unclassified	97	

* For sale by the National Technical Information Service, Springfield, Virginia 22161

NASA-C-168 (Rev. 10-75)

TABLE OF CONTENTS

LIST OF TABLES

LIST OF FIGURES

LIST OF FIGURES (cont.)

LIST OF FIGURES (cont.)

SUMMARY

The creep-rupture behavior of nine iron-base and one cobalt-base candidate Stirling engine alloys was evaluated at 650° to 925°C in 15 MPa H_2 and air. The test alloys included six wrought alloys for tube application (CG-27, N-155, 19-9DL, 12RN72, INCOLOY Alloy 800H, and A-286) and four cast alloys for cylinders and regenerator housing (SA-F11, HS-31, CRM-6D, and XF-818). Two heats of CRM-6D and XF-818 were tested in two different heat treated conditions--CRM-6D (aged vs. braze-cycled) and XF-818 (as-cast vs. braze-cycled), and SA-F11 and HS-31 with braze-cycle treatment only.

Rupture life, minimum creep rate, and time to 1% strain data were analyzed using the Orowan-Sherby-Dorn temperature-compensated technique, and 3500-h rupture life stress and stress to obtain 1% strain in 3500 h were estimated. The analysis indicated that tube alloys CG-27, N-155, and 19-9DL meet the design stress level of 28 MPa for 3500-h rupture life in 15 MPa H_2, and cast alloys HS-31 (braze-cycled), CRM-6D (aged), and SA-F11 (braze-cycled) also adequately meet the design stress of 119 MPa for 3500-h rupture life at 775°C in 15 MPa H_2 for MOD 1A Stirling engine design criteria.

The hydrogen environment had no significant adverse effect, compared to air, on 3500-h rupture life stress and stress to obtain 1% creep strain in 3500-h or on minimum creep rate, and in a few cases, a positive effect was noted. However, ductility was adversely affected in hydrogen environment, more for the tube alloys than for the cast materials.

INTRODUCTION

The Department of Energy and NASA-Lewis Research Center have a joint program under way to develop the Stirling engine as an alternative to the automotive internal combustion engine. Advantages of the Stirling engine include the potential for high fuel efficiency, multiple fuel capability, low pollution, and low noise. To achieve these operating characteristics, the Stirling engine will operate near 820°C and use high-pressure hydrogen as the working fluid.

The long-term effects of high-pressure hydrogen at high temperature on the physical and mechanical properties of high-temperature alloys are unknown. The most critical component in the engine is the heater head which consists of the cylinders, tubings, and regenerator housing. Candidate alloys for these applications must not only meet all the property requirements in air as well as in high-pressure hydrogen, but must also be of low cost to be compatible with automotive application. With these considerations in mind, the creep-rupture properties of the candidate alloys were evaluated over the temperature range of 650°-925°C in air as well as in 15 MPa H_2. The air test results of six alloys were published earlier in NASA CR-168071.[1] This report analyzes the 15 MPa H_2 data and compares them with the air data for ten different alloys.

MATERIALS, EQUIPMENT, AND EXPERIMENTAL PROCEDURES

Test Materials and Analysis

In all, ten different superalloys were evaluated. Nine of them were iron base and one was cobalt base, and their nominal compositions are given in Table 1.

Of these ten alloys, HS-31, SA-F11, CRM-6D, and XF-818 are casting alloys, and the other six are sheet alloys in the thickness range of 0.79 to 0.99 mm (0.031 to 0.039 in.)--comparable to the wall thickness of the tubes used in the Stirling engine. Five of the sheet alloys--A-286, INCOLOY Alloy 800H (or 800H),* N-155, 19-9DL, and CG-27--were purchased from U.S. commercial suppliers; 12RN72, a Sandvik alloy, is specially rolled into sheet form for United Stirling AB, Sweden (US/AB), the supplier who provided the material.

*INCOLOY Alloy 800H is a registered trademark of Huntington Alloys, Inc. In the text, tables, and figures, the alloy is either identified fully or as 800H.

The CRM-6D and XF-818 investment cast specimens were obtained from two sources: Climax Molybdenum Co., Research Laboratory, Ann Arbor, Michigan, USA, and United Stirling AB, Sweden. The HS-31 and SA-F11 investment cast specimens were obtained from United Stirling AB, Sweden.

Specimen Design and Preparation

The specimen drawings and dimensions are shown in Fig. 1. They conform to ASTM E-8. All specimen surfaces were finished to 0.8 μm (32 μin.) rms or better. The CG-27 and 12RN72 sheet specimens were supplied by NASA fully machined with a 9.53 mm (3/8 in.) wide gage section--in CG-27 only, the gage section was remachined to the standard width of 6.25 mm (1/4 in.).

All investment cast specimens were radiographed either by IITRI or United Stirling AB, Sweden, and those with no detectable flaws were selected for testing.

Heat Treatment and Microstructure

The alloys were given their recommended heat treatments as outlined in Table 2. The heat treated hardness values and average grain diameters are also indicated in Table 2.

All the wrought alloys have solid solution-strengthened single-phase austenitic structures with fine second phase and inclusions indicating the rolling direction. N-155, 12RN72, and CG-27 show some twinning in austenite. Undissolved micron size carbides and nitrides may be seen in 12RN72. Fine precipitates in CG-27 relate to its high Al and Ti contents. Of the six sheet alloys, CG-27 is significantly stronger than all the rest, and 12RN72 and 800H are the softest while A-286, N-155, and 19-9DL have similar hardnesses. Selected microstructures are shown in Fig. 2.

Typical dendritic structures of all the cast alloys are shown in Fig. 3. With the exception of braze-cycle heat treated HS-31, the interdendritic arm spacings are very similar in the other alloys. In HS-31, the structural continuity at the boundaries is much less in evidence and only traces of lamellar structure are noted. The boron content of XF-818 is reflected in the distribution of lamellar M_3B_2 in the eutectic structure of the dendrite walls. At higher magnifications, the structures clearly indicate discrete precipitates constituting the dendrite walls, and some coring effect is noted in CRM-6D.

High-Pressure Hydrogen Multispecimen Creep-Rupture Test Equipment

All high-pressure creep-rupture tests were carried out in a specially designed pressure vessel rated at 20.7 MPa at a maximum temperature of 925°C.

The following features are central to the overall satisfactory performance of the tests:

- Six specimens tested simultaneously within a single vessel
- Continuous direct measurement of creep extension within the vessel
- Specimen loading by dead weight with 10:1 lever ratio
- All specimens mounted on a central support column which may be assembled outside the vessel
- All temperature and strain data recorded for computer analysis
- Double-wall vessel design with balanced pressure across the inner wall
- Double-studded pressure vessel to avoid all welding
- Vessel, trunion-mounted for low headroom operation
- Vessel mounted on vibration dampening frame.

The schematic of the high-pressure vessel assembly is shown in Fig. 4.

High-Pressure Hydrogen Creep-Rupture Tests

Six specimens were tested simultaneously in the specially designed high-pressure test equipment shown in Fig. 4. Specimens were deadweight loaded to their initial stress levels and adjustments were made for both internal pressure effect and friction between the Teflon seal and stainless steel pullwire; the overall accuracy of the initial stress was better than 1% at stress levels exceeding 100 MPa and between 1 and 2% at stresses less than 100 MPa.

Two Chromel-Alumel thermocouples were mounted on each specimen just outside the gage length and monitored continuously. Temperatures were uniform between the specimens as well as between the two thermocouples on the same specimen with the standard deviation not exceeding 1.1°C. New thermocouples were used in each test.

The specimens were heated by a resistance-wound elements of 4 kW capacity controlled by a Barber-Colman Model 560 temperature controller. The two halves of the furnace elements could be controlled separately, and furnace element temperatures were monitored and controlled.

Capacitance-type transducers with a sensitivity of 0.25 μm (10 μin.), connected to specially designed concentric tube extensometers, are located in the upper cooler region of the reactor, and creep extension signals were recorded at any desired intervals. During loading, signals were recorded at 3

second intervals which were later increased to 10 min invervals during the first 2 h and further changed to 4 h intervals for long-term tests.

Automatic timers recorded test duration. A mercury cut-off switch mounted on the loading arm indicated rupture when the arm dropped from the horizontal position.

Hydrogen pressure inside the inner reactor vessel was balanced against nitrogen pressure outside it using a differential pressure gage. When the pressure between the inner vessel and the outer chamber exceeded ±70 kPa, automatic demand-operated solenoid valves fed the desired gas (either H_2 to inside or N_2 to outside) to keep the pressure balanced across the hot wall of the reactor inner vessel.

Before start, the vessel interior was flushed with nitrogen (obtained from liquid N_2); nitrogen was pressurized to 3.5 MPa and cycled to ambient pressure three times. Research grade test hydrogen (<1 ppm O_2) from 41.4 MPa tanks were introduced to 3.5 MPa pressure and cycled twice to ambient pressure, and then the test hydrogen was introduced to a pressure somewhat lower than the final test pressure of 15 MPa. The reactor was heated until the desired temperature level was obtained and stabilized (about 4 h), and the H_2 pressure was adjusted to 15 MPa.

Before each test, specimen dimensions were measured to ±25.4 μm, and the cross-sectional areas were calculated to three significant digits. Extensometers were attached to the specimen shoulders. The fractured specimens were fitted, and the extensometer position marks were remeasured to obtain the total extension. To calculate elongation (as percent), the divisor was taken as the adjusted length of the reduced sections, as defined in ASTM E-139.

Incremental loading was used, and extension on loading was noted. Extensometer readings on full loading were taken as the zero base for all subsequent creep strain measurements as a function of time recorded from the conclusion of full load.

In several tests, one or more specimens did not rupture before the tests were discontinued. While no definite rupture life data were obtained in these tests, other valuable information on minimum creep rate and time to 1% creep strain were documented and used in the analysis.

The internal transducers gave excellent results most of the time. One or two transducers, however, malfunctioned in a few tests. To avoid a total loss of creep strain information, externally mounted dial gages, reading to the nearest 25 μm (0.001 in.), were attached to the horizontal loading arms and these data were documented. Later, these dial gages were replaced by LVDTs for automatic recording.

Air Creep-Rupture Tests

Tests in air conducted by IITRI were reported in NASA-CR-168071.[1] Additional air tests conducted on several alloys by NASA-Lewis Research Center will be published separately.[2]

EXPERIMENTAL RESULTS AND ANALYSES

Basic Data

The complete set of high-pressure hydrogen creep-rupture data are given in Table 3. The corresponding air creep-rupture data for A-286, 800H, N-155, 19-9DL, CMR-6D (Climax, aged), and XF-818 (Climax, as-cast) are given in NASA-CR-168071.[1] Air creep-rupture data for wrought alloys 12RN72 and CG-27, and cast US/AB alloys HS-31,SA-F11, CRM-6D, and XF-818 (braze-cycle treated) were evaluated by NASA-LeRC and will be published separately.[2]

The data can be broadly grouped into two categories, namely, independent (controlled) and dependent (derived). The independent category covers the data from columns (2) to (5): environment--15 MPa H_2, alloy type--any one of the ten alloys, temperature--705° to 870°C, and applied initial stress--50 to 275 MPa; column 1 identifies the test number.

The values in columns (6) to (11) are the observed data, i.e., rupture life (t_r), minimum creep rate ($\dot{\varepsilon}_m$), time to reach 1% creep strain ($t_{0.01}$), time to reach tertiary stage (t_{ter}), and total elongation (ε), and for the cast alloys, the reduction in area is given in column (11).

Creep Curves

The creep elongation vs. time curves for tests in 15 MPa H_2 were computer plotted at different temperatures and stress levels. Several typical curves shown in Figs. 5 to 10 illustrate the creep behavior of casting alloys XF-818, CRM-6D, HS-31, and SA-F11, and the wrought alloys, 12RN72 and CG-27.

In Fig. 5, seven XF-818 specimen creep curves from both Climax and US/AB heats/heat treatments are shown on one plot with the longest test discontinued without rupture after 1492 h. Essentially, both the (Climax, as-cast and US/AB, braze-cycled) XF-818 specimens behaved in a similar manner exhibiting the three stages of creep, namely, primary, secondary or steady state, and tertiary. These curves were obtained from data transmitted from the transducers located inside the pressure chamber.

From the same Climax heat of XF-818 (as-cast) specimens, five air creep curves are compared with four 15 MPa H_2 creep curves in Fig. 6. The essential equivalence in creep performance in the two environments is evident from these curves. The only significant difference appears to be in the shorter time to rupture (from the onset of tertiary stage) in 15 MPa H_2, and the consequent lower elongation ductility. For the two longer duration tests, only the first 500 h portions of the curves are shown.

The SA-F11 (US/AB braze-cycled) results for 760° and 815°C tests in 15 MPa H_2 (Fig. 7) indicate the essential similarity with the 15 MPa H_2 XF-818 (Climax, as-cast) results (Fig. 6) except that the total elongations were lower than those of XF-818. The almost identical behavior of Fig. 7 creep

curves at 257 MPa/760°C and 160 MPa/815°C is to be noted--the 815°C specimen, however, exhibited higher ductility and elongation in the tertiary stage.

Figure 8 shows the creep behavior of four CG-27 specimens tested in 15 MPa H_2 at 815°C. In two tests, the internal transducer had malfunctioned and the dial gage data (at 24 h intervals) were plotted. The somewhat uneven nature of the curve reflects the dial gage division marks of 25.4 μm (1×10^{-3} in.). The longest test shown in Fig. 8 (140 MPa/819 h) indicates an initial low creep rate, which increased after about 50 h and then decreased to a steady state creep condition for about 300 h before entering the tertiary stage; this behavior may be due to transducer malfunction at the initial period.

Wrought alloys 12RN72 and CG-27 creep strains plotted in Fig. 9 show that 12RN72 has a relatively shorter secondary stage, a longer tertiary stage, and higher ductility when compared with CG-27. The uneven nature of one curve reflects readings from dial gages.

The creep behavior of four cast alloys from one single test is plotted in Fig. 10. The smoothness of the curves indicates that when specimens broke successively at different time periods, no permanent disturbing effect was noted on the creep-elongation behavior of the remaining specimens. This reflects the special design feature of the massive A-286 central column around which the six specimens are grouped in their isolated cells. The adequacy of this unique design feature points to the development of high-pressure test apparatuses which can simultaneously test 12, 24, or an even larger number of specimens under a single high-temperature high-pressure environment.

Temperature-Compensated Analyses of Rupture Life, Minimum Creep Rate, and Time to 1% Creep Strain

The Orowan-Sherby-Dorn (O-S-D) method was selected by NASA-Lewis as the method of analysis combining stress and temperature.[3-8] The O-S-D relationship is given by:

$$\ln Y = \ln k + n \ln \sigma + Q/RT \qquad (1)$$

where

Y = t_r, $t_{0.01}$, or $\dot{\varepsilon}_m$

Q = the apparent activation energy, J/mol

σ = the initial stress, MPa

T = the test temperature, K

R = the universal gas constant, 8.314 J/K mol

n = stress exponent

k = a constant.

A linear regression analysis of Eq. 1 determines the apparent activation energy, Q, and the slope of the fitted line, n, which is the stress exponent based on the power-law creep relationship. Equation 1 can be rearranged in the following manner:

$$(\ln Y - Q/RT) = \ln k + n \ln \sigma \qquad (2)$$

The rupture life, time to reach 1% creep strain, and minimum creep rate data for the different alloys tested in 15 MPa H_2 and given in Table 3 were analyzed using the O-S-D relationship according to Eq. 2. The results of this analysis are compared, where available, with the results of a similar analysis for tests in air reported in NASA CR-168071.[1] Finally, based on this analysis, stresses for 3500-h rupture lives in air and 15 MPa H_2 were estimated and compared with the design criteria stresses for the automotive Stirling engine.

The comparative analysis of air and 15 MPa H_2 creep-rupture data of the four casting and six wrought alloys are grouped in the following manner:

- Cast alloys CRM-6D (aged) and XF-818 (as-cast): Climax Molybdenum Co., Michigan
- Cast alloys HS-31, SA-F11, CRM-6D, and XF-818 (braze-cycled): United Stirling AB, Sweden
- Wrought alloys A-286, 800H, N-155, 19-9DL, 12RN72, and CG-27.

Climax Cast Alloys CRM-6D (Aged) and XF-818 (As-cast) Tested in Air and 15 MPa H_2

The regression analysis results for rupture life (t_r), time to reach 1% creep strain ($t_{0.01}$), and the minimum creep rate ($\dot{\varepsilon}_m$) are given in Table 4. Table 4 includes both air[1] and 15 MPa H_2 data analysis. Based on the regression analysis parameters, temperature-compensated rupture life, minimum creep rate, and time to 1% creep strain values were plotted against stress in air and 15 MPa H_2 tests. The 15 MPa H_2 figures are compared with air data where available; the air curves and analyses were given in reference 1.

The temperature-compensated rupture life data of Climax heats of CRM-6D (aged) and XF-818 (as-cast) in 15 MPa H_2 and air environments are graphically compared in Fig. 11. Similarly, Fig. 12 compares the minimum creep rate behavior in two environments for Climax CRM-6D (aged) and XF-818 (as-cast). The stress exponent and activation energies of these alloys for rupture life and minimum creep rate are summarized below:

Rupture Life (t_r):

Alloy	Environment	Stress Exponent (n)	Apparent Activation Energy (Q), kJ/mol
CRM-6D (aged)	Air	-9.12	461
	15 MPa H_2	-13.3	720
XF-818 (as-cast)	Air	-7.52	505
	15 MPa H_2	-7.93	436

Minimum Creep Rate ($\dot{\varepsilon}_m$):

Alloy	Environment	Stress Exponent (n)	Apparent Activation Energy (Q), kJ/mol
CRM-6D (aged)	Air	11.8	-551
	15 MPa H_2	11.8	-574
XF-818 (as-cast)	Air	7.47	-545
	15 MPa H_2	7.55	-450

Rupture Life Analysis

For the Climax alloy CRM-6D (aged), testing in 15 MPa H_2 results in the rupture life stress exponent (n) being more negative than that tested in air. Increases in the apparent activation energy in H_2 over the air environment also were noted. These two trends oppose each other. The larger sensitivity to small changes in stress in H_2 as revealed in the large negative exponent (n) makes CRM-6D (Climax, aged) more susceptible to rupture due to smaller stress fluctuations. On the other hand, a significantly large apparent activation energy (Q) makes the alloy less susceptible to deterioration due to sudden large changes in temperature. The opposing trend effects of n and Q on rupture life in CRM-6D (Climax, aged) tend to compensate each other, and the overall effect on 3500-h rupture life stress in H_2 may not be significantly different from that in air, as discussed in a later section. The combined effect of n and Q on t_r is further strongly influenced by the constant term, ln k, which itself is observed to be strongly affected by H_2.

In Climax XF-818 (as-cast) alloys, the rupture life stress exponent (n) is slightly more negative in H_2 than that in air, and the Q is also about 15% less. The very similar n values indicate that the alloy does not become more stress-sensitive in H_2 than in air, while the slightly different Q will not make it more sensitive to temperature fluctuations.

In Fig. 11, rupture life is combined (compensated) with the quotient (Q/T) obtained from test temperature (T) and the apparent activation energy (Q). The slopes (n) indicate the differences in the stress exponents while the near-parallel shift is due to the combined effect of rupture life and Q values.

Minimum Creep Rate Analysis

While H_2 environment effect has some influence on rupture lives of both Climax CRM-6D (aged) and XF-818 (as-cast) when compared to air environment, the effect of H_2 on minimum creep rate appears to be negligible. The stress exponent (n) remained unaffected by environment, and Q was only affected in XF-818 (Climax, as-cast). A less negative Q in H_2, by itself, will tend to increase the minimum creep rate in H_2 over air, and the more positive n for H_2 environment will also have a positive effect; however, the differences in Q and n are small, and the total effect in increasing $\dot{\varepsilon}_m$ is likely to be small. The parallel lines in Fig. 12 indicate that the stress exponents are similar and the shifts between air and H_2 lines are due to the combined effect of $\dot{\varepsilon}_m$ and Q values.

United Stirling AB, Cast Alloys CRM-6D, XF-818, HS-31, and SA-F11 (All Braze-Cycled) Tested in 15 MPa H_2

The temperature-compensated analysis data of the four cast alloys in the braze-cycle heat treated condition, tested in the 15 MPa H_2 environment are summarized in Table 5. Based on this analysis, temperature-compensated rupture life and minimum creep rate parameters vs. stress in 15 MPa H_2 were plotted in Figs. 13 and 14, respectively. The stress exponent and activation energies for rupture life and minimum creep rate are summarized below:

Rupture Life (t_r) in 15 MPa H_2:

Alloy	Stress Exponent (n)	Apparent Activation Energy (Q), kJ/mol
CRM-6D	-6.94	273
XF-818	-8.43	591
HS-31	-10.2	551
SA-F11	-6.85	508

Minimum Creep Rate ($\dot{\varepsilon}_m$) in 15 MPa H_2:

Alloy	Stress Exponent (n)	Apparent Activation Energy (Q), kJ/mol
CRM-6D	6.76	-239
XF-818	9.74	-708
HS-31	12.6	-600
SA-F11	6.58	-505

Rupture Life Analysis

The similarity and difference in n and Q between the four cast alloys (US/AB, braze cycled) tested in 15 MPa H_2 are reflected in the line slopes and the degree of shift between the lines as shown in Fig. 13. The n values range from -6.85 to -10.2, with CRM-6D and SA-F11 having very similar values of about -7. XF-818 with -8.43 and HS-31 with -10.2 (n) values indicate a more sensitive rupture life dependency on stress.

The CRM-6D and XF-818 (US/AB, braze-cycled) alloys belong to different heats than CRM-6D (Climax, aged) and XF-818 (Climax, as-cast). Their n and Q values in 15 MPa H_2 are compared below:

Alloy	Stress Exponent (n)	Apparent Activation Energy (Q), kJ/mol
CRM-6D (Climax, aged)	-13.3	720
CRM-6D (US/AB, braze-cycled)	-6.94	273
XF-818 (Climax, as-cast)	-7.93	436
XF-818 (US/AB, braze-cycled)	-8.43	591

The large difference between the n and Q values in CRM-6D from the two suppliers may also be due to the two different casting procedures followed in this very high C-Mn alloy--namely, Climax castings were made by feeding the molten alloy from the side while the US/AB alloys were fed from one end. In XF-818, the values do not indicate the sensitivity shown by CRM-6D due to different cast/heat treatment/casting procedures between Climax and US/AB castings.

Minimum Creep Rate Analysis

The slopes of lines and the shift in the lines between the four cast alloys shown in Fig. 14 indicate the relative behavior of these four braze-cycled US/AB cast alloys. The n values range from 6.58 to 12.6 with SA-F11 and CRM-6D having very similar values near 7. XF-818 with 9.74 and HS-31 with 12.6 (n) values indicate a more sensitive minimum creep rate dependency on stress. Thus, rupture life vs. stress and minimum creep rate vs. stress dependencies in these four alloys show a significant parallelism.

The CRM-6D and XF-818 9 (US/AB, braze-cycled) alloys belong to different cast/heat treatment/casting procedures than CRM-6D (Climax, aged) and XF-818 (Climax, as-cast), and their n and Q values in 15 MPa H_2 are compared below:

Alloy	Stress Exponent (n)	Apparent Activation Energy (Q), kJ/mol
CRM-6D (Climax, aged)	11.8	-574
CRM-6D (US/AB, braze-cycled)	6.76	-239
XF-818 (Climax, as-cast)	7.55	-450
XF-818 (US/AB, braze-cycled)	9.74	-708

There are significant differences in both n and Q values between the different heats and heat treatments of alloys of the same nominal composition when tested in 15 MPa H_2 with the possibility that the different casting procedures had also contributed to these differences, particularly in the high Mn alloy, CRM-6D.

Wrought Alloys N-155, 19-9DL, 800H, and A-286 Tested in Air and 15 MPa H_2, and CG-27 and 12RN72 Tested in 15 MPa H_2

The temperature-compensated data analysis for rupture life and minimum creep rate of the six wrought alloys in 15 MPa H_2 is summarized in Table 6; the air data analysis for A-286, 800H, N-155, and 19-9DL was published earlier.[1] In Figs. 15 and 16, respectively, the temperature-compensated rupture life and minimum creep rate in 15 MPa H_2 are compared for the six alloys.

Rupture Life Analysis

The stress slope (n) in 15 MPa H_2 (Table 6) varies from -4.67 to -7.92 and the apparent activation energy from 359 to 530 kJ/mol. 800H, N-155, and 19-9DL with n very near to minus 8 (-8) have the largest stress sensitivity, and CG-27 and A-286 with n about -4.5 to -5, the smallest.

In alloys A-286, 800H, N-155, and 19-9DL, the n values for tests in air (Table 6) were in all cases slightly less negative, i.e., the sensitivity to stress is slightly less in air than in 15 MPa H_2.

Minimum Creep Rate Analysis

Except for A-286 and CG-27, the stress slope (n) for the other four wrought alloys in 15 MPa H_2 (Table 6) ranged from 7.63 to 9.83. The A-286 and CG-27 values are 4.09 and 3.31, respectively, indicating their lesser sensitivity to stress. The four alloys (A-286, 800H, N-155, and 19-9DL) had the n values uniformly smaller in air (Table 6), indicating a lesser dependence on stress compared to 15 MPa H_2 environment.

Analysis of Time to 1% Creep Strain Data

Tables 4, 5, and 6 summarize the temperature-compensated analysis data for time to 1% creep strain. Based on these data, regression lines were fitted as shown in Figs. 17, 18, and 19 for the following alloys:

Fig. 17 - Two Climax cast alloys, CRM-6D (aged) and XF-818 (as-cast)

Fig. 18 - Four United Stirling AB cast alloys, HS-31, SA-F11, CRM-6D, and XF-818; all braze-cycled.

Fig. 19 - Six wrought alloys, A-286, 800H, N-155, 19-9DL, 12RN72, and CG-27.

These plots show significant scatter around the fitted lines indicating low regression coefficients (resulting from a small data set) as well as due to the derived nature of the data from the observed elongation vs. time curves. The n and Q values, however, have similar ranges comparable to those observed for rupture life. Only in the case of US/AB HS-31 was a large difference noted between t_r and $t_{0.01}$ (n) and (Q) values in 15 MPa H_2 tests, as indicated below:

Analysis	Stress Exponent (n)	Apparent Activation Energy (Q), kJ/mol
Rupture life (t_r)	-10.2	551
Time to 1% creep strain ($t_{0.01}$)	-4.54	256

In other words, in HS-31 (braze cycled), $t_{0.01}$ is significantly less sensitive to stress changes than t_r.

Analysis of Stress Exponent (n) and Apparent Activation Energy (Q) in the Ten Different Alloys

All the n and Q values are summarized in Table 7. For rupture life and minimum creep rate, the alloys with different n values are arranged in increasing order of sensitivity to stress and temperature changes, as given below:

Stress-Life Exponent (n):

Rupture Life		Minimum Creep Rate	
Air	15 MPa H_2	Air	15 MPa H_2
A-286	CG-27	A-286	CG-27
N-155	A-286	19-9DL	A-286
19-9DL	12RN72	N-155	SA-F11[a]
800H	SA-F11[a]	XF-818[b]	CRM-6D[a]
XF-818[b]	CRM-6D[a]	800H	XF-818[b]
CRM-6D[b]	19-9DL	CRM-6D[b]	800H
	N-155		19-9DL
	800H		12RN72
	XF-818[b]		XF-818[a]
	XF-818[a]		N-155
	HS-31[a]		CRM-6D[b]
	CRM-6D[b]		HS-31[a]

[a]United Stirling AB. These alloys were braze-cycle heat treated.

[b]Climax castings, CRM-6D (aged), XF-818 (as-cast).

The above tabulation indicates that for rupture life the stress-life exponents (n) of the cast alloys generally make them relatively more sensitive to stress fluctuations than the wrought alloys, in both air and high pressure hydrogen environments. For minimum creep rate, no such trend is noted.

Under O-S-D analysis of the form

$$\ln Y = \ln k + n \ln \sigma + Q/RT \tag{1}$$

for Y = rupture life, n is negative and Q is positive; and for Y = minimum creep rate, n is positive and Q is negative.

Thus, with constant ln k and Q, for rupture life (t_r), when $n_{air} > n_{H2}$ (for example, $n_{air} = -7$ and $n_{H_2} = -8$), then

$$(t_r)_{air} > (t_r)_{H_2}$$

at the same stress (σ) level, and rupture life will also vary more significantly in H_2 environment with smaller stress changes. For example, when stress increases, say, by 5%, with other Eq. 1 quantities remaining constant, rupture lives in air (n = -7) and hydrogen (n = -8) are decreased by the following factors:

$$\text{Air:} \quad (1.05)^{-7} = 0.71$$

$$15 \text{ MPa } H_2\text{:} \quad (1.05)^{-8} = 0.68$$

and it is readily seen that stress sensitivity on rupture life is higher under H_2 ($n = -8$) than under air ($n = -7$) environment.

In minimum creep rate, n is positive, and when $n_{air} > n_{H_2}$--for example, $n_{air} = 8$, and $n_{H_2} = 7$--then

$$(\dot{\varepsilon}_m)_{air} > (\dot{\varepsilon}_m)_{H_2}$$

at the same stress (σ) level, and in air the minimum creep rate will vary more significantly with smaller stress changes. For example, when stress increases, say, by 5%, with other Eq. 1 quantities remaining constant, the minimum creep rates in air ($n = 8$) and hydrogen ($n = 7$) are increased by the following factors:

$$\text{Air:} \quad (1.05)^{8} = 1.48$$

$$15 \text{ MPa } H_2\text{:} \quad (1.05)^{7} = 1.41$$

The form of Eq. 1, with the temperature parameter (T) expressed as a ratio to the apparent activation energy (Q), indicates that as Q becomes more positive, Q/T will increase and affect both t_r and $\dot{\varepsilon}_m$ positively. For example, in rupture life where Q has a negative value, with other quantities remaining constant in Eq. 1, if $Q_{air} > Q_{H_2}$ (for example, $Q_{air} = 600$ kJ/mol and $Q_{H_2} = 500$ kJ/mol), $(t_r)_{air} > (t_r)_{H_2}$.

If T is decreased by 10%, say, from 1100K (827°C) to 990K (717°C) in both air and H_2 environment, Q/RT will change to Q/0.9 RT, i.e., an increase of 11% from the energy term, and a larger more positive Q for rupture life in air will mean a more significant increase in rupture life. And, of course, the reverse will be true if $(Q)_{air} < (Q)_{H_2}$.

In the case of the minimum creep rate, Q is negative, and with $(Q)_{air} > (Q)_{H_2}$--for example, $Q_{air} = -500$ kJ/mol and $(Q)_{H_2} = -600$ kJ/mol--then

$$(\dot{\varepsilon}_m)_{air} > (\dot{\varepsilon}_m)_{H_2}$$

with other quantities in Eq. 1 remaining unchanged. Also, following the analysis of Q for t_r, a more positive Q will thus have less effect in decreasing the minimum creep rate.

The above analysis presupposes that only either n or Q is varying with the other quantities in Eq. 1 remaining constant. However, both n and Q vary, and the environment also appears to significantly affect the fitting constant, k, and the total effect shows up as the overall change in t_r and $\dot{\varepsilon}_m$ in the two environments. In the next section, the combined effect of these changes is reflected in the estimation of 3500 h rupture life stress and stress to reach 1% creep strain in 3500 h for each alloy.

Predicted Stresses for Rupture and 1% Creep in 3500 Hours

Based on the temperature-compensated analytical data given in Tables 4, 5, and 6, mean stresses for 3500-h rupture lives in air and and 15 MPa H_2 were estimated and are summarized in Table 8. Similar estimates of mean stresses to obtain 1% creep strain in 3500 h in air and 15 MPa H_2 were made and are given in Table 9. By statistical methodology, the 90% confidence limits on these estimated stresses were calculated and are summarized in Tables 8 and 9 along with the mean stresses.

3500-Hour Rupture Stress

The wrought and cast alloys are ranked below in terms of decreasing stresses for 3500-h rupture life both in air and 15 MPa H_2:

Wrought alloys (Temp. = 870°C)		Cast Alloys (Temp. = 775°C)	
Air	15 MPa H_2	Air	15 MPa H_2
N-155	CG-27	CRM-6D[a]	HS-31[b]
19-9DL	N-155	XF-818[a]	CRM-6D[a]
800H	19-9DL	______[c]	SA-F11[b]
______[c]	A-286		XF-818[a]
A-286	12RN72		XF-818[b]
	800H		______[c]
	______[c]		CRM-6D[a]

[a]Climax cast alloys, CRM-6D (aged) and XF-818 (as-cast).

[b]United Stirling AB cast alloys, braze cycle heat treated.

[c]Design stress levels of 28 MPa at 870°C and 119 MPa at 775°C for wrought and cast alloys, respectively.

The MOD 1A design criteria stress for 3500-h rupture life for wrought tube material is 28 MPa at 870°C, and although in air the A-286 alloy did not meet the requirements, in 15 MPa H_2 all the alloys appear to meet the criteria. In 15 MPa H_2, out of the different cast alloys, only CRM-6D (US/AB, braze-cycled) failed to meet the 119 MPa at 775°C criteria.

If one considers the lower value of the 90% confidence limits, then for the tube alloys in 15 MPa H_2 both 800H and A-286 will fail to meet the 28 MPa (870°C) design stress requirements, and 12RN72 barely exceeds it at 30.7 MPa. Similarly, for the cast alloys, both CRM-6D (US/AB, braze-cycled) and XF-818 (Climax, as-cast) will fail to meet the level of 119 MPa (775°C) while XF-818 (US/AB, braze-cycled) barely exceeds it at 122 MPa.

Several graphical presentations of 3500-h rupture stress levels of the different alloys over the temperature range of 775° to 870°C (with estimated graphical extensions to 705°C and 925°C) for both air and 15 MPa H_2 environments are given in Figs. 20 to 24. These figures not only illustrate the relative strength levels at the different temperatures, but their extrapolations indicate (on the assumption that the creep mode does not change) what the effect of small but expected temperature fluctuations (due to different Q values) will be on their strength levels.

H_2 vs. Air Effect on 3500-h Rupture Stress

As indicated earlier, Fig. 20 shows that A-286 performance improves in 15 MPa H_2 to exceed the 28 MPa design stress level though, the 90% confidence range being large, its lower 90% limit does not meet the specification. 800H, 12RN72, and 19-9DL mean stress levels in 15 MPa H_2 meet the requirements barely. Only N-155 and CG-27 are significantly stronger to fully meet the design stress level. N-155 performance appears to improve in 15 MPa H_2 while 800H decreases marginally.

Among the cast alloys, Fig. 21 shows that CRM-6D (Climax, aged) and HS-31 and SA-F11 (US/AB, braze-cycled) are adequate to meet the 119 MPa (775°C) design criteria, and CRM-6D (US/AB, braze-cycled) is inadequate. CRM-6D (Climax, aged) indicates a performance improvement in 15 MPa H_2 over air. In both the XF-818 heats, the mean stress values barely satisfy the design stress criteria, and in XF-818 (Climax, as-cast), 15 MPa H_2 environment tends to decrease rupture stress level and exhibits a larger scatter than that noted in air environment.

Operating Temperature Fluctuation Effect on 3500-h Rupture Stress in 15 MPa H_2

If these predicted mean stresses in the range of 775° and 870°C for tube alloys tested in 15 MPa H_2 are extrapolated to a higher temperature of, say 925°C, then except for N-155 and CG-27, none of the other alloys will meet the 28 MPa criteria level, as shown in Fig. 22. Figure 23 shows that with four US/AB cast alloys, the mean stress levels when extrapolated to a higher temperature indicate that at about 825°C ($10^4/T = 9.1$), alloy SA-F11 (US/AB, braze-cycled) barely meets the 119 MPa design stress requirement in 15 MPa H_2, and its lower 90% confidence value is below the specification. Similarly, Fig. 24 shows that Climax cast alloy XF-818 (as-cast) fail to meet the 119 MPa stress criterion when a temperature excursion to 825°C takes place; CRM-6D (Climax, aged), however, remains strong in 15 MPa H_2.

Stress to 1% Creep Strain in 3500 Hours

The predicted stresses for reaching 1% creep strain in 3500 h were analyzed in a manner similar to that for stress to 3500 h rupture and the alloys are ranked below in order of decreasing stress levels.

Wrought Alloys (Temp. = 870°C)		Cast Alloys (Temp. = 775°C)	
Air	15 MPa H_2	Air	15 MPa H_2
N-155	CG-27	CRM-6D[a]	CRM-6D[a]
800H	N-155	XF-818[a]	SA-F11[b]
19-9DL	12RN72		XF-818[a]
A-286	19-9DL		XF-818[b]
	800H		CRM-6D[b]
			HS-31[b]

[a]Climax, CRM-6D (aged), XF-818 (as-cast).

[b]United Stirling, AB, braze-cycled.

The above analysis indicates that CG-27 and N-155 are the strongest tube alloys in 15 MPa H_2, and the mean stress to reach 1% creep strain in 3500 h follows the ranking for 3500-h rupture life stress. Within the cast alloys, CRM-6D (Climax, aged), SA-F11 (US/AB, braze-cycled), and XF-818 (Climax, as-cast) are the strongest in terms of stress to 1% creep strain in 3500 h and rank differently in 3500-h rupture life stress, where HS-31 (US/AB, braze cycled) was the strongest.

Effect of Environment on Rupture Elongation

The complete rupture elongation data of the ten alloys in both air and 15 MPa H_2 are summarized in Table 10. As expected, the total elongation on rupture was strongly dependent on temperature and stress in both the environments. Elongation increased with increasing stress and temperature but tended to decrease at the highest temperatures. Total elongation on rupture in 15 MPa H_2 environment in tube and cast alloys is summarized below.

Maximum Total Elongation on Rupture in 15 MPa H_2, %

Tube Alloys (815°C)		Cast Alloys (760°C)	
N-155	35.3	HS-31[a]	28.1
12RN72	24.7	CRM-6D[a]	21.1
800H	21.4	XF-818[a]	14.7
A-286	8.1	XF-818[b]	10.7
19-9DL	11.7	CRM-6D[b]	7.4
CG-27	7.3	SA-F11[a]	6.3

[a]United Stirling AB, braze-cycled.

[b]Climax, CRM-6D (aged), XF-818 (as-cast).

Only a few tube alloys were tested at 815°C and 870°C in both air and 15 MPa H_2 and these elongation (%) data show some serious deteriorating effect of H_2 as indicated below, along with reduction indicated as a percent of air value.

Alloy	Max Total Elongation on Rupture (815°C), %		Change from Air, %
	Air	15 MPa H_2	
N-155	58.3	35.3	-39
19-9DL	44.8	9.4	-79
800H	59.6	21.4	-64
A-286	44.6	8.1	-82

In the case of Climax cast alloys at 760°C, this deteriorating effect of H_2 on elongation was not as greatly pronounced as in the tube alloys.

Alloy	Max Total Elongation on Rupture (760°C), %		Change from Air, %
	Air	15 MPa H_2	
CRM-6D (aged)	8.7	7.4	-15
XF-818 (as-cast)	13.6	10.4	-16

When the creep-rupture elongation air test data on tube alloy 12RN72 and CG-27 and US/AB braze-cycled XF-818, CRM-6D, HS-31, and SA-F11 become available,[2] it will be possible to compare the selective effect of hydrogen on the ductility of these alloys.

Without extensive microstructural analysis using transmission electron microscopy, the reason for loss of ductility due to high pressure H_2 will be speculative. The hydrogen environment diffusion through the structure might activate and promote cavity nucleation at grain boundaries and may also act in cavity enlargement--the total effect evident as a reduction in total elongation on rupture.

FRACTOGRAPHY AND MICROSTRUCTURAL ANALYSIS

Fracture Location and Appearance

Typical fractured specimens tested in 15 MPa H_2 are shown in Figs. 25 to 27. Figure 25 shows 19-9DL and XF-818 (Climax, as-cast) specimens tested in the temperature range of 705° to 815°C. The largest elongations for 19-9DL and XF-818 (Climax, as-cast) specimens were 28.5% and 10.4%, respectively.

In Fig. 26, all six alloy specimens from two different tests are compared with elongations indicating the higher ductility of the wrought alloys. Multiple fracture initiation occasionally resulted in fracture pieces almost detaching, as shown for A-286 and 19-9DL.

Fractured specimens from two tests are shown in Fig. 27. In both tests, 12RN72 appears to have fractured, with pieces almost detaching from the specimen. The low ductility of CG-27 and SA-F11 is evident in these figures.

Several fracture surfaces were evaluated by SEM, and a few of the specimens were polished through the midsection parallel to their longitudinal direction to observe the nature of grain-boundary movement and crack distribution in the specimen interior.

Fractographs

Fracture analysis was done on a selected number of specimens of various alloys tested in 15 MPa H_2. Analyses of air test specimens were published earlier.[1]

Wrought Alloys

In A-286, the fracture mode was essentially intergranular (Fig. 28a), while in some areas a transgranular dimple rupture mode was observed (Fig. 28b); in Fig. 28c, the intergranular fracture showed second-phase particles which need additional studies for identification.

Figure 29a shows a typical dimple rupture in alloy 800H which is very similar to those shown in Figs. 29b and c, respectively, for N-155 and 19-9DL. Multiple crack sites near specimen edges, more numerous near the final fracture, are typical in all these highly ductile wrought alloys.

12RN72 fracture surfaces (760° and 815°C) are shown in Fig. 30. Earlier, in Fig. 27, multiple cracking in 12RN72 leading almost to separation of pieces indicated low strength and significant ductility at these temperatures. However, in different areas on the same fracture surface one observed very ductile dimple rupture with adjoining areas showing intergranular decohesive rupture with particles decorating the grain surfaces, as seen earlier for A-286 (Fig. 28c). For example, Figs. 30a and b show low-magnification fractographs showing dimple rupture and decohesive mode; whereas at higher magnifications, Figs. 30c and d clearly reveal the details of dimples and intergranular modes. In contrast to 12RN72, CG-27, which had the lowest ductility among the wrought alloys, showed quasi-cleavage type fracture (Fig. 31a) that revealed only very few dimples at higher magnifications (Fig. 31b).

Cast Alloys

In 15 MPa H_2, difference in fracture appearance between CRM-6D (aged) and CRM-6D (braze-cycled) is not significant, as shown in Fig. 32. Figures 32a, b, and c compare the fractographs at different temperatures, and Figs. 32d, e, and f compare these structures at higher magnifications; the similarity is evident. The fracture surfaces are jagged, and the region marked A in Fig. 32a

is crescent-shaped and very rough. Region B covers more than 60% of the area and shows interdendritic pullout, and region C is narrow and rough. Similar features are discerned in varying degrees on Figs. 32b and c. At higher magnifications, a mixture of interdendritic and transdendritic fracture of similar nature is noted on Figs. 32d, e, and f.

The braze-cycled vs. as-cast XF-818 fractographs are shown in Fig. 33. Figures 33a and b compare macrofractographs, and Figs. 33c and d present the same fractures at higher magnification. Area A in Fig. 33a is smooth and shiny with a significant shear angle following a dendritic colony. Area B, covering 40% of the area, appeared less shiny and rougher while area C, considerably more rugged, appeared to be the overload area for rupture; similar features were noted on Fig. 33b. At higher magnification, some fine dimples were noted on both fracture surfaces, as shown in Figs. 33c and d.

The significant ductility shown by HS-31 (braze-cycled) specimens is clearly evident in Fig. 34. Figures 34a and b show that the fracture path had followed a dendritic pattern over certain regions. Very fine dimples are present on the entire fracture surface, and dendritic spines are clearly outlined in Figs. 34c and d.

The low ductility of SA-F11 (braze-cycled) is evident in Figs. 35a and b where the fracture paths are seen to follow the dendritic pattern of the cast structure. At higher magnifications, a dimple network may be seen on several areas including dendrite spines and arms.

Cross-Section Examination

One-half of several fractured specimens were metallurgically polished in their longitudinal cross-section approximately halfway through the thickness. All the specimens were electrolytically etched with 10% oxalic acid to reveal various constituents and their microstructures.

Figures 36a to d show typical creep cavities due to grain boundary movement in A-286, 800H, N-155, and 19-9DL, respectively. Determining whether hydrogen had assisted in the growth of these cavities at the initial stages will require detailed TEM examination of thin sections near the cracks. Although A-286 and 800H did not show any substructure, a fine second phase appears to be present in Figs. 36c and d.

Similarly, grain boundary cavity formation due to creep is seen in Figs. 37a and b for 12RN72 and CG-27. The cavities are not significantly different in size in the two alloys, and CG-27 shows some twinned structure.

Fracture surfaces of CRM-6D and XF-818 specimens for the different heats are shown in Figs. 38a to d. No obvious differences were noted between the differently heat treated structures at 50X as well as at 200X and higher magnifications. The higher ductility of the lower strength braze-cycle treated alloys are evident in extensive reduction in area seen in Figs. 38b and d.

Specimen fracture surfaces of the two high-strength alloys HS-31 (cobalt-base) and SA-F11 (iron-base) are shown in Figs. 39a and b, respectively. The

high ductility of HS-31 is readily contrasted with the low ductility of SA-F11. Adjacent to the fracture, significant grain boundary movements have created cavities in HS-31, as seen in Fig. 39a. At higher magnifications, for both HS-31 and SA-F11, a significant number of creep voids are seen, Figs. 39c and d, respectively; in the case of SA-F11, however, the presence of some casting cavities is suspected along the dendrite orientation.

SUMMARY OF RESULTS

Nine iron-base and one cobalt-base alloys were tested in air and 15 MPa H_2 for creep rupture at 650° to 925°C. The rupture life (t_r), minimum creep rate ($\dot{\varepsilon}_m$), and time to 1% creep strain ($t_{0.01}$) were analyzed using Orowan-Sherby-Dorn temperature-compensated analysis, and rupture ductility and microstructures were evaluated. The analyses indicate the following:

- At the MOD 1A engine operating temperature of 870°C and design stress level of 28 MPa for a 3500 h rupture life in 15 MPa H_2, tube alloys CG-27, N-155, and 19-9DL adequately meet the design stress criterion. In air, N-155, and 19-9DL (in that order) met the design stress requirements and 15 MPa H_2 did not change the order. In terms of elongation at rupture in 15 MPa H_2, N-155 is significantly better than 19-9DL, and CG-27 showed the least ductility.

- At the MOD 1A engine operating temperature of 775°C for cylinders and regenerator housing, and with 119 MPa design stress level for a 3500-h rupture in 15 MPa H_2, the cast alloys HS-31 (US/AB, braze-cycled), CRM-6D (Climax, aged), and SA-F11 (US/AB, braze-cycled) adequately meet the design stress criterion, with XF-818 (Climax, as-cast) also satisfying the criterion but less adequately.

- The analysis of stress to reach 1% creep strain in 3500 h in 15 MPa H_2, however, indicates a different ranking in which HS-31 (US/AB, braze-cycled) has the lowest value of 46.2 MPa while the top three alloys, CRM-6D (Climax, aged), SA-F11 (US/AB, braze-cycled), and XF-818 (Climax, cast) had values of 130, 126, and 105 MPa, respectively. Thus, in combination with the high predicted stress for rupture in 3500 h, it appears that CRM-6D (Climax, aged) and SA-F11 (US/AB, braze-cycled) will be the best selections. However, when rupture ductility is taken into consideration, HS-31 (US/AB, braze-cycled) with 28% elongation is the highest and exceeds significantly CRM-6D (Climax, aged) which had 7.4%, and SA-F11 (US/AB, braze-cycled), which had 6.3%. XF-818 (Climax, as-cast) with elongation at 10.7% and meeting the design stress criterion may then be considered a suitable candidate engine material.

- Ductility was affected by hydrogen environment in both wrought and cast alloys with reductions from values in air up to 70% noted in wrought alloys and 30% in the cast alloys (excluding the braze-cycled alloys).

- No significant effect of hydrogen on fracture mechanism was noted. In wrought alloys, the main fracture mechanism was dimple rupture with fracture initiating at multiple locations. In cast alloys, interdendritic planar fractures along with transdendritic fracture modes were noted with occasional dimples noted in the areas last to rupture.

REFERENCES

1. S. Bhattacharyya, "Creep-Rupture Behavior of Six Candidate Stirling Engine Iron-Base Superalloys in High-Pressure Hydrogen, Vol. I - Air Creep-Rupture Behavior," NASA CR-168701, December 1982.

2. R. H. Titran, unpublished data, NASA-Lewis Research Center, Cleveland, Ohio.

3. F. R. Larson, and J. Miller, Trans. ASME, Vol. 74, 1952, p. 765.

4. S. S. Manson and A. M. Haferd, "A Linear Time-Temperature Relation for Extrapolation of Creep and Stress-Rupture Data," NACA Technical Note 2890, March 1952.

5. S. S. Manson and W. R. Brown, Proc. ASTM, ASTEA, Vol. 53, 1953, p. 693.

6. O. D. Sherby, "Factors Affecting the High Temperature Strength of Polycrystalline Solids," Acta Met., Vol. 10, No. 2, 1962, pp. 135-147.

7. J. E. Dorn, "The Spectrum of Activation Energies for Creep," in Creep and Recovery, ASM, Metals Park, Ohio, 1957, pp. 255-283.

8. R. M. Goldhoff, " The Evaluation of Elevated Temperature Creep and Rupture Strength Data: An Historical Perspective," in Characterization of Materials for Service at Elevated Temperatures, G. V. Smith, Ed., Publ. No. MPC-7, ASME, New York, 1978, pp. 247-265.

TABLE 1. SUPERALLOY COMPOSITIONS

Alloys	Nominal Composition, %													
	C	Mn	Si	Cr	Ni	Co	Mo	W	Nb	Ti	Al	B	Fe	Others
A-286[a]	0.05	1.40	0.40	15	26	-	1.25	-	-	2.15	0.2	0.003	Bal	0.03 V
INCOLOY Alloy 800H[a,b]	0.08	0.8	0.5	21	32.5	-	-	-	-	0.4	0.4	-	Bal	0.4 Cu
N-155[a]	0.12	1.5	0.5	21	20	20	3.0	2.5	1.0[c]	-	-	-	Bal	0.15 N, 0.5 Cu max
19-9DL[a]	0.30	1.10	0.60	19	9.0	-	1.25	1.20	0.40	0.30	-	-	Bal	-
12RN72[d]	0.1	1.8	0.4	19	25	-	1.4	-	-	0.5	-	0.006	Bal	0.030 P, 0.015 S max
CG-27[a]	0.05	0.1	0.1	13	38	-	5.5	-	0.6	2.5	1.5	0.01	Bal	
HS-31[e]	0.5	0.75	0.75	25.5	10.5	Bal	-	7.5	-	-	-	-	-	-
SA-F11[f]	0.63	0.5	0.6	23.0	16.0	-	-	12.0	-	-	-	0.4	Bal	-
CRM-6D[a]	1.05	5.00	0.50	22	5.0	-	1.0	1.0	1.0	-	-	0.003	Bal	-
XF-818[g]	0.21	0.29	0.34	18.3	18.0	-	7.32	-	0.43	-	-	0.75	Bal	0.106 N, 0.007 P, 0.010 S

[a] 1983 Materials & Processing Databook, Metal Progress, Vol. 124, No. 1, p. 64.

[b] INCOLOY Alloy 800H is a registered trademark of Huntington Alloys, Inc. In all subsequent tables, figures, and in the text, the alloy is identified either fully or as 800H.

[c] Includes tantalum.

[d] Sandvik Lecture No. 56-10E, Paper presented at the Mi Con 78 Symposium, Houston, Texas, April 1978, Steel Research Center, Sandvik, Sandviken, Sweden.

[e] ASM Metals Handbook, Vol. 3, 9th Ed., p. 268.

[f] Composition supplied by NASA-Lewis Research Laboratory, Cleveland, Ohio.

[g] Climax Molybdenum Co., Research Laboratory, Ann Arbor, Michigan.

TABLE 2. HEAT TREATMENT, HARDNESS, AND GRAIN SIZE OF TESTED ALLOYS

Alloy	Heat Treatment	Average Hardness, HRA (HV)[a]	Average Grain Dia., μm
A-286	Solution annealed at 1149°C,[b,c] aged at 718°C for 16 h and air cooled.	51.9 (163)	108
800H	Solution annealed at 1149°C[b,c]	40.0 (108)	64
N-155	Solution annealed at 1177°C[b,c]	51.5 (161)	42
19-9DL	Solution annealed at 1204°C-10 min[c]	50.5 (156)	33
12RN72	Solution annealed at 1150°C-15 min[c]	39.7 (107)	56
CG-27	Solution annealed at 1150°C in vacuum for 10 min, furnace cooled to room temperature, aged at 790°C in vacuum for 16 h, cooled to 650°C, held for 4 h, and furnace cooled.	69.7 (378)	194
HS-31[d]	Simulative brazing cycle heat treatment, 1 h at 1150°C in 10^{-6} mm vacuum followed by furnace cooling	61.0 (243)	-
SA-F11[d]		62.1 (256)	-
CRM-6D[d]		61.6 (249)	-
XF-818[d]		52.1 (164)	-
CRM-6D[e]	Aged at 650°C-100 h	62.4 (260)	-
XF-818[e]	As-cast	50.5 (156)	-

[a]Vicker's hardness number (HV) converted from Rockwell hardness A scale (HRA).

[b]Solution annealing time 142 s/mm (1 hr/in.) thickness minimum.

[c]Rapidly cooled from solution temperature.

[d]Cast by United Stirling AB, Sweden. The molten alloy was fed in the mold from one end. Simulative braze cycle heat treatment by NASA-LeRC, Cleveland, Ohio.

[e]Cast by Climax Molybdenum Co., Ann Arbor, Michigan. The molten alloy was fed in the mold from the side.

TABLE 3. HIGH-PRESSURE (15 MPa) HYDROGEN CREEP-RUPTURE DATA

(1) Test No.	(2) Env.	(3) Alloy[a]	(4) Temp., °C	(5) Stress, MPa	(6) t_r, h	(7) Min Creep Rate, s^{-1}	(8) $t_{0.01}$, h	(9) t_{ter}, h	(10) El., %	(11) R.A., %
H03	HYD	CRM[b]	705	395	9.0	7.11E-07	1.0	5.0	5.6	19.6
H04	HYD	CRM	705	385	15.7	4.86E-07	0.9	8.0	6.0	12.2
H05	HYD	CRM	705	369	25.8	3.03E-07	4.0		7.8	17.6
H19	HYD	CRM	760	220	306	3.18E-08	17.2	233	7.0	22.6
H06	HYD	CRM	760	195	470+	1.04E-08	65.0	350	3.1+	2.1+
H08	HYD	CRM	760	196	749	7.16E-09	99.0	579	7.4	37.2
H07	HYD	CRM	815	162	111	5.21E-08	16.5	70.0	8.1	58.3
H20	HYD	CRM	815	160	238	1.94E-08	61.9	150	8.5	45.0
H10	HYD	CRM	815	151	842	4.40E-09	131	500	7.0	21.5
H09	HYD	CRM	870	116	383+	5.90E-09	7.5		1.6+	
H13	HYD	CRM[c]	760	252	3.7	5.21E-06	0.4	1.0	20.1	35.0
H14	HYD	CRM	760	130	357	6.54E-08	27.0	150	14.8	43.3
H18	HYD	CRM	760	117	742	3.35E-08	75.0	300	21.1	55.6
H15	HYD	CRM	815	105	273	9.56E-08	12.5	140	27.3	50.4
H16	HYD	CRM	815	100	504	3.77E-08	43.5	140	20.8	39.3
H17	HYD	CRM	815	87	1210	1.34E-08	125	330	24.7	39.2
H05	HYD	XF8[d]	705	396	6.4	7.46E-07	1.2	2.2	5.0	11.9
H03	HYD	XF8	705	395	15.0				6.0	6.2
H06	HYD	XF8	760	216	182	5.44E-08	27.5	47.0	10.4	36.6
H19	HYD	XF8	760	210	167	7.86E-08	23.5	80.0	8.5	24.7
H19	HYD	XF8	760	195	424	2.98E-08	44.4	150	10.7	23.9
H08	HYD	XF8	760	166	1492+	5.99E-09	198	750	6.6+	11.4+
H01	HYD	XF8	815	176	56.7	1.17E-07	7.8	41.0	10.3	30.6
H07	HYD	XF8	815	133	275	4.00E-08	41.8	75.0	14.2	57.3
H12	HYD	XF8	815	131	200	5.51E-08	14.0	80.0	10.1	47.3
H20	HYD	XF8	815	125	387	3.94E-08		200	11.0	47.8
H10	HYD	XF8	815	118	1091	8.78E-09	200	200	16.2	21.1
H09	HYD	XF8	870	93.6	221	5.90E-08	38.0		15.4	47.2
H13	HYD	XF8[c]	760	192	258	6.32E-08	35.0	55.0	11.6	20.7
H14	HYD	XF8	760	185	325	5.72E-08	36.0	100	14.7	21.1
H18	HYD	XF8	760	158	1303	1.07E-08	90.6	620	12.9	22.6
H15	HYD	XF8	815	135	141	1.59E-07	10.2	47.0	19.7	40.6
H16	HYD	XF8	815	120	460	4.41E-08	25.0	147	19.0	34.7
H17	HYD	XF8	815	106	1082	1.46E-08	105	375	15.6	33.3
H13	HYD	HS3[c]	760	242	193	2.04E-07	3.0	125	23.2	42.6
H14	HYD	HS3	760	235	245	1.73E-07	2.6	165	28.1	51.0
H18	HYD	HS3	760	220	895	3.02E-08	5.4	556	20.7	48.0
H15	HYD	HS3	815	180	209	1.13E-07	2.6	107	18.3	40.3
H16	HYD	HS3	815	165	551	3.71E-08	3.9	292	17.9	43.9
H17	HYD	HS3	815	157	500	3.87E-08	4.0	280	13.5	30.6
H13	HYD	SAF[c]	760	257	336	2.33E-08	62.0	150	6.1	8.4
H14	HYD	SAF	760	230	605	1.11E-08	113	210	5.0	6.3
H18	HYD	SAF	760	220	1023	7.57E-09	156	324	6.3	7.7
H15	HYD	SAF	815	180	198	3.63E-08	35.0	76.0	8.6	8.3
H16	HYD	SAF	815	160	364	2.50E-08	61.0	127	7.0	12.0
H17	HYD	SAF	815	145	886	9.12E-09	190	300	7.1	6.3

TABLE 3 (cont.)

(1) Test No.	(2) Env.	(3) Alloy[a]	(4) Temp., °C	(5) Stress, MPa	(6) t_r, h	(7) Min Creep Rate, s^{-1}	(8) $t_{0.01}$, h	(9) t_{ter}, h	(10) El., %
H04	HYD	A28	705	446	0.5	1.50E-05			14.0
H03	HYD	A28	705	365	15.0+	7.76E-08	2.5		2.0+
H05	HYD	A28	705	359	26.4	1.32E-07	6.9	17.0	7.0
H02	HYD	A28	760	254	45.5	1.31E-08	36.2	21.0	4.7
H06	HYD	A28	760	160	437	4.60E-10	270	80.0	9.8
H08	HYD	A28	760	131	1202	7.25E-10	570	130	8.1
H01	HYD	A28	815	138	27.7	1.12E-09	17.0	12.5	7.9
H07	HYD	A28	815	70.2	571+	9.17E-09	195	50.0	2.7+
H20	HYD	A28	815	70.0	533	1.46E-10	163	20.0	8.1
H10	HYD	A28	815	55.6	1331+	1.95E-09	25.0	1100	4.8+
H09	HYD	A28	870	24.7	383+	1.17E-07	3.5		21.0+
H04	HYD	IN8	705	230	3.8	8.00E-06	0.1	2.0	30.0
H03	HYD	IN8	705	193	14.3	3.40E-06	0.2	9.4	32.0
H02	HYD	IN8	760	124	24.8	1.76E-06	0.3	17.0	26.3
H19	HYD	IN8	760	95.0	96.7	2.04E-07	9.5	57.5	13.8
H06	HYD	IN8	760	78.0	470+	6.04E-08	23.0	100	13.8+
H08	HYD	IN8	760	74.9	1391	2.82E-08	54.0	752	29.1
H01	HYD	IN8	815	107	2.7	1.22E-07	0.2	1.0	19.2
H07	HYD	IN8	815	62.5	107	3.92E-07	0.5		21.4
H12	HYD	IN8	815	60.7	240	1.27E-07	9.7	175	16.4
H10	HYD	IN8	815	54.8	1331+	2.31E-08	11.0	1000	16.3+
H09	HYD	IN8	870	41.0	383+	1.32E-07	10.0		22.8+
H04	HYD	N15	705	319	11.2	1.19E-06	0.3	8.0	17.0
H05	HYD	N15	705	283	39.0	5.24E-07	0.7	17.0	24.0
H02	HYD	N15	760	193	30.4	9.28E-07	0.7	15.0	35.0
H06	HYD	N15	760	138	460		210		30.0
H08	HYD	N15	760	118	1193	1.18E-08	41.0	550	25.8
H01	HYD	N15	815	124	46.2+	8.81E-07	1.4	29.0	24.0+
H12	HYD	N15	815	107	146	2.09E-07	4.7	30.0	35.3
H07	HYD	N15	815	97.0	349	8.15E-08	19.0	100	33.9
H12	HYD	N15	815	89.1	573	3.15E-08	25.0	175	24.6
H10	HYD	N15	815	80.0	1331+	5.50E-09	300	500	6.1+
H04	HYD	199	705	306	1.7	1.60E-06			8.0
H05	HYD	199	705	237	28.4	2.40E-07	4.7	8.0	15.0
H02	HYD	199	760	163	20.7	4.53E-07	1.6	2.0	28.5
H06	HYD	199	760	109	304	4.07E-08	29.4	125	9.3
H08	HYD	199	760	88.5	1195	4.71E-09	85.0	579	7.9
H01	HYD	199	815	93.4	32.1	2.09E-07	7.8	12.5	9.4
H07	HYD	199	815	72.7	342	3.13E-08	31.1	200	9.3
H12	HYD	199	815	71.3	508	1.86E-08	50.0	240	9.0
H20	HYD	199	815	68.0	439	2.64E-08	92.5	229	11.7
H10	HYD	199	815	57.8	1331+	1.10E-09	1000	1080	2.9+
H13	HYD	12R	760	97	450+		7.0	350	3.8+
H14	HYD	12R	760	90	247	1.14E-07	32.5	195	18.4
H19	HYD	12R	760	85	456+	2.64E-08	71.7	81.7	15.4+
H18	HYD	12R	760	75	891	1.75E-08	131	200	21.1
H15	HYD	12R	815	60	350+	5.26E-08	33.5	129	7.8+
H16	HYD	12R	815	57	650	2.03E-08	104	67.6	24.7
H17	HYD	12R	815	50	1323	8.02E-09	225	80.0	20.9
H19	HYD	CG2	760	275	277	3.96E-09	275	85.5	2.6
H18	HYD	CG2	760	250	599			135	
H13	HYD	CG2	760	198	450+		5.0		4.4+
H15	HYD	CG2	815	190	189	2.59E-08	62.5	62.0	5.77
H16	HYD	CG2	815	165	313	2.23E-08	80.0	104	7.25
H20	HYD	CG2	815	145	499	1.36E-08	71.6	475	3.8
H17	HYD	CG2	815	140	819	8.64E-09	280	420	6.46

TABLE 3 (concl.)

Notes

[a]Alloy code:

CRM	=	CRM-6D castings	
XF8	=	XF-818 castings	
HS3	=	HS31 castings	
SAF	=	SA-F11 castings	
A28	=	A-286	
IN8	=	INCOLOY Alloy 800H	
N15	=	N-155	
199	=	19-9DL	
12R	=	12RN72	
CG2	=	CG-27	

[b]Aged (Climax Molybdenum Co.).

[c]Braze-cycled (United Stirling AB, Sweden).

[d]As-cast (Climax Molybdenum Co.).

TABLE 4. STATISTICAL DATA ON TEMPERATURE-COMPENSATED ANALYSIS OF CAST ALLOYS CRM-6D AND XF-818 IN AIR AND 15 MPa H_2

Alloy[a]	Environment	No. of Data	R^2	ln k	n	Q, kJ/mol
			Rupture Life (t_r)			
CRM-6D	Air	26	0.843	0.829	-9.12	461
	15 MPa H_2	8	0.962	-6.35	-13.3	720
XF-818	Air	14	0.991	-13.2	-7.52	505
	15 MPa H_2	10	0.894	-3.51	-7.93	436
			Time to Reach 1% Creep Strain ($t_{0.01}$)			
CRM-6D	Air	29	0.973	5.59	-10.6	468
	15 MPa H_2	9	0.938	3.48	-11.1	512
XF-818	Air	14	0.988	-20.8	-6.86	522
	15 MPa H_2	9	0.833	-10.1	-8.70	512
			Minimum Creep Rate ($\dot{\varepsilon}_m$)			
CRM-6D	Air	28	0.947	-16.9	11.8	-551
	15 MPa H_2	9	0.948	-14.2	11.8	-574
XF-818	Air	14	0.990	6.85	7.47	-545
	15 MPa H_2	10	0.825	-4.51	7.55	-450

[a]Alloys cast by Climax Molybdenum Co., Ann Arbor, Michigan. CRM-6D and XF-818 were tested in aged and as-cast conditions, respectively.

TABLE 5. STATISTICAL DATA ON TEMPERATURE-COMPENSATED ANALYSIS OF BRAZE-CYCLED CAST ALLOYS HS-31, SA-F11, CRM-6D, AND XF-818 IN 15 MPa H_2

Alloy[a]	No. of Data	R^2	ln k	n	Q, kJ/mol
		Rupture Life (t_r)			
HS-31	6	0.769	-2.91	-10.2	551
SA-F11	6	0.972	-15.3	-6.85	508
CRM-6D	6	0.998	7.89	-6.94	273
XF-818	6	0.993	-18.9	-8.43	591
		Time to Reach 1% Creep Strain ($t_{0.01}$)			
HS-31	6	0.710	-3.83	-4.54	256
SA-F11	6	0.942	-16.2	-7.06	510
CRM-6D	6	0.968	1.07	-6.90	309
XF-818	6	0.919	-26.1	-7.76	603
		Minimum Creep Rate ($\dot{\varepsilon}_m$)			
HS-31	6	0.793	-15.1	12.6	-600
SA-F11	6	0.949	4.68	6.58	-505
CRM-6D	6	0.987	-21.6	6.76	-239
XF-818	6	0.991	14.8	9.74	-708

[a]Alloys cast and supplied by United Stirling AB, Sweden. Simulative braze cycle heat treatment was given by NASA-LeRC, Cleveland, Ohio.

TABLE 6. STATISTICAL DATA ON TEMPERATURE-COMPENSATED ANALYSIS OF WROUGHT ALLOYS A-286, INCOLOY ALLOY 800H, N-155, 19-9DL, 12RN72, AND CG-27

Alloy	Environment	No. of Data	R^2	ln k	n	Q, kJ/mol
			Rupture Life (t_r)			
A-286	Air	15	0.858	-38.4	-3.82	544
	15 MPa H_2	6	0.800	-18.2	-4.81	413
800H	Air	23	0.941	-10.8	-6.79	406
	15 MPa H_2	8	0.977	-20.7	-7.92	530
N-155	Air	19	0.976	-13.9	-6.28	435
	15 MPa H_2	8	0.994	-13.1	-7.85	496
19-9DL	Air	19	0.975	-17.6	-6.44	461
	15 MPa H_2	9	0.975	-18.5	-7.84	523
12RN72	15 MPa H_2	4	0.990	-7.09	-6.49	359
CG-27	15 MPa H_2	6	0.917	-14.9	-4.67	403
			Time to Reach 1% Creep Strain ($t_{0.01}$)			
A-286	Air	12	0.946	-39.4	-3.54	535
	15 MPa H_2	8	0.620	-0.429	-3.67	199
800H	Air	14	0.886	-17.0	-8.86	515
	15 MPa H_2	8	0.962	-29.5	-9.42	635
N-155	Air	17	0.988	-17.4	-7.04	467
	15 MPa H_2	9	0.957	-16.6	-9.59	573
19-9DL	Air	16	0.955	-26.8	-7.38	559
	15 MPa H_2	9	0.897	-16.2	-7.51	473
12RN72	15 MPa H_2	7	0.898	-24.0	-10.5	639
CG-27	15 MPa H_2	4	0.985	70.7	-4.98	-367
			Minimun Creep Rate ($\dot{\varepsilon}_m$)			
A-286	Air	9	0.767	35.9	3.09	-613
	15 MPa H_2	7	0.916	-43.0	4.09	18.9
800H	Air	22	0.849	-0.803	6.49	-384
	15 MPa H_2	8	0.981	-0.279	7.63	-428
N-155	Air	17	0.980	8.85	7.39	-527
	15 MPa H_2	9	0.979	15.1	9.83	-693
19-9DL	Air	19	0.948	15.2	7.38	-573
	15 MPa H_2	10	0.941	11.8	8.12	-581
12RN72	15 MPa H_2	6	0.858	4.45	9.41	-542
CG-27	15 MPa H_2	5	0.951	25.8	3.31	-548

TABLE 7. RANGE OF VALUES OF STRESS EXPONENT (n) AND APPARENT ACTIVATION ENERGY (Q)

Alloy	n		Q, kJ/mol	
	Air	15 MPa H_2	Air	15 MPa H_2
		Rupture Life		
Cast Alloys				
HS-31[a]		-10.2		551
SA-F11[a]		-6.85		508
CRM-6D[b]	-9.12	-13.3	461	720
CRM-6D[b]		-6.94		273
XF-818[b]	-7.52	-7.93	505	436
XF-818[b]		-8.43		591
Wrought Alloys				
CG-27		-4.67		403
12RN72		-6.49		359
19-9DL	-6.44	-7.84	461	523
N-155	-6.28	-7.85	435	496
800H	-6.79	-7.92	406	530
A-286	-3.82	-4.81	544	413
		Minimum Creep Rate		
Cast Alloys				
HS-31[a]		12.6		-600
SA-F11[a]		6.58		-505
CRM-6D[b]	11.8	11.8	-551	-574
CRM-6D[a]		6.76		-239
XF-818[b]	7.47	7.55	-545	-450
XF-818[a]		9.74		-708
Wrought Alloys				
CG-27		3.31		-548
12RN72		9.41		-542
19-9DL	7.38	8.12	-573	-581
N-155	7.39	9.83	-527	-693
800H	7.63	6.49	-384	-428
A-286	3.09	1.40	-613	-518

[a]United Stirling AB castings, braze-cycle treated.

[b]Climax Molybdenum Co. castings, CRM-6D (aged), XF-818 (as-cast).

TABLE 8. PREDICTED STRESSES FOR 3500-HOUR RUPTURE LIFE IN AIR AND 15 MPa HYDROGEN

Alloy	Environment	Temp., °C (°F)	Estimated Stress, MPa (ksi) Mean	90% Conf. Limits Low	High
A-286	Air	775 (1427)	63.4 (9.20)	48.3	83.2
		870 (1600)	16.3 (2.36)	12.4	21.4
	15 MPa H_2	775 (1427)	78.4 (11.4)	50.8	121
		870 (1600)	34.6 (5.02)	22.4	53.4
800H	Air	775 (1427)	58.5 (8.48)	52.4	65.3
		870 (1600)	33.1 (4.80)	29.6	36.9
	15 MPa H_2	775 (1427)	56.6 (8.21)	51.4	62.1
		870 (1600)	29.9 (4.34)	27.2	32.8
N-155	Air	755 (1427)	84.6 (12.3)	78.0	91.8
		870 (1600)	43.7 (6.34)	40.3	47.4
	15 MPa H_2	775 (1427)	93.7 (13.6)	90.2	97.4
		870 (1600)	51.3 (7.44)	49.4	53.3
19-9DL	Air	775 (1427)	67.2 (9.75)	61.3	73.8
		870 (1600)	34.0 (4.93)	31.0	37.3
	15 MPa H_2	775 (1427)	71.0 (10.3)	64.6	78.0
		870 (1600)	37.6 (5.45)	34.2	41.3
12RN72	15 MPa H_2	775 (1427)	55.0 (7.98)	52.0	58.1
		870 (1600)	32.4 (4.70)	30.7	34.2
CG-27	15 MPa H_2	775 (1427)	143 (20.7)	131	157
		870 (1600)	62.9 (9.12)	57.3	68.9
CRM-6D[a]	Air	775 (1472)	147 (21.3)	130	167
		870 (1600)	91.1 (13.2)	80.5	103
CRM-6D[a]	15 MPa H_2	775 (1427)	164 (23.8)	154	174
		870 (1600)	97.9 (14.2)	92.3	104
CRM-6D[b]	15 MPa H_2	775 (1427)	87.7 (12.7)	84.7	90.9
		870 (1600)	60.3 (8.75)	58.2	62.5
XF-818[a]	Air	775 (1427)	130 (18.9)	124	136
		870 (1600)	68.4 (9.92)	65.3	71.6
XF-818[a]	15 MPa H_2	775 (1427)	126 (18.3)	110	144
		870 (1600)	74.5 (10.8)	64.9	85.4
XF-818[b]	15 MPa H_2	775 (1427)	125 (18.1)	122	128
		870 (1600)	64.0 (9.28)	62.5	65.6

TABLE 8 (cont.)

Alloy	Environment	Temp., °C (°F)	Estimated Stress MPa (ksi) Mean	90% Conf. Limits Low	90% Conf. Limits High
HS-31[b]	15 MPa H_2	775 (1427)	169 (24.5)	156	183
		870 (1600)	101 (14.6)	93.0	109
SA-F11[b]	15 MPa H_2	775 (1427)	160 (23.2)	154	167
		870 (1600)	79.1 (11.5)	75.8	82.5

[a]Climax Molybdenum Co.; castings, CRM-6D (aged), XF-818 (as-cast).

[b]United Stirling AB, Sweden; castings, braze-cycle treated.

TABLE 9. PREDICTED STRESS TO 1 PERCENT CREEP IN 3500 HOURS IN AIR AND 15 MPa H_2

Alloy	Environment	Temp., °C (°F)	Estimated Stress, MPa (ksi) Mean	90% Conf. Limits Low	90% Conf. Limits High
A-286	Air	775 (1427)	49.8 (7.22)	41.2	60.1
		870 (1600)	11.8 (1.71)	9.74	14.2
	15 MPa H_2	775 (1427)	48.4 (7.02)	22.9	102
		870 (1600)	28.8 (4.18)	13.7	60.9
800H	Air	775 (1427)	46.4 (6.73)	40.8	52.7
		870 (1600)	26.6 (3.86)	23.4	30.3
	15 MPa H_2	775 (1427)	37.7 (5.47)	31.9	44.5
		870 (1600)	21.9 (3.18)	18.5	25.9
N-155	Air	775 (1427)	53.7 (7.79)	50.7	56.9
		870 (1600)	28.5 (4.13)	26.9	30.2
	15 MPa H_2	775 (1427)	71.5 (10.4)	64.1	79.7
		870 (1600)	40.5 (5.87)	36.3	45.1
19-9DL	Air	775 (1427)	52.6 (7.63)	46.7	59.5
		870 (1600)	25.5 (3.70)	22.6	28.9
	15 MPa H_2	775 (1427)	54.0 (7.83)	45.2	64.5
		870 (1600)	29.6 (4.29)	24.8	35.4
12RN72	15 MPa H_2	775 (1427)	50.7 (7.35)	46.5	55.3
		870 (1600)	28.4 (4.12)	26.0	31.0
CG-27[a]	15 MPa H_2	775 (1427)	60.1 (8.72)	48.6	74.4
		870 (1600)	121 (17.6)	98.1	150
CRM-6D[b]	Air	775 (1427)	127 (18.4)	121	134
		870 (1600)	83.4 (12.1)	79.2	87.7
CRM-6D[b]	15 MPa H_2	775 (1427)	130 (18.9)	118	143
		870 (1600)	83.7 (12.1)	76.2	91.9
CRM-6D[c]	15 MPa H_2	775 (1427)	61.5 (8.92)	53.0	71.3
		870 (1600)	40.1 (5.82)	34.6	46.5
XF-818[b]	Air	775 (1427)	90.8 (13.2)	85.6	96.3
		870 (1600)	43.9 (6.37)	41.4	46.6
XF-818[b]	15 MPa H_2	775 (1427)	105 (15.2)	88.9	123
		870 (1600)	59.7 (8.66)	50.7	70.3
XF-818[c]	15 MPa H_2	775 (1427)	90.0 (13.1)	82.5	98.1
		870 (1600)	42.9 (6.22)	39.3	46.8
HS-31[c]	15 MPa H_2	775 (1427)	46.2 (6.70)	42.0	50.7
		870 (1600)	27.0 (3.92)	24.5	29.6
SA-F11[c]	15 MPa H_2	775 (1427)	126 (18.3)	119	134
		870 (1600)	63.5 (7.97)	59.7	67.4

[a]CG-27 data revealed an apparent anomaly, mentioned earlier.

[b]Climax Molybdenum Co.; castings, CRM-6D (aged), XF-818 (as-cast).

[c]United Stirling AB, Sweden; castings, braze-cycle treated.

TABLE 10. ELONGATION DATA

Environment	Temp., °C	Stress Range, MPa	Elongation Range, %
		Alloy A-286	
Air	650	441, 483	8.4, 11.4
Air	705	179-379	3.4-21.0
15 MPa H_2	705	359, 446	7.0, 14.0
Air	760	124-345	8.7-26.3
15 MPa H_2	760	131-254	4.7-9.8
Air	815	55-138	10.7-44.6
15 MPa H_2	815	70, 138	12.5, 20.0
Air	870	21-55	29.8-87.2
15 MPa H_2	870	24.7	21.0[a]
Air	925	17-28	38.7-58.4
		INCOLOY Alloy 800H	
Air	650	207-276	15.0-32.2
Air	705	110-186	19.6-36.8
15 MPa H_2	705	193-230	2.0-9.4
Air	760	70-152	28.1-53.0
15 MPa H_2	760	74.9-124	13.8-29.1
Air	815	45-110	18.1-59.6
15 MPa H_2	815	54.8-62.5	16.3[a]-21.4
Air	870	26-76	15.9-32.2
15 MPa H_2	870	41.0	22.8[a]
Air	925	31-48	19.7-24.0
		N-155	
Air	650	276-414	19.9-26.2
Air	705	159-276	28.3-46.0
15 MPa H_2	705	283, 319	17.0, 24.0
Air	760	97-241	18.0-51.5
15 MPa H_2	760	118-193	25.8-35.0
Air	815	63-165	12.1-58.3
15 MPa H_2	815	80-124	6.1[a]-35.3
Air	870	47-110	26.3-65.0
Air	925	41-69	27.7-43.4
		19-9DL	
Air	650	276-414	10.1-18.8
Air	705	131-276	12.1-24.2
15 MPa H_2	705	237, 306	8.0, 15.0
Air	760	86-193	12.1-37.4
15 MPa H_2	760	88.5-163	7.9-28.5
Air	815	59-138	10.1-44.8
15 MPa H_2	815	68-93.4	9.0-11.7
Air	870	33-103	20.8-61.6
	925	35-69	27.5-47.6

TABLE 10 (cont.)

Environment	Temp., °C	Stress Range, MPa	Elongation Range, %
		12RN72	
15 MPa H_2	760	75, 90	18.4, 21.1
15 MPa H_2	815	50, 57	20.9, 24.7
		CG-27	
15 MPa H_2	760	275	2.6
15 MPa H_2	815	140-190	6.5-7.3
		CRM-6D[b]	
Air	650	379, 393	4.2, 5.6
Air	705	276-345	7.8-8.4
15 MPa H_2	705	369-395	5.6-7.8
Air	760	193-290	7.7-10.7
15 MPa H_2	760	196, 220	7.0, 7.4
Air	815	131-241	4.6-13.9
15 Mpa H_2	815	151-162	7.0-8.5
Air	870	97-172	2.8-21.7
15 MPa H_2	870	116	1.6[a]
Air	925	90-117	5.5-12.5
		CRM-6D[c]	
15 MPa H_2	760	117-252	14.8-21.1
15 MPa H_2	815	87-105	20.8-27.3
		XF-818[b]	
Air	650	393, 414	7.5, 8.0
Air	705	283-414	6.7-10.1
15 MPa H_2	705	395, 396	5.0, 6.0
Air	760	207-331	8.2-13.6
15 MPa H_2	760	195-216	8.5-10.7
Air	815	103-241	14.1-23.8
15 MPa H_2	815	118-176	10.1-16.2
Air	870	63-172	12.9-20.6
15 MPa H_2	870	93.6	15.4
Air	925	55-103	18.4-25.2
		XF-818[c]	
15 MPa H_2	760	158-192	11.6-14.7
15 MPa H_2	815	106-135	15.6-19.7

TABLE 10 (cont.)

Environment	Temp., °C	Stress Range, MPa	Elongation Range, %
		HS-31[c]	
15 MPa H_2	760	220-242	20.7-28.1
15 MPa H_2	815	157-180	13.5-18.3
		SA-F11[c]	
15 MPa H_2	760	220-257	5.0-6.3
15 MPa H_2	815	145-180	7.0-8.6

[a]Tests discontinued without failure.

[b]Climax Molybdenum Co.; castings, CRM-6D (aged), XF-818 (as-cast).

[c]United Stirling AB, Sweden; castings, braze-cycle treated.

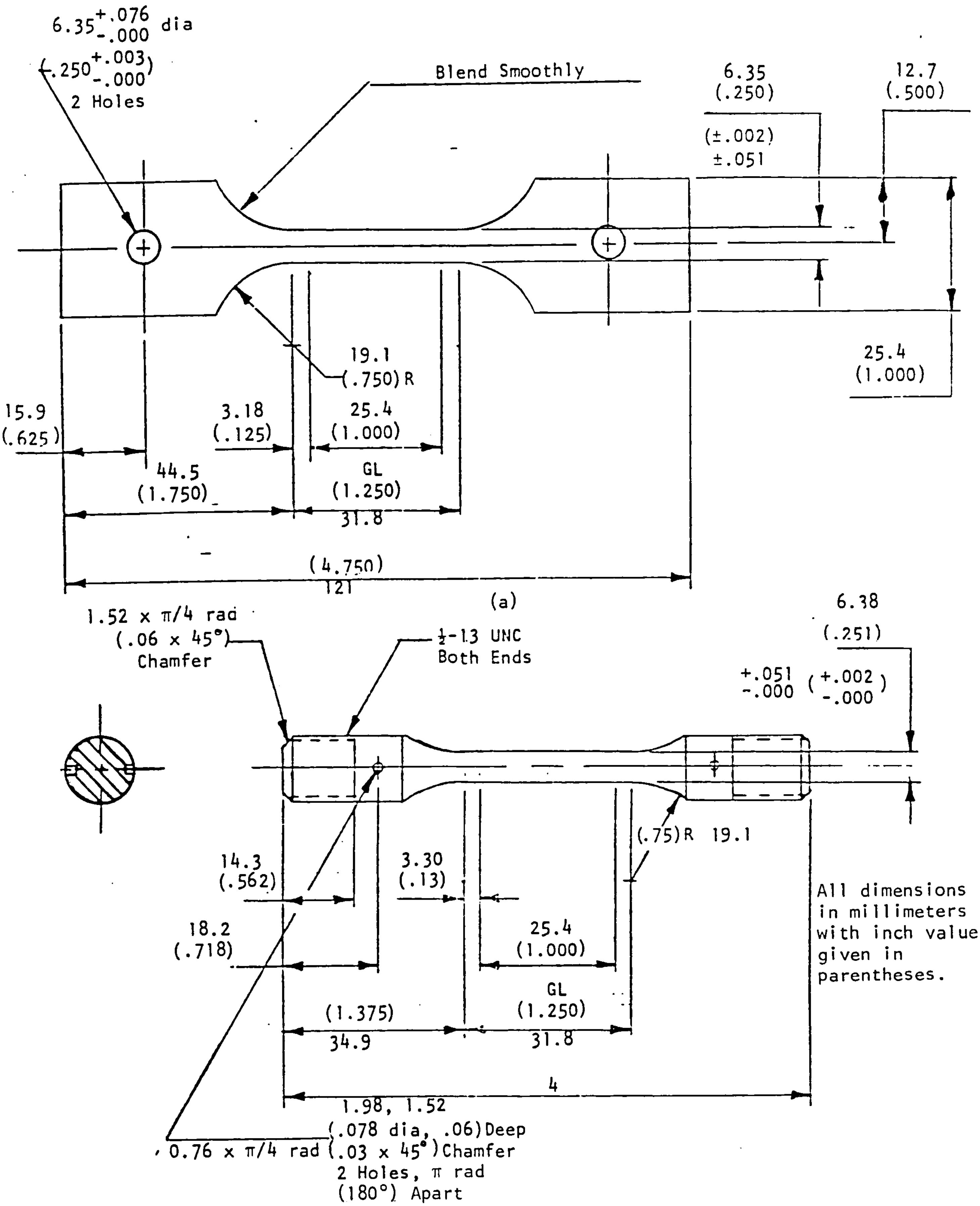

Figure 1. Creep-rupture specimen design. (a) Wrought (sheet), (b) cast.

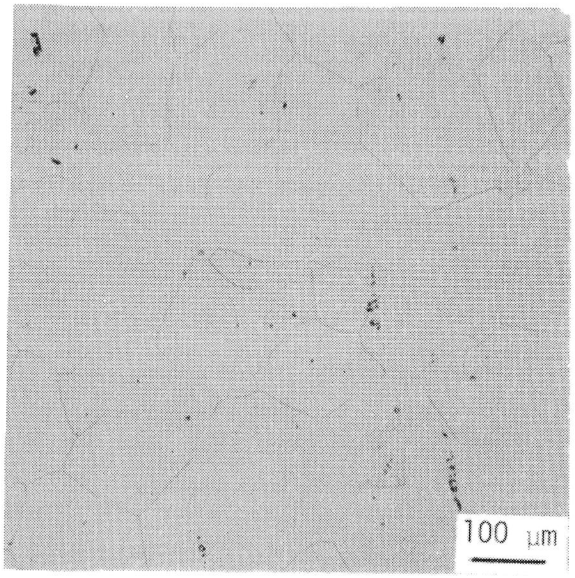

Neg. No. 52209

(a)

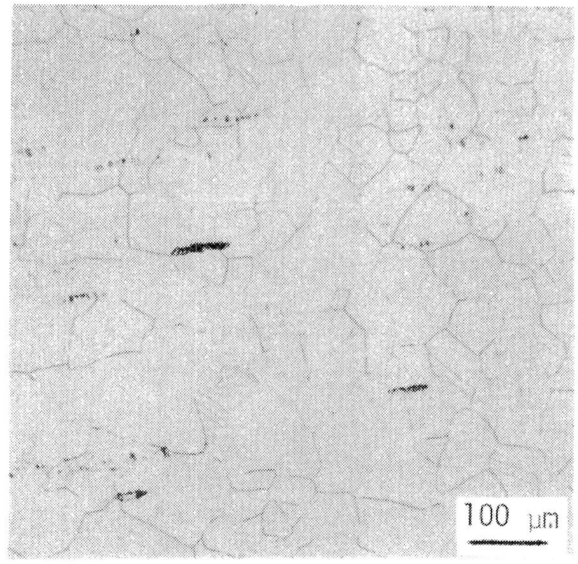

Neg. No. 52207

(b)

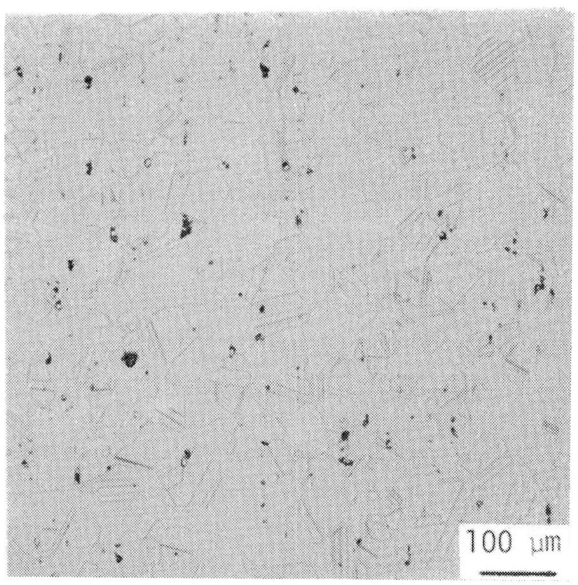

Neg. No. 52208

(c)

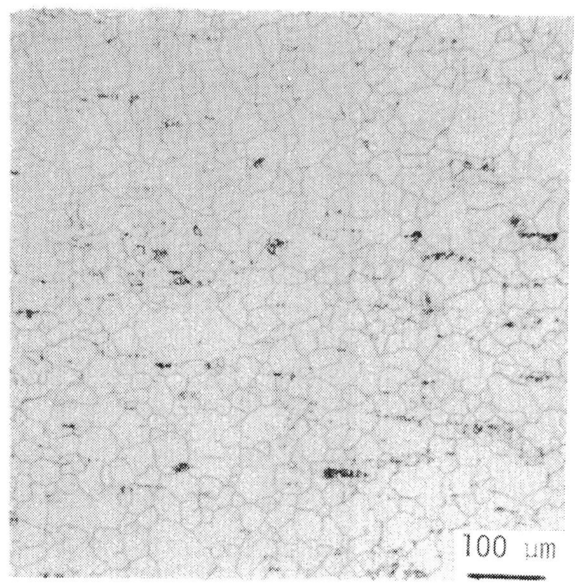

Neg. No. 52206

(d)

Figure 2. Microstructures of wrought alloys. (a) A-286, (b) 800H, (c) N-155, (d) 19-9DL, (e) 12RN72, (f) CG-27. Etchant: 10% oxalic acid, electrolytic.

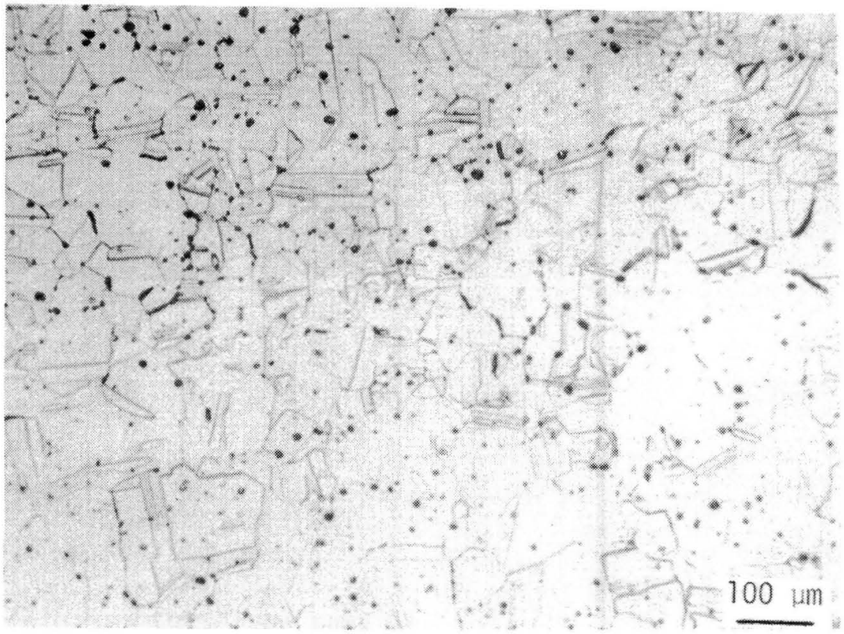

Neg. No. 56112

(e)

Neg. No. 56113

(f)

Figure 2 (cont.)

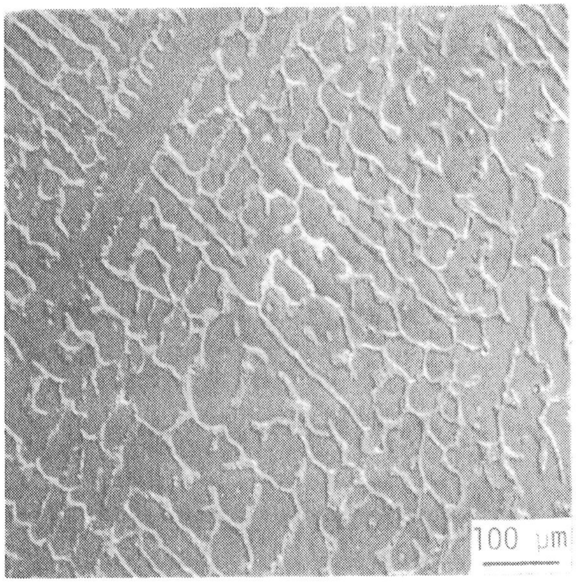

SEM No. 5486

(a) CRM-6D (Climax), aged

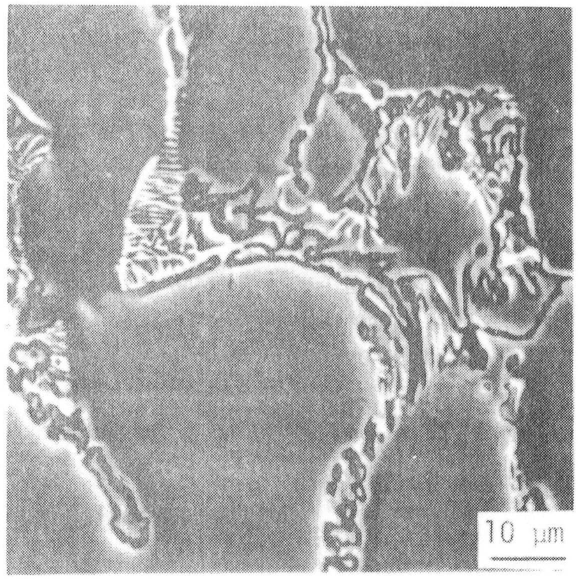

SEM No. 5488

(b) CRM-6D (Climax), aged

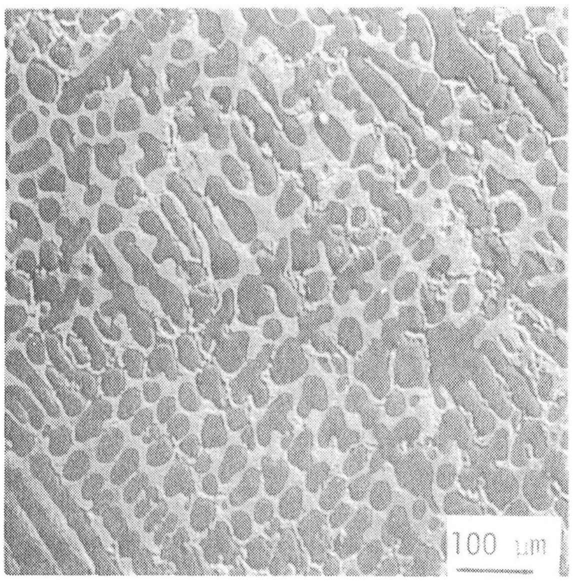

SEM No. 5489

(c) XF-818 (Climax), as-cast

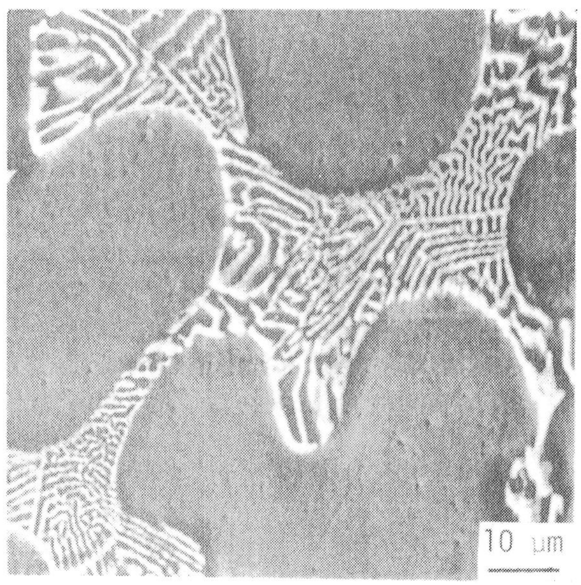

SEM No. 5491

(d) XF-818 (Climax), as-cast

Figure 3. Microstructures of cast alloys. (a-d) Climax heat, side gating, (e-l) United Stirling AB heat, end gating. Etchant: 10% oxalic acid, electrolytic.

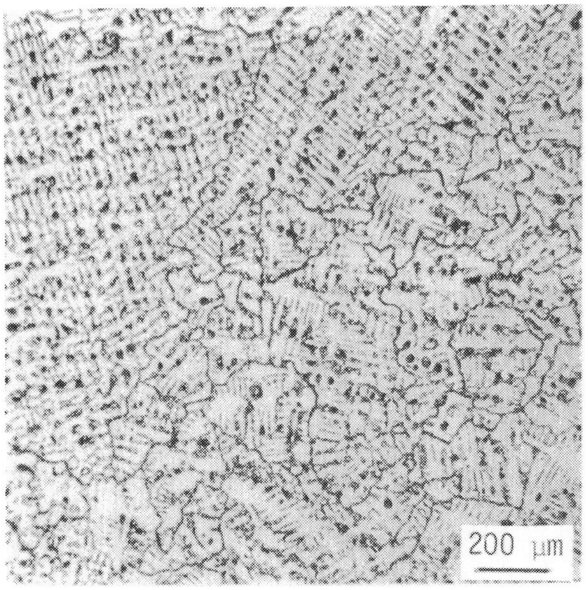

Neg. No. 54966

(e) XF-818 (US/AB), braze-cycled

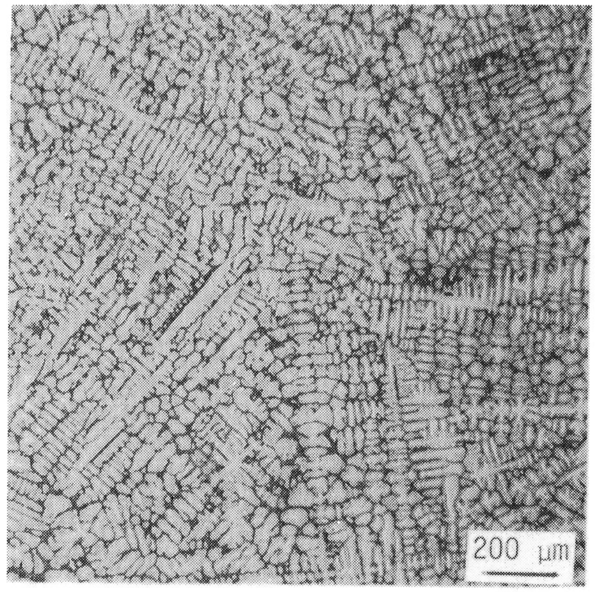

Neg. No. 45968

(f) CRM-6D (US/AB), braze-cycled

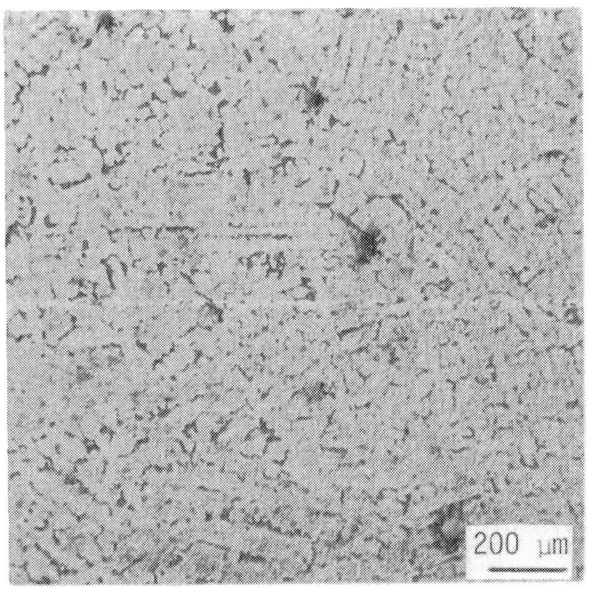

Neg. No. 54961

(g) HS-31 (US/AB), braze-cycled

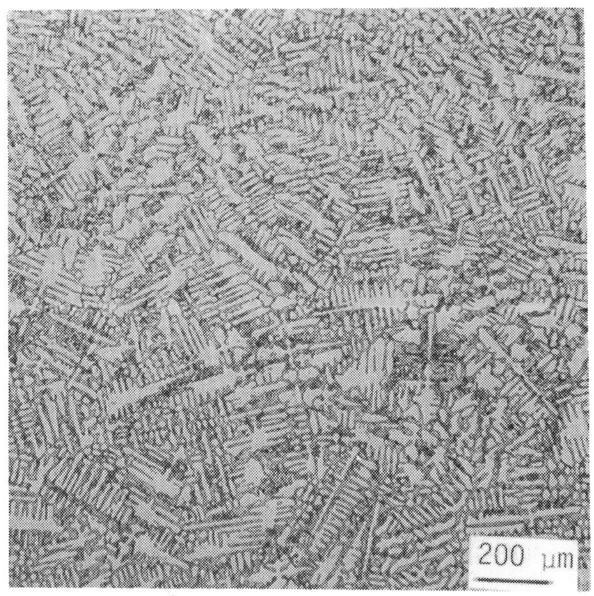

Neg. No. 54970

(h) SA-F11 (US/AB), braze-cycled

Figure 3 (cont.)

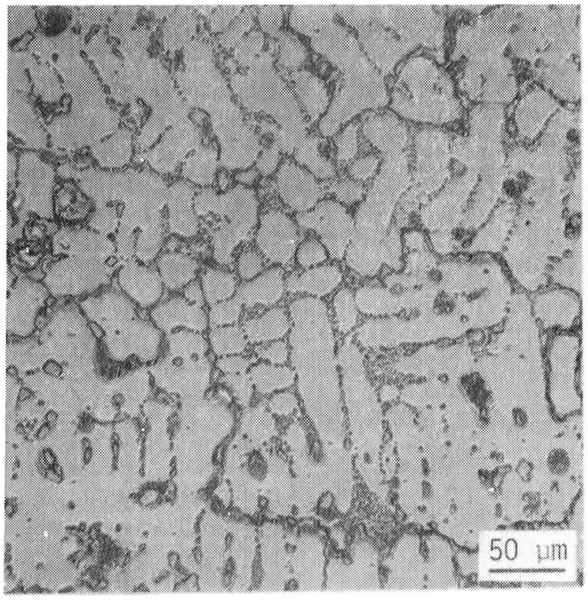

Neg. No. 54967

(i) XF-818 (US/AB), braze-cycled

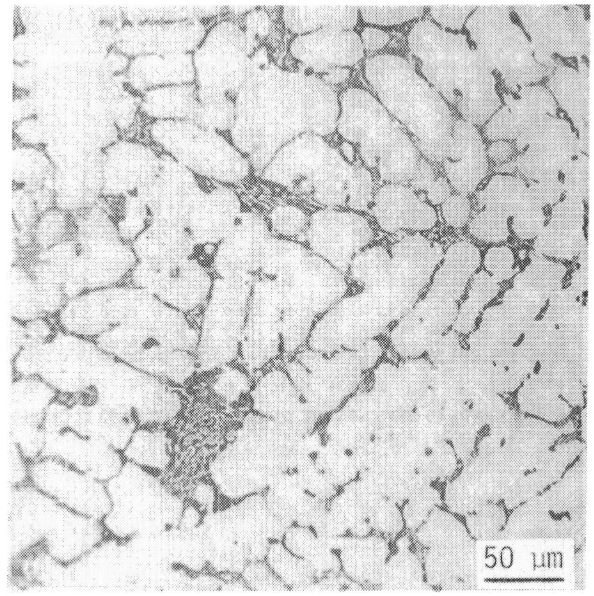

Neg. No. 54969

(j) CRM-6D (US/AB), braze-cycled

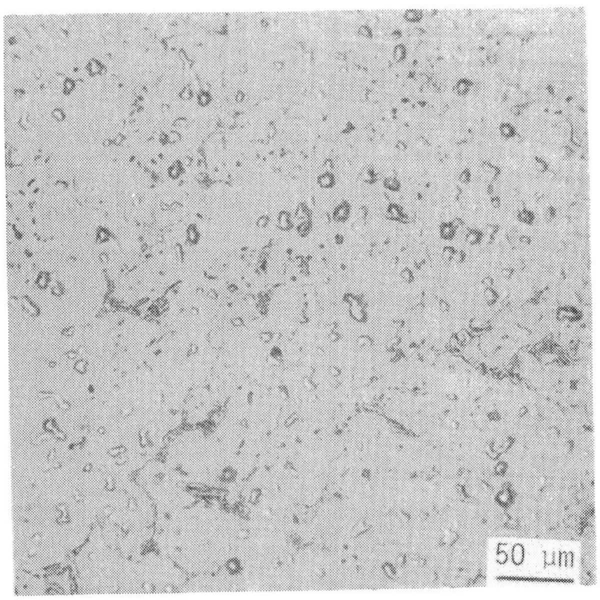

Neg. No. 54962

(k) HS-31 (US/AB), braze-cycled

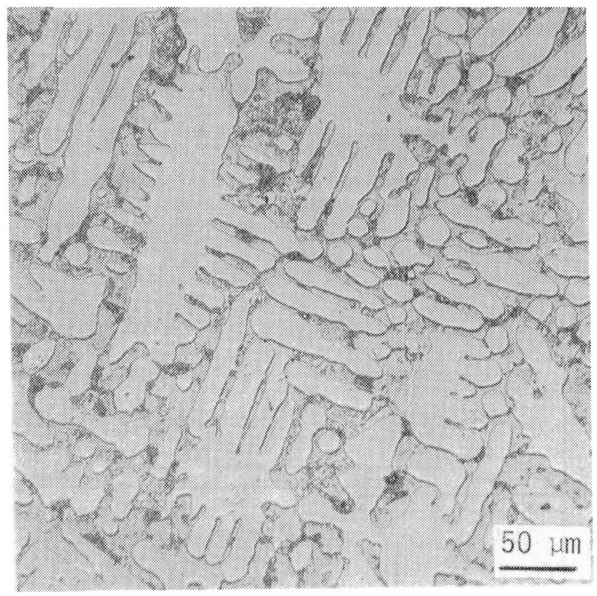

Neg. No. 54971

(l) SA-F11 (US/AB), braze-cycled

Figure 3 (cont.)

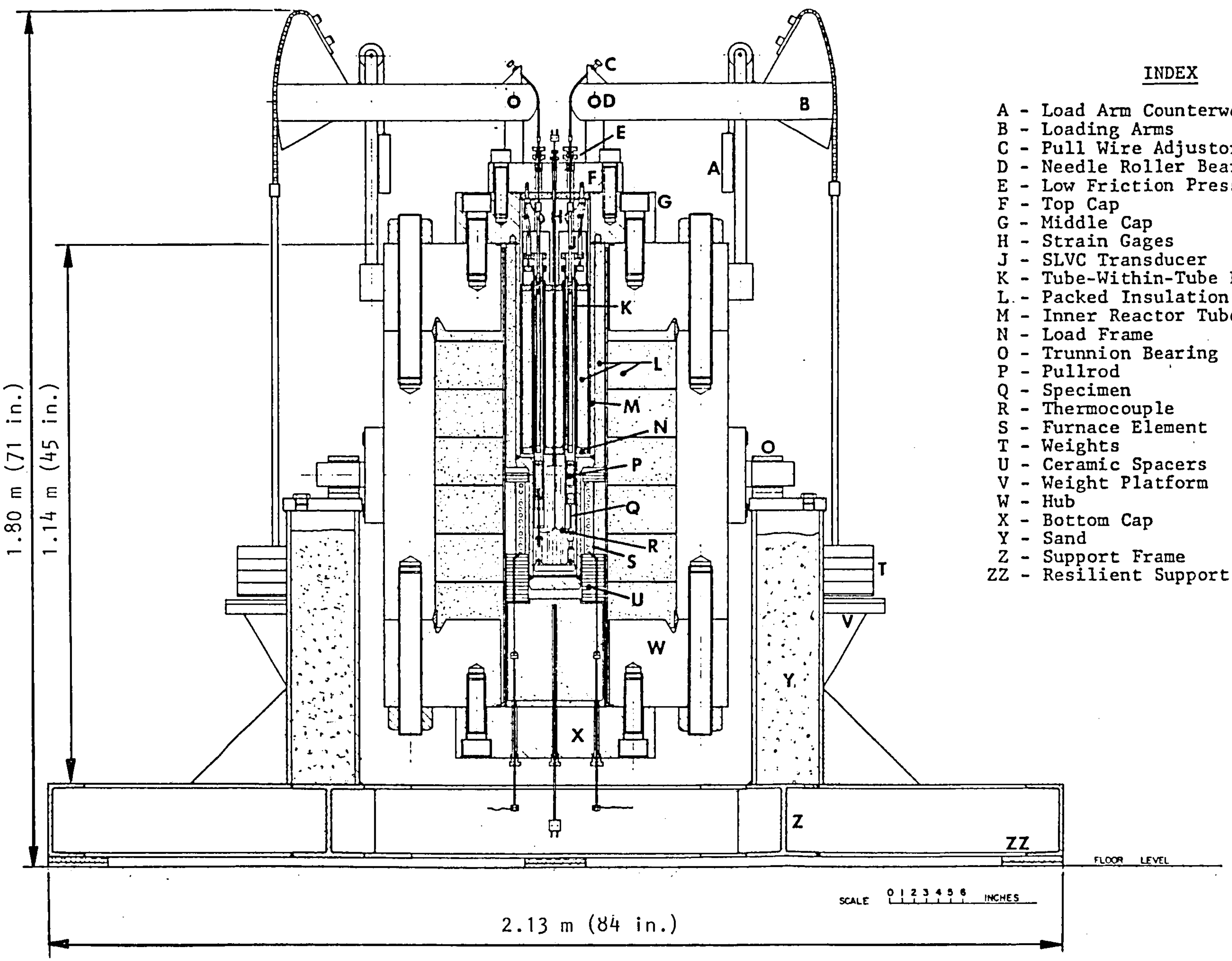

INDEX

A - Load Arm Counterweight
B - Loading Arms
C - Pull Wire Adjustors
D - Needle Roller Bearings
E - Low Friction Pressure Seal
F - Top Cap
G - Middle Cap
H - Strain Gages
J - SLVC Transducer
K - Tube-Within-Tube Extensometer
L - Packed Insulation
M - Inner Reactor Tube
N - Load Frame
O - Trunnion Bearing
P - Pullrod
Q - Specimen
R - Thermocouple
S - Furnace Element
T - Weights
U - Ceramic Spacers
V - Weight Platform
W - Hub
X - Bottom Cap
Y - Sand
Z - Support Frame
ZZ - Resilient Support Pads

Figure 4. High-pressure multispecimen test facility for creep-rupture evaluation of materials in controlled environments.

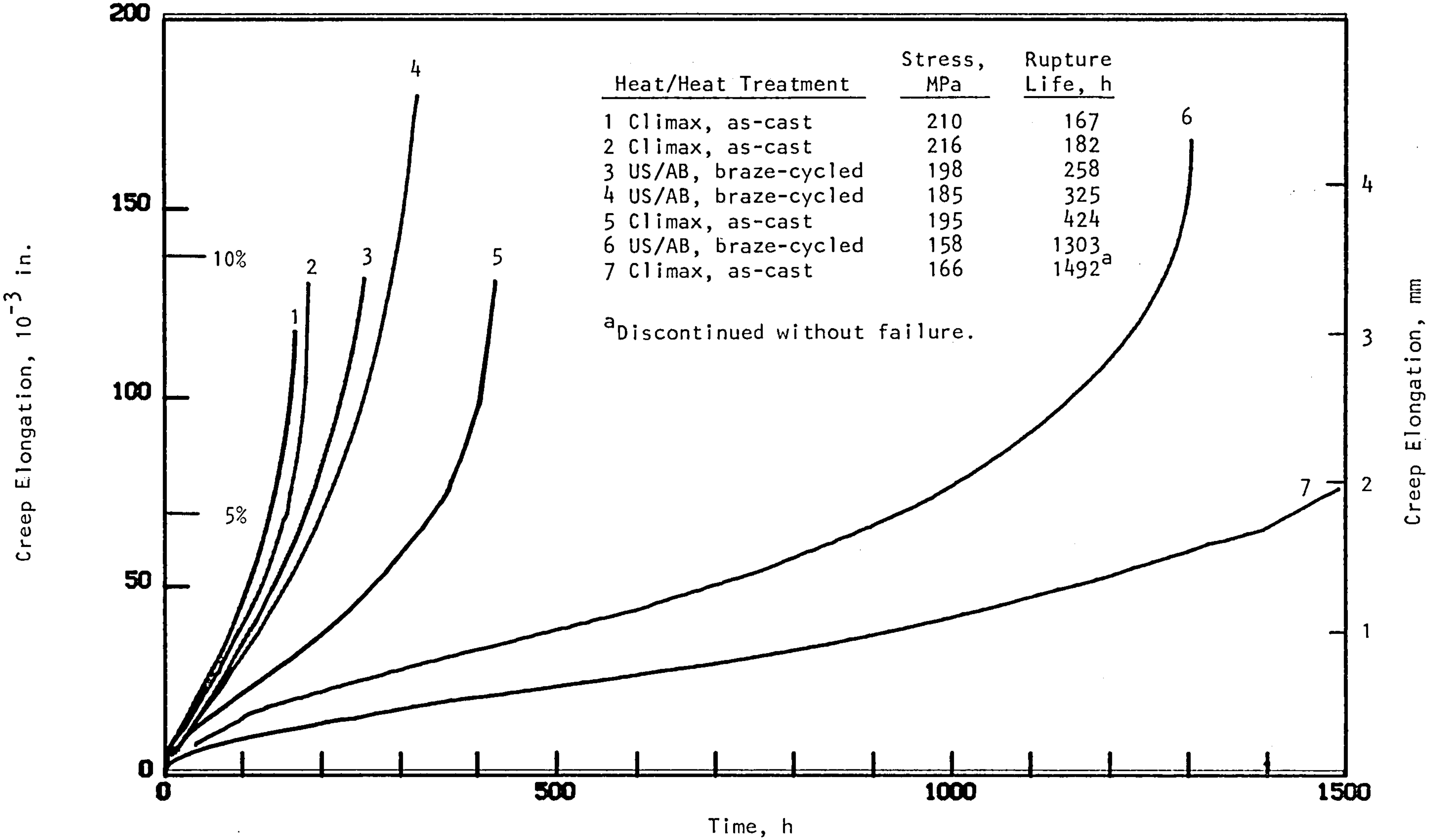

Figure 5. Creep elongation curves for two heats of XF-818 (Climax and US/AB) tested in 15 MPa H_2 at 760°C.

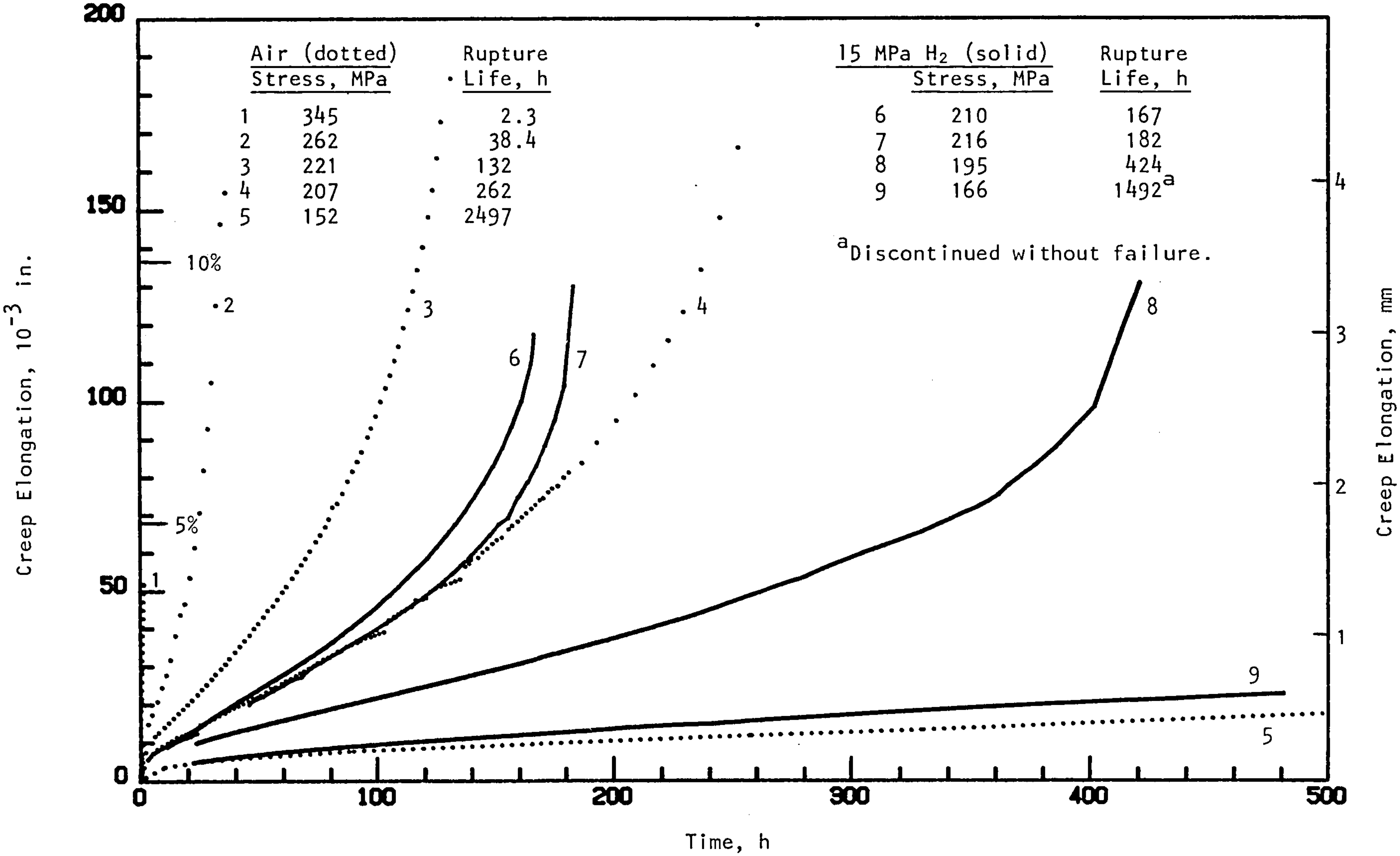

Figure 6. Creep elongation curves for XF-818 (Climax, as-cast) tested in air and 15 MPa H_2 at 760°C.

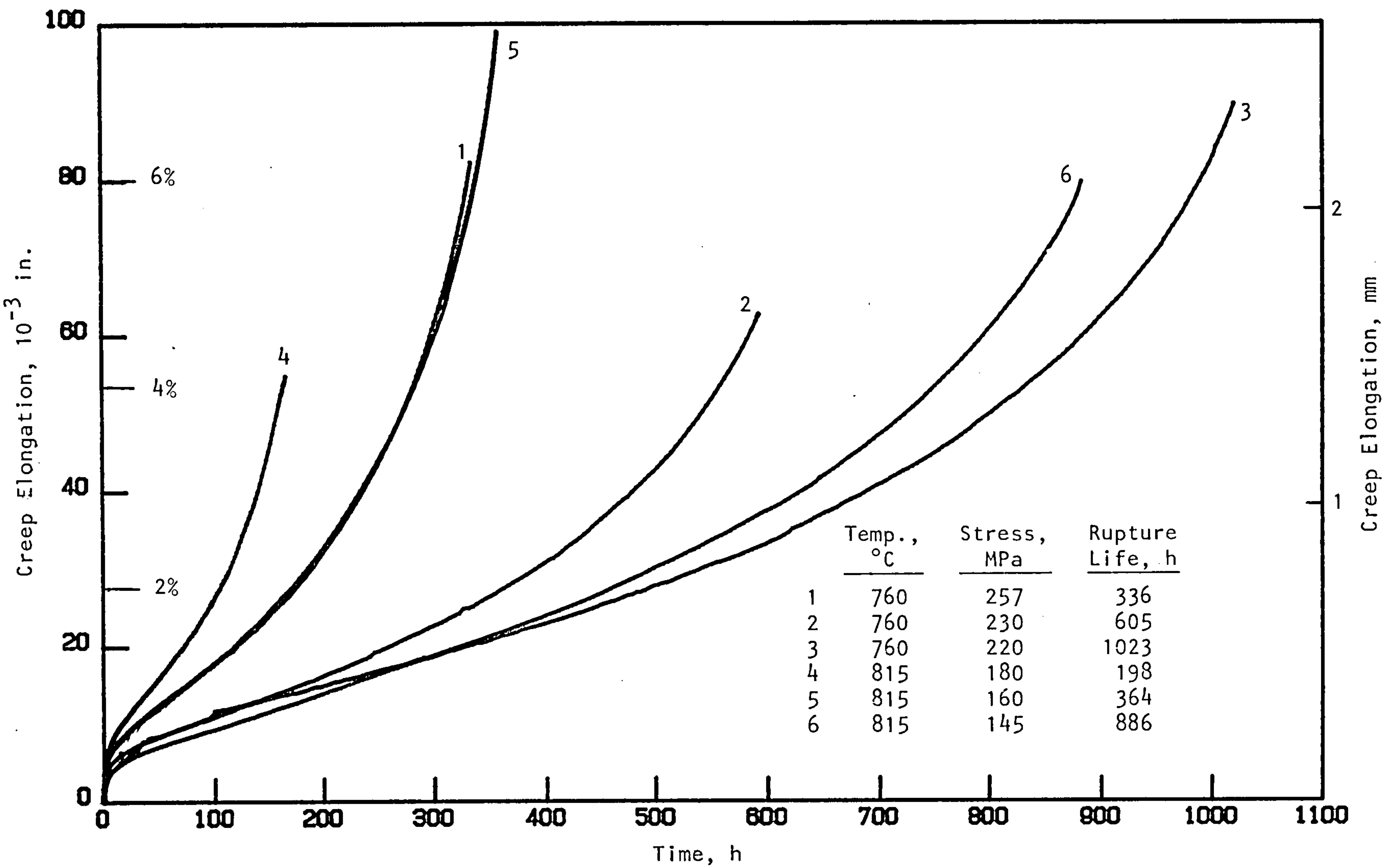

Figure 7. Creep elongation curves for SA-F11 (US/AB, braze-cycled) tested in 15 MPa H_2.

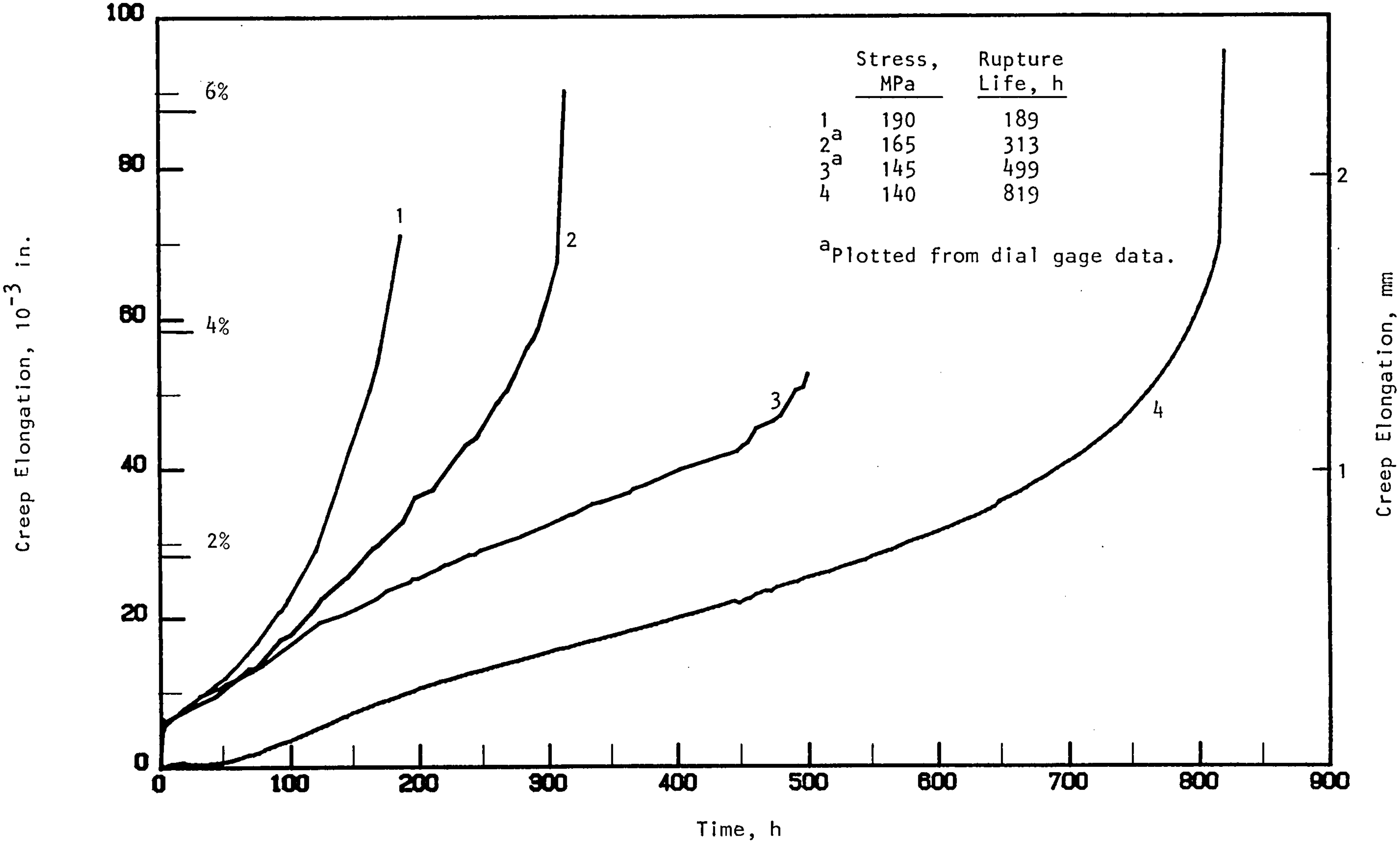

Figure 8. Creep elongation curves for CG-27 tested in 15 MPa H_2 at 815°C.

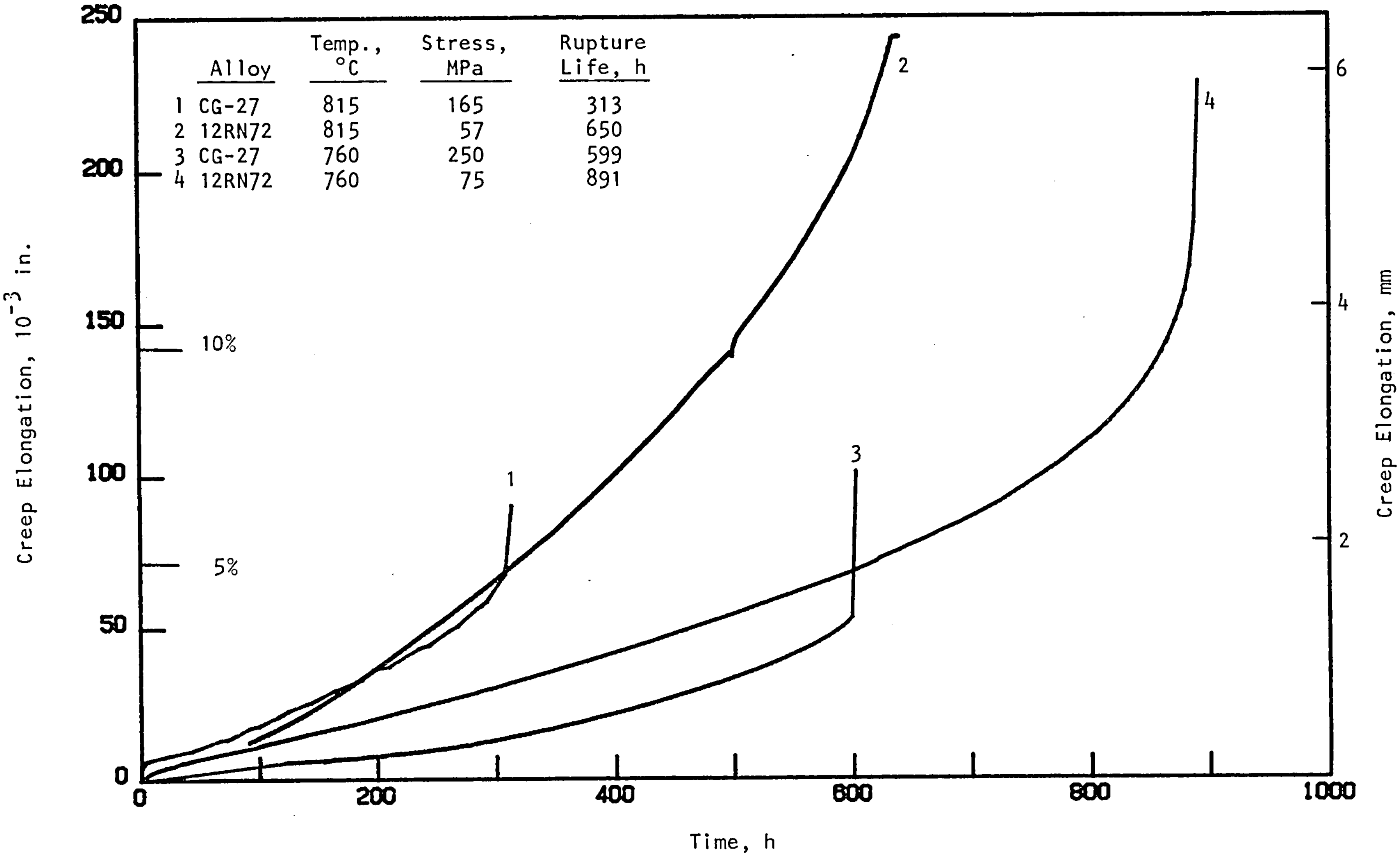

Figure 9. Creep elongation curves for 12RN72 and CG-27 tested in 15 MPa H_2.

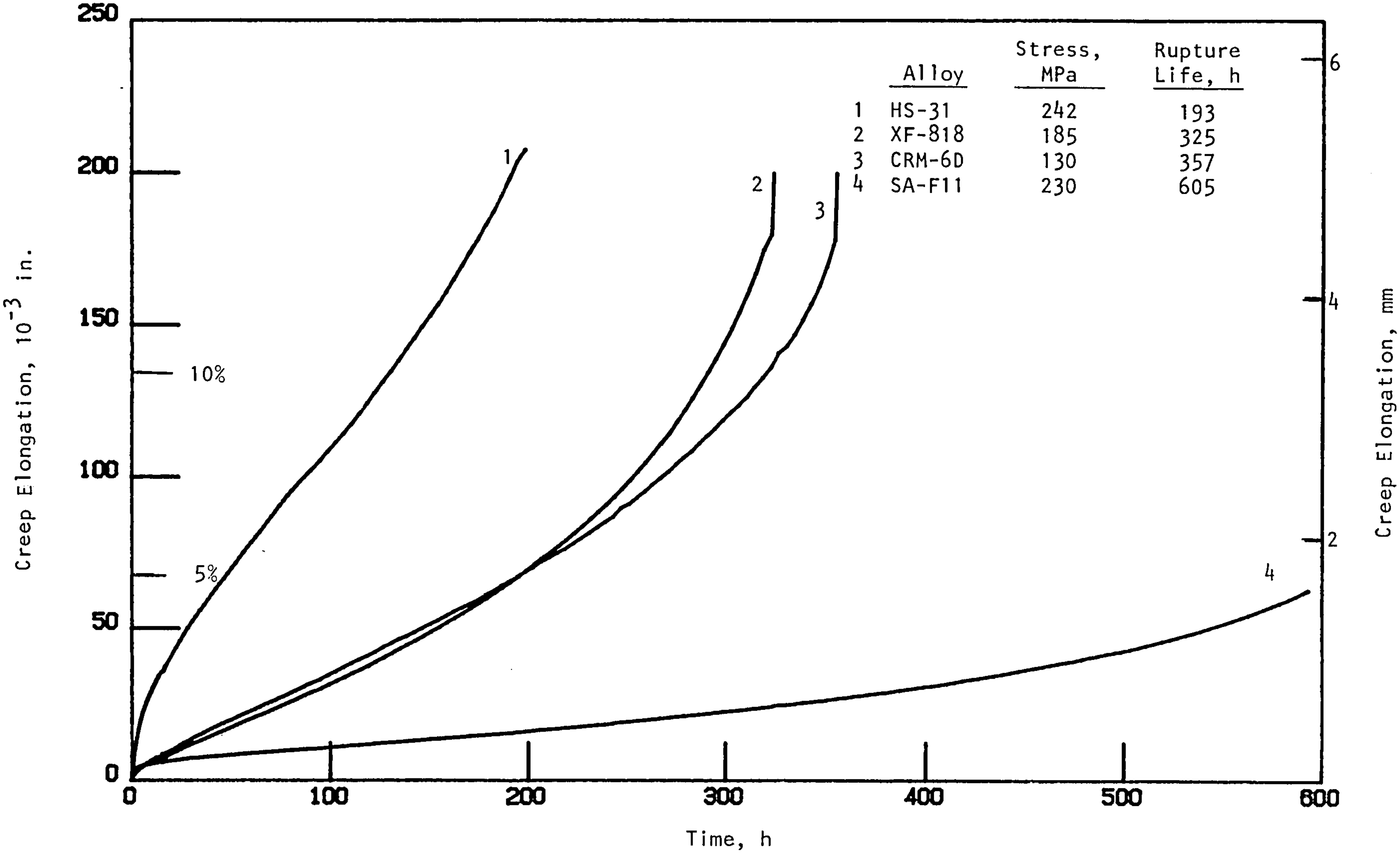

Figure 10. Creep elongation curves for HS-31, XF-818, CRM-6D, and SA-F11 (US/AB, braze-cycled) tested in a single test (H14) in 15 MPa H_2 at 760°C.

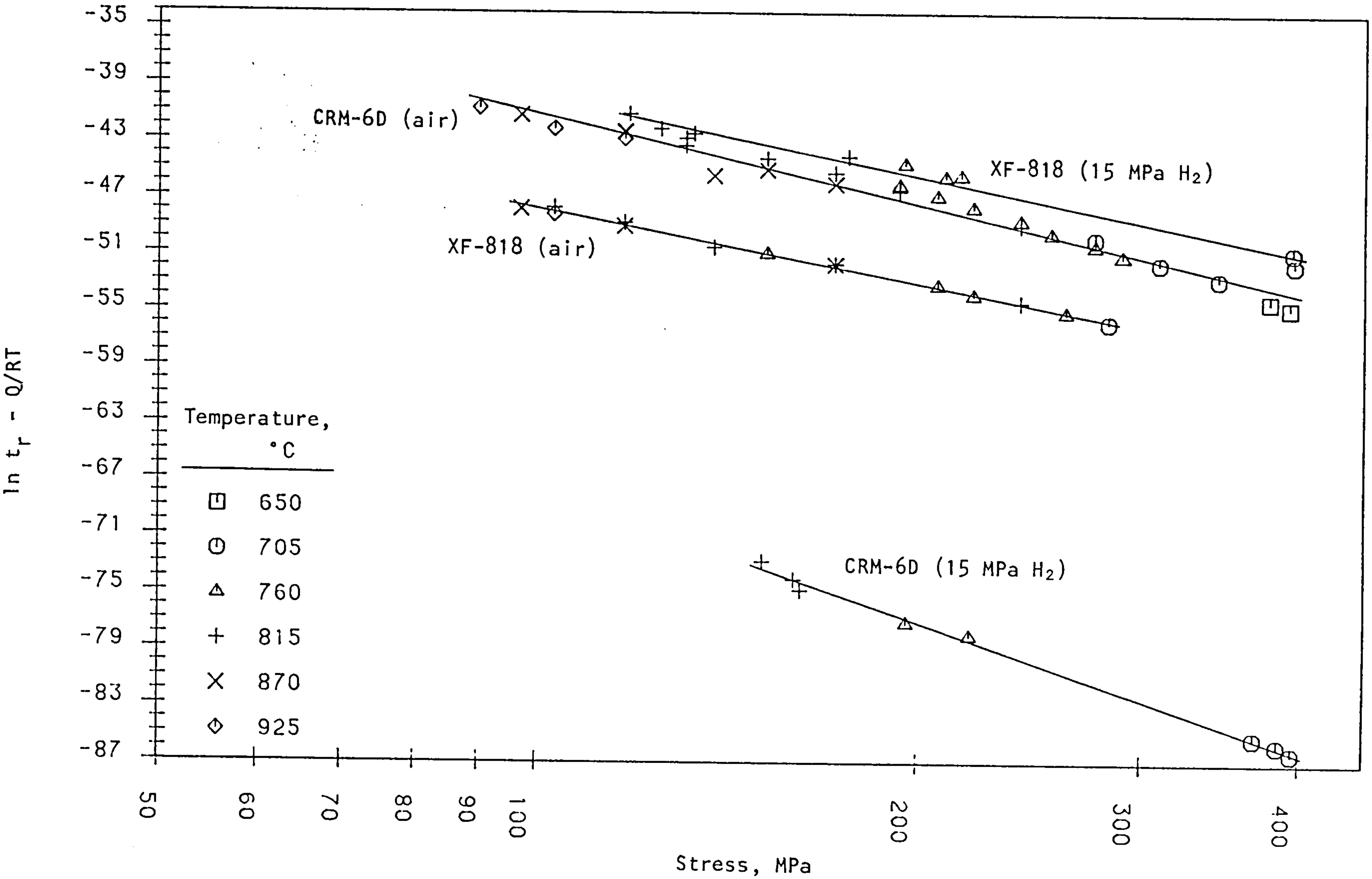

Figure 11. Temperature-compensated rupture life vs. stress for Climax CRM-6D (aged) and XF-818 (as-cast) tested in 15 MPa H_2 and air.

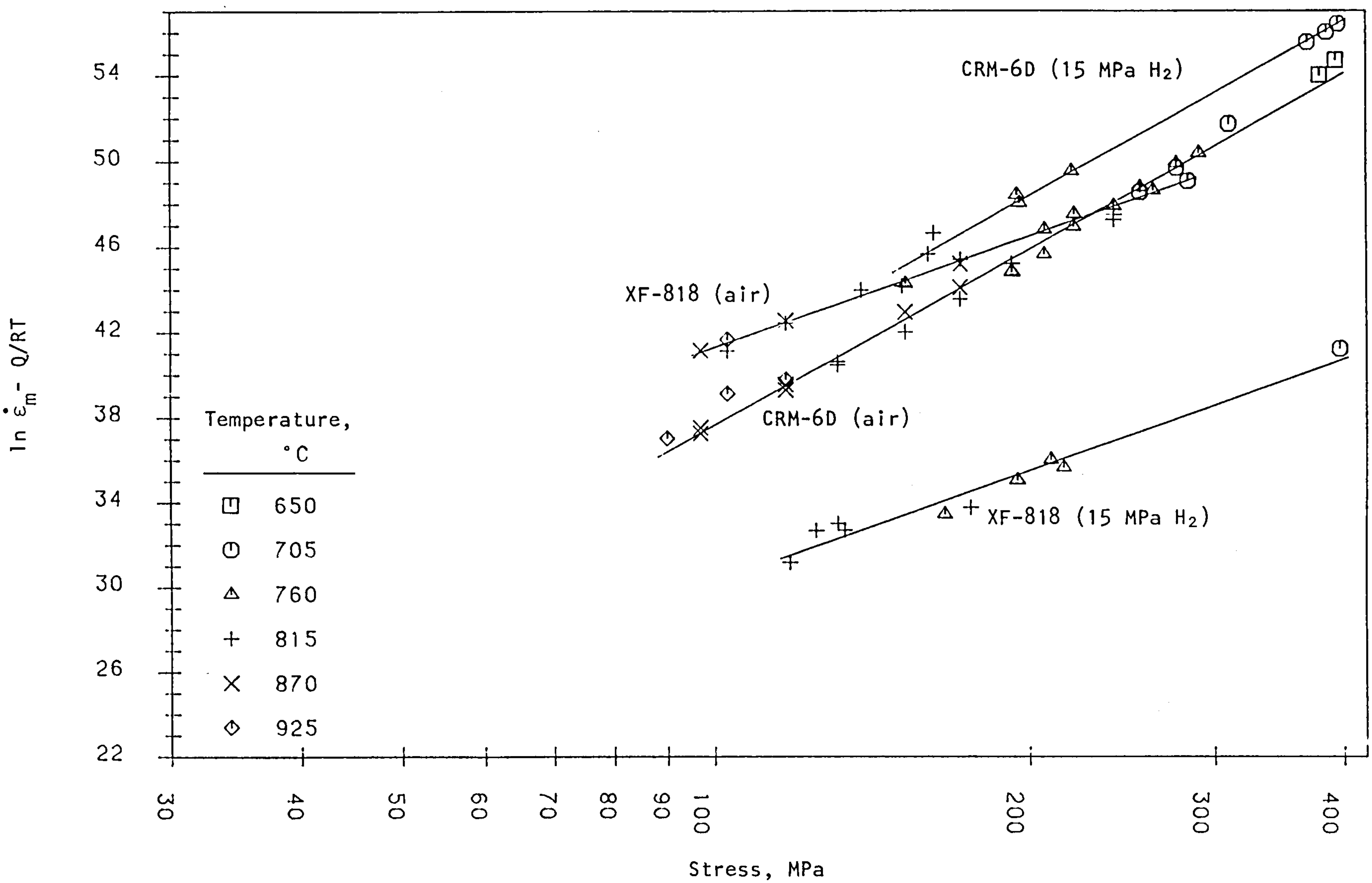

Figure 12. Temperature-compensated minimum creep rate vs. stress for Climax CRM-6D (aged) and XF-818 (as-cast) tested in 15 MPa H_2 and air.

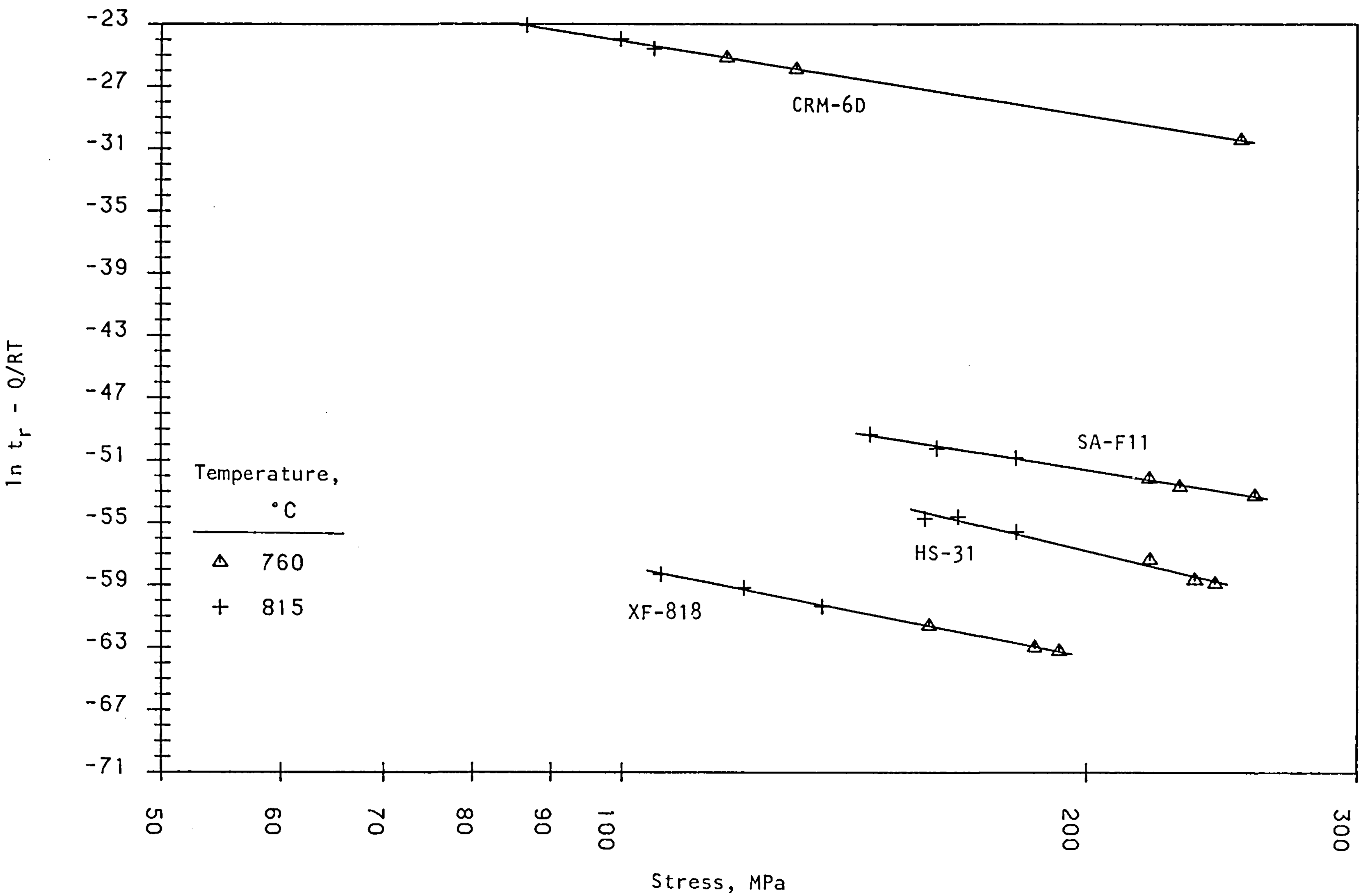

Figure 13. Temperature-compensated rupture life vs. stress for United Stirling AB braze-cycled HS-31, SA-F11, CRM-6D, and XF-818 tested in 15 MPa H_2.

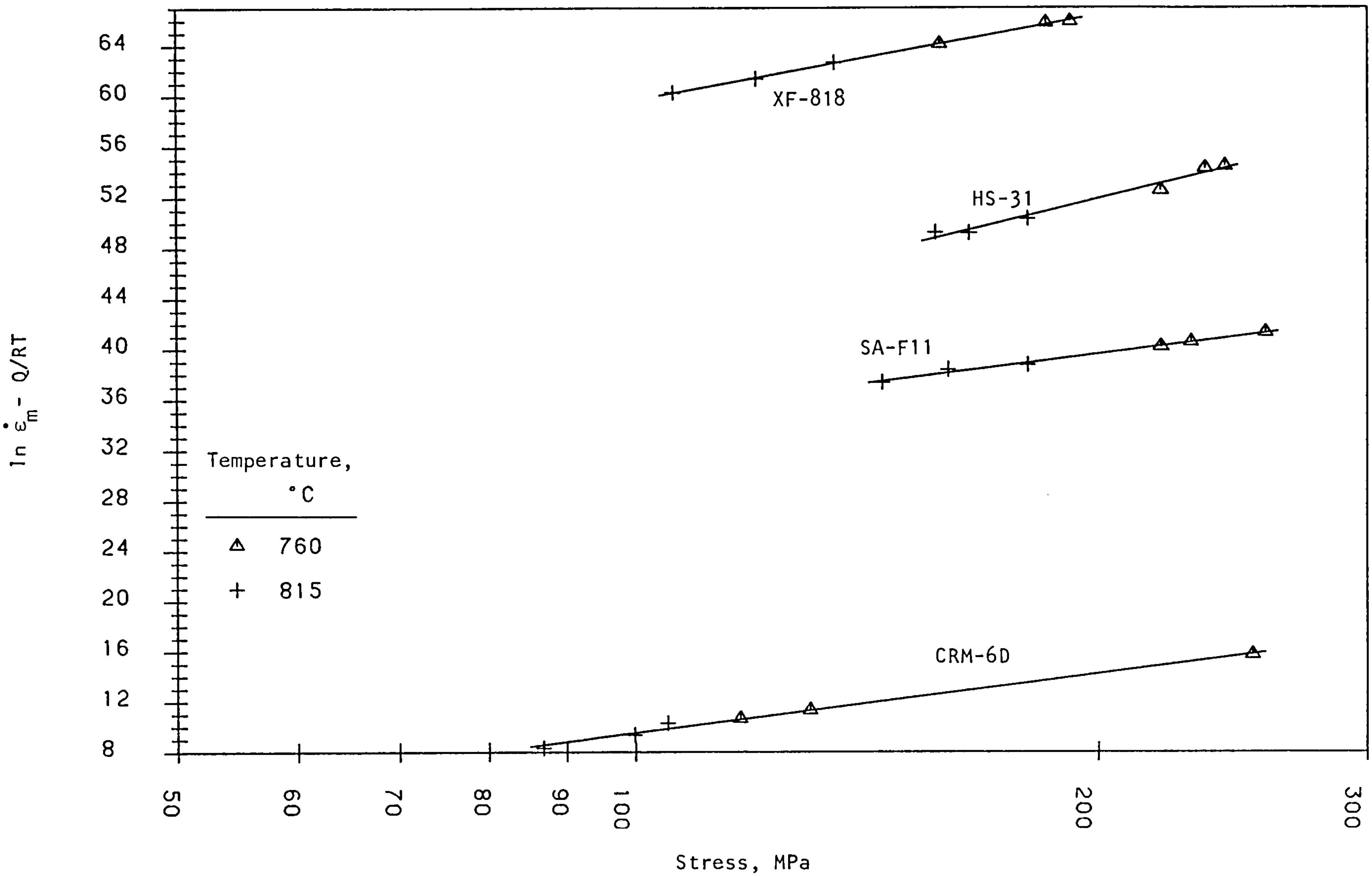

Figure 14. Temperature-compensated minimum creep rate vs. stress for United Stirling AB braze-cycled HS-31, SA-F11, CRM-6D, and XF-818 tested in 15 MPa H_2.

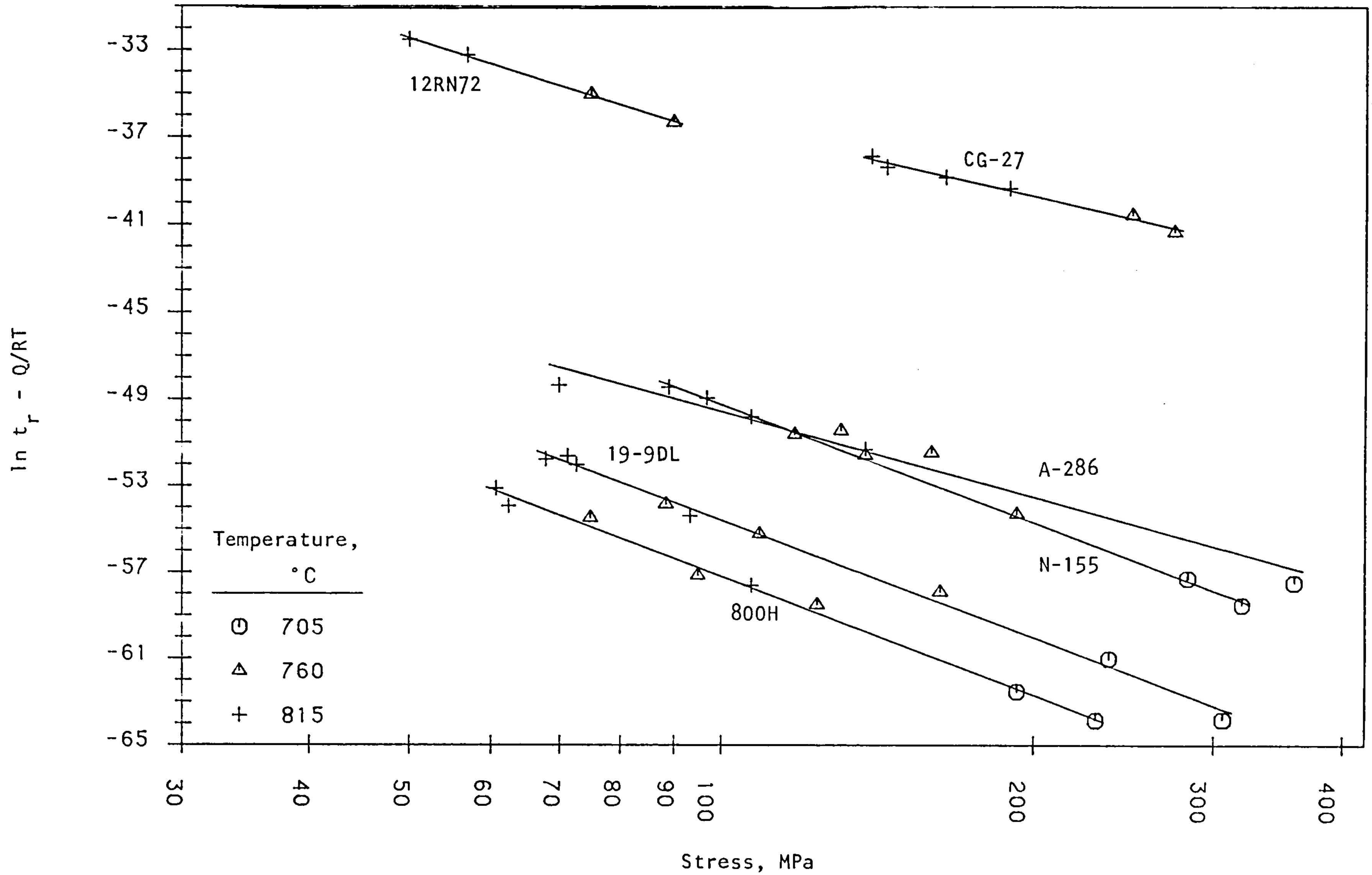

Figure 15. Temperature-compensated rupture life vs. stress for A-286, 800H, 19-9DL, N-155, 12RN72, and CG-27 tested in 15 MPa H_2.

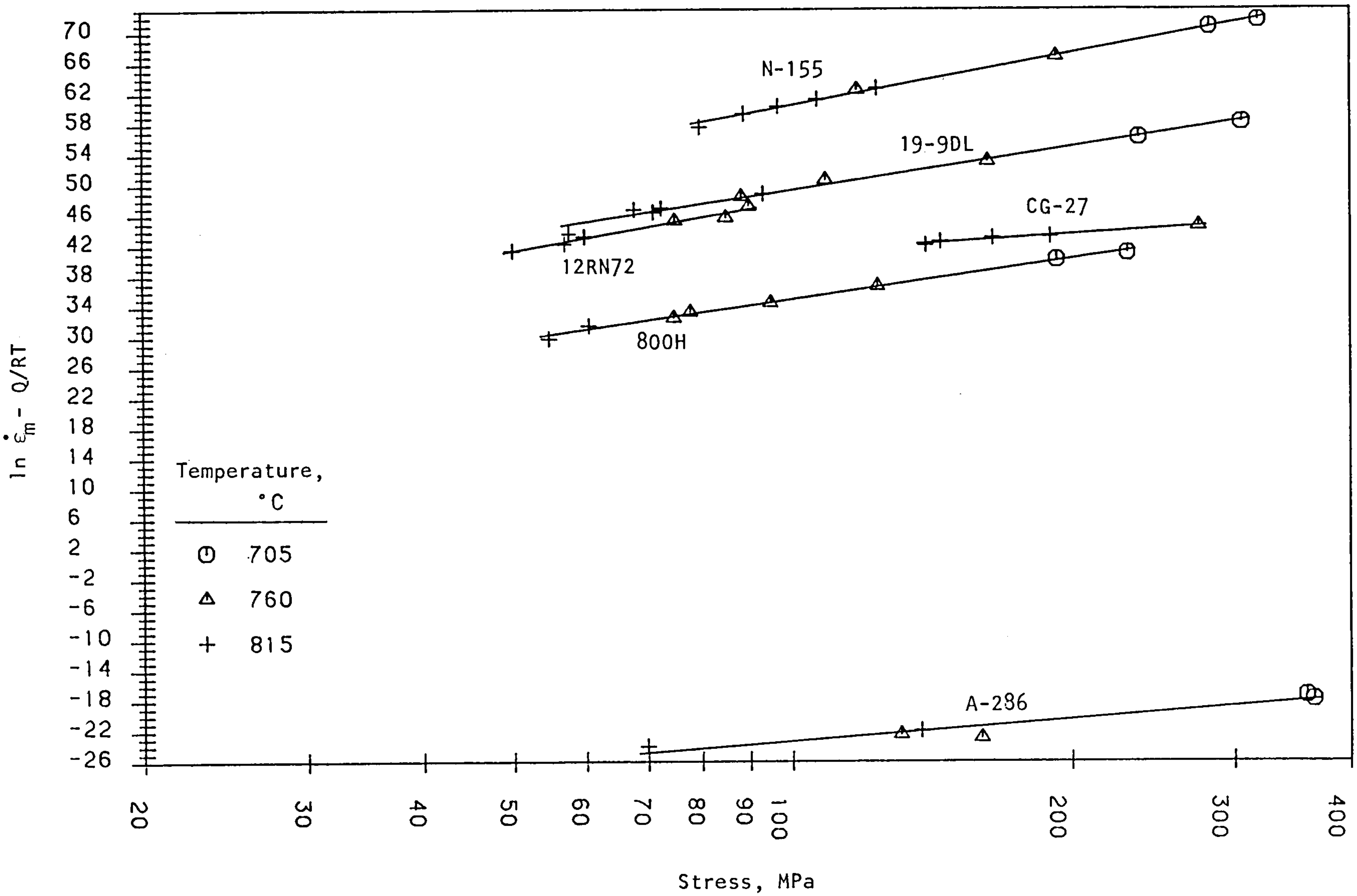

Figure 16. Temperature-compensated minimum creep rate vs. stress for A-286, 800H, 19-9DL, N-155, 12RN72, and CG-27 tested in 15 MPa H_2.

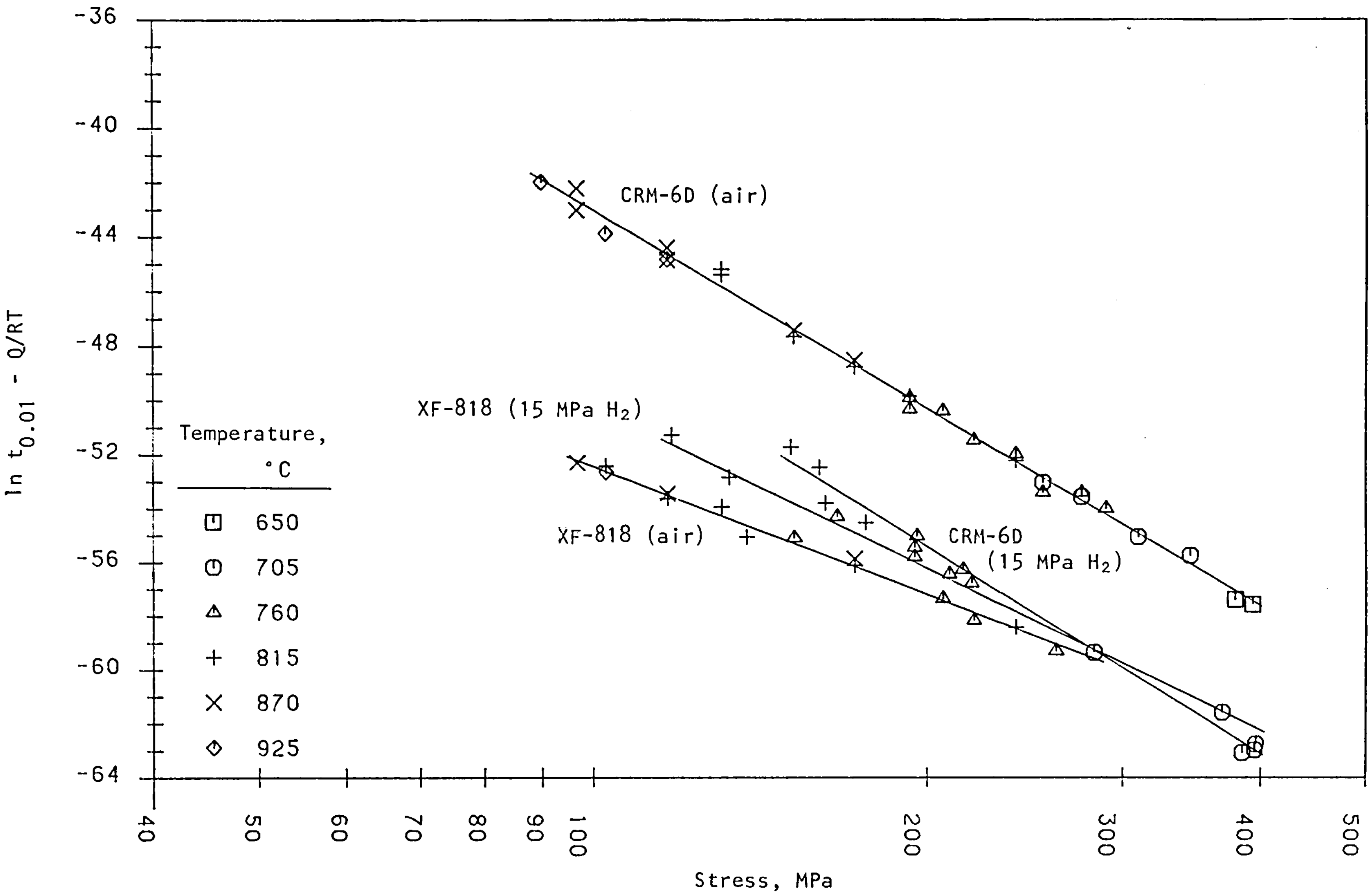

Figure 17. Temperature-compensated time to 1% creep strain vs. strain for Climax CRM-6D (aged) and XF-818 (as-cast) tested in 15 MPa H_2 and air.

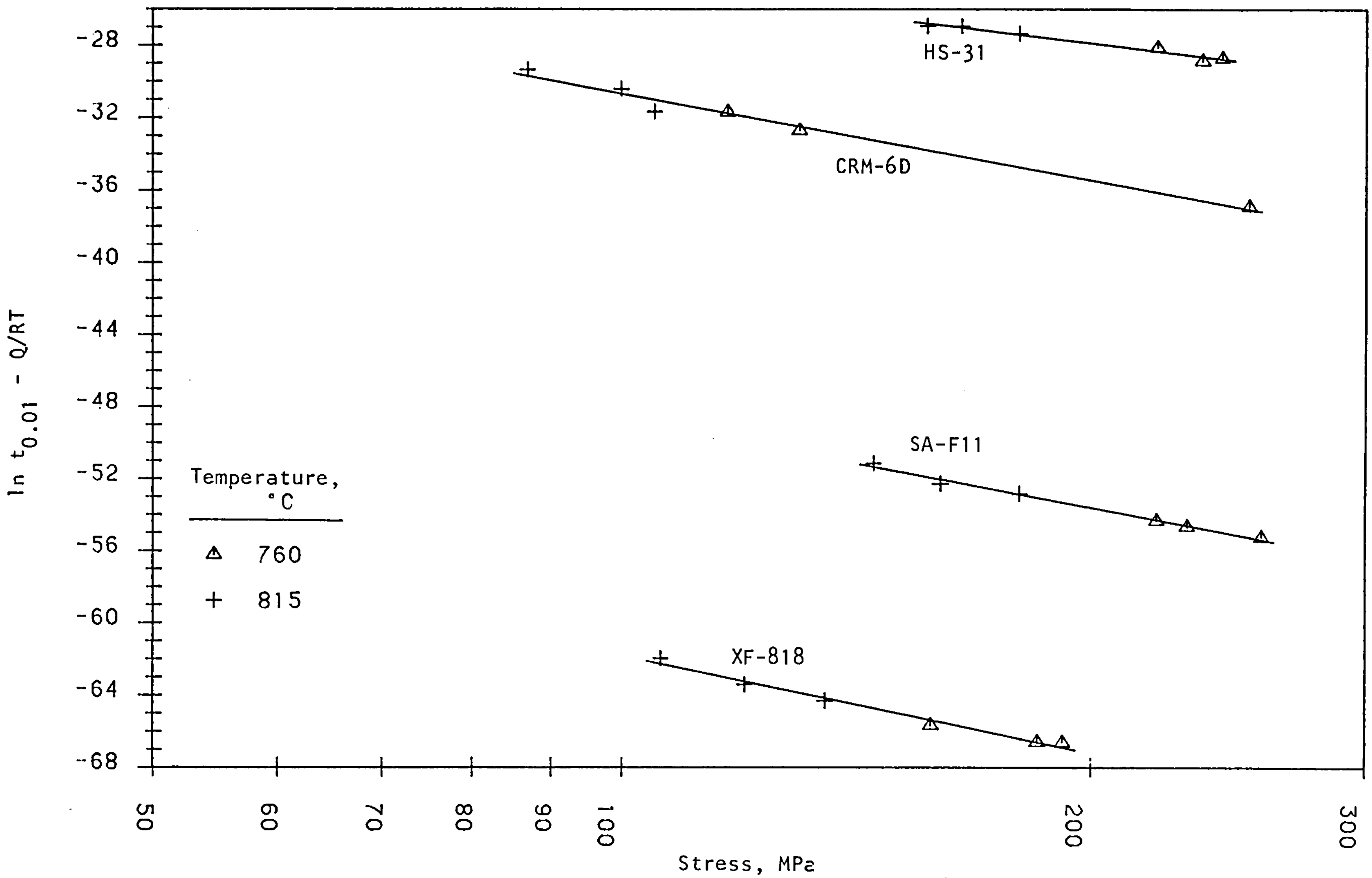

Figure 18. Temperature-compensated time to 1% creep strain vs. strain for United Stirling AB braze-cycled HS-31, SA-F11, CRM-6D, and XF-818 tested in 15 MPa H_2.

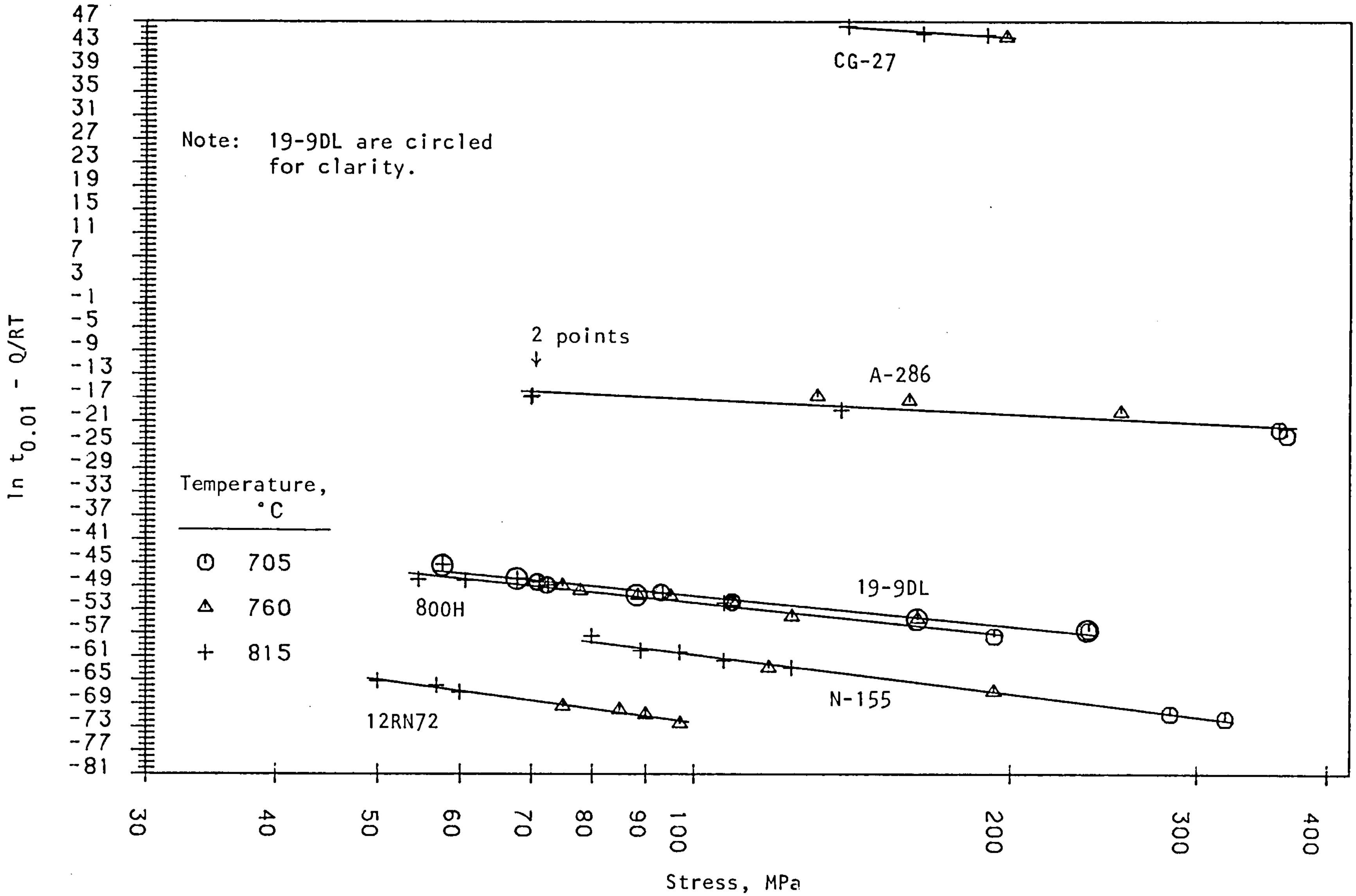

Figure 19. Temperature-compensated time to 1% creep strain vs. strain for A-286, 800H, 19-9DL, N-155, 12RN72, and CG-27 tested in 15 MPa H_2.

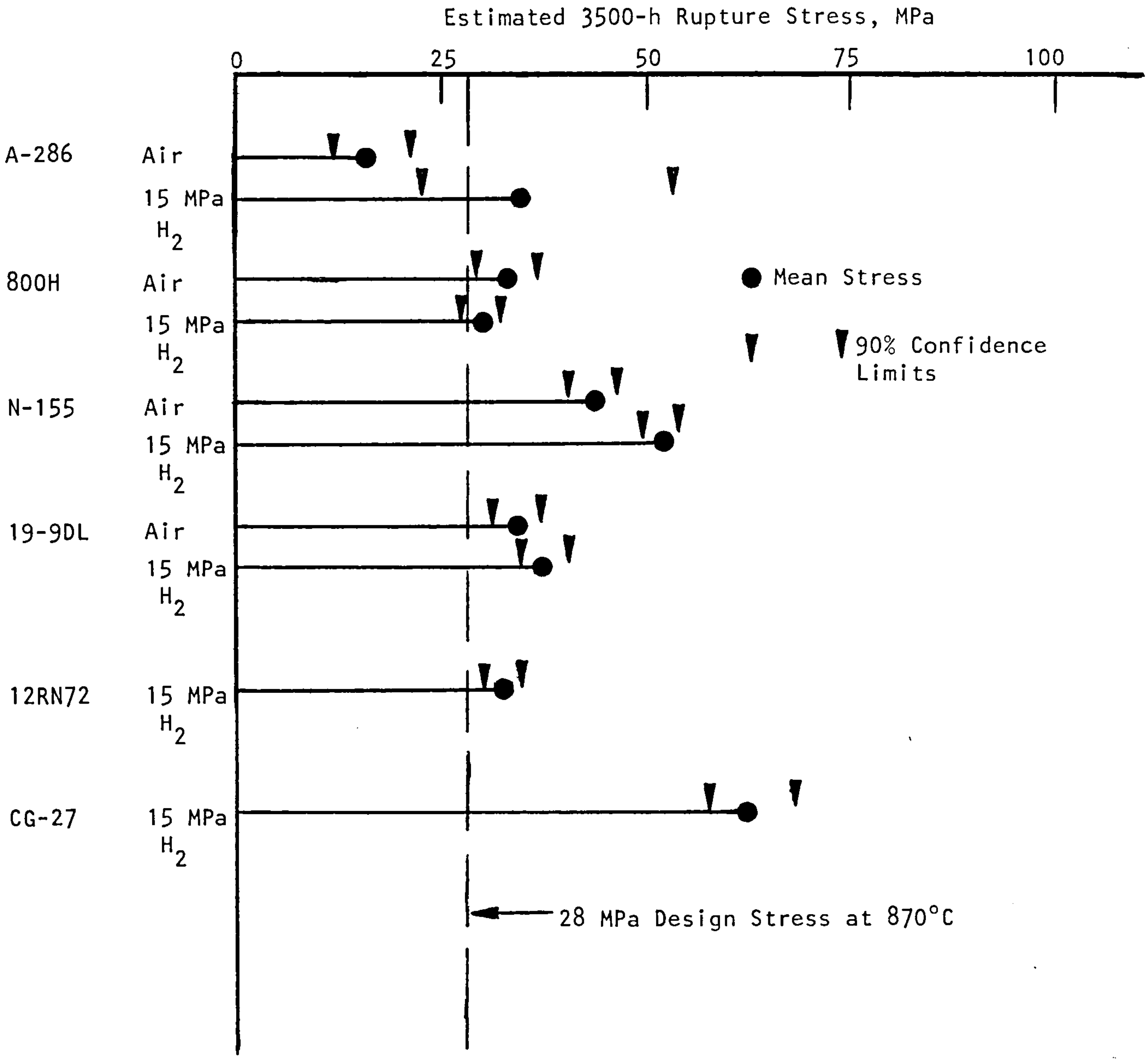

Figure 20. Estimated 3500-h rupture stress for tube alloys tested at 870°C in air and 15 MPa hydrogen.

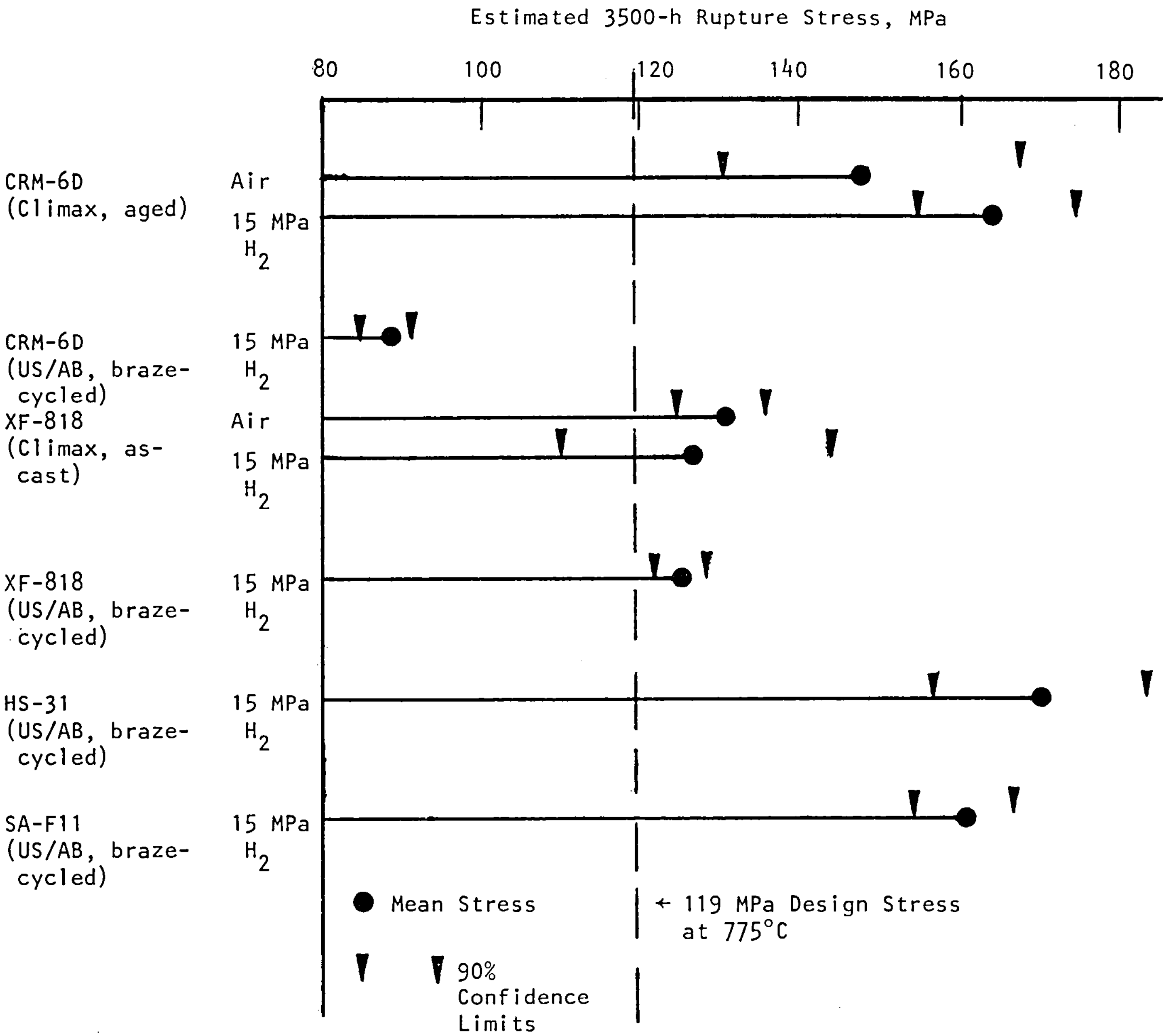

Figure 21. Estimated 3500-h rupture stress for cast alloys tested at 775°C in air and 15 MPa hydrogen.

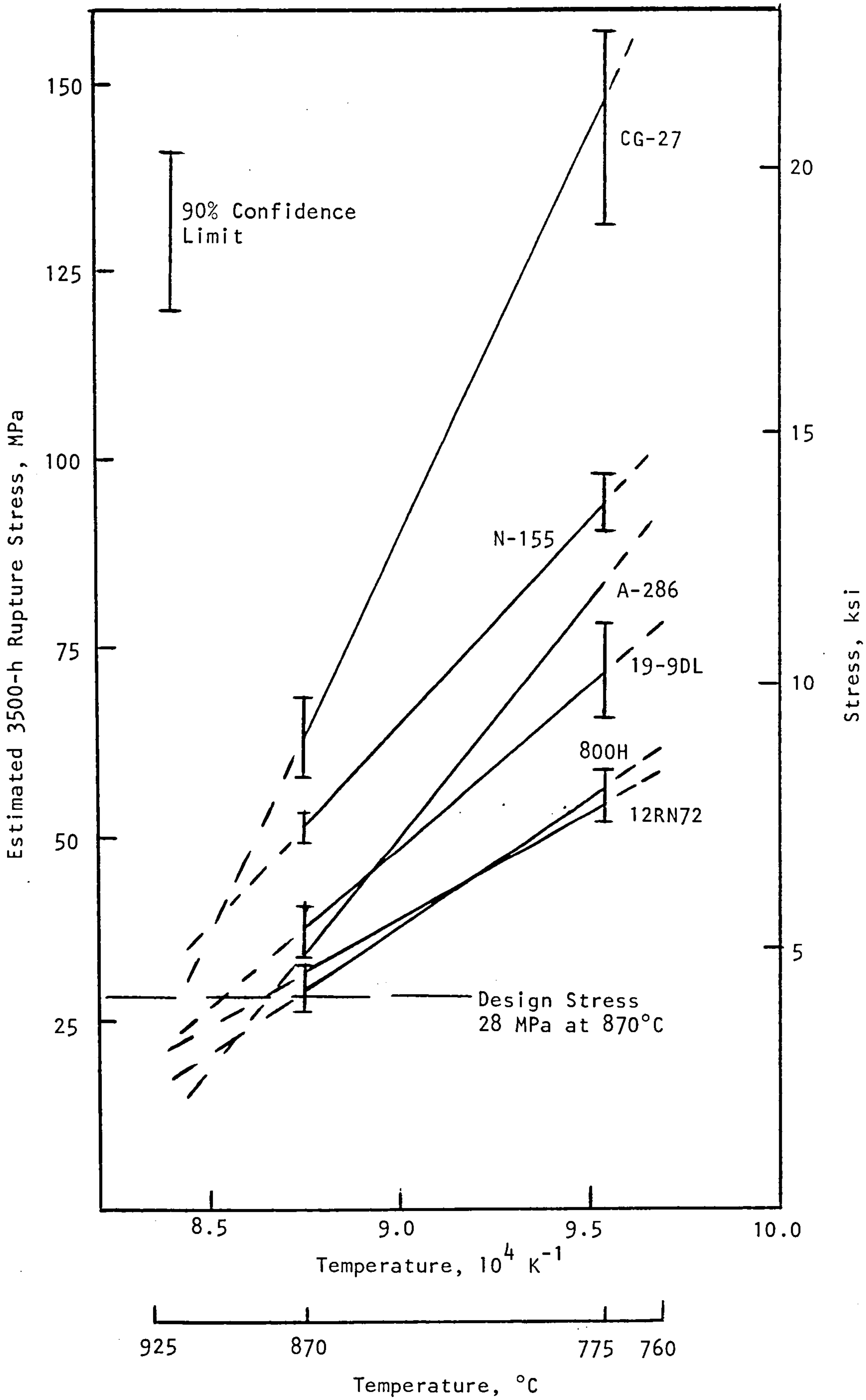

Figure 22. Estimated 3500-h rupture stress of six tube alloys as a function of temperature tested in 15 MPa hydrogen.

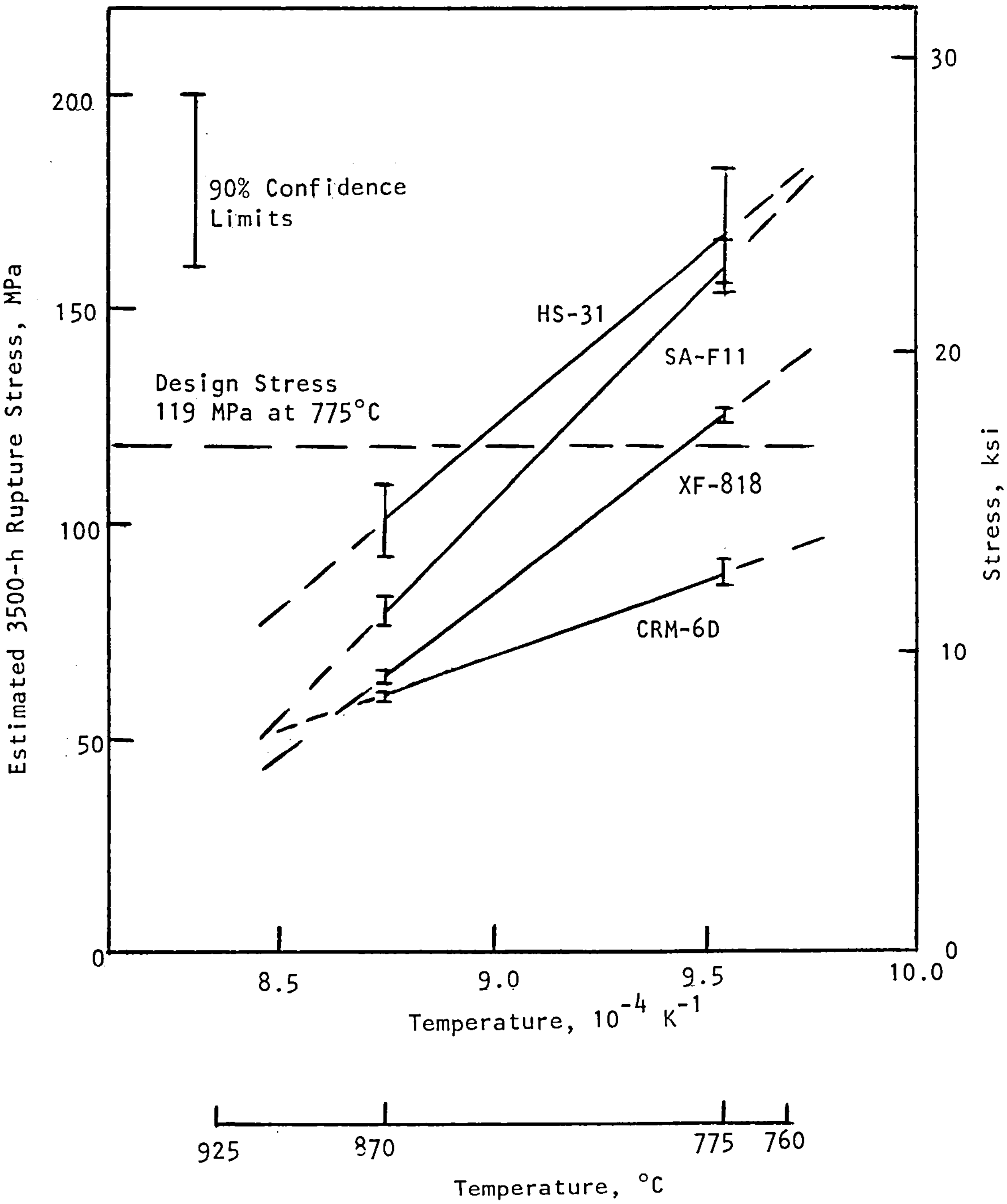

Figure 23. Estimated 3500-h rupture stress of United Stirling AB braze-cycled cast alloys as a function of temperature, tested in 15 MPa hydrogen.

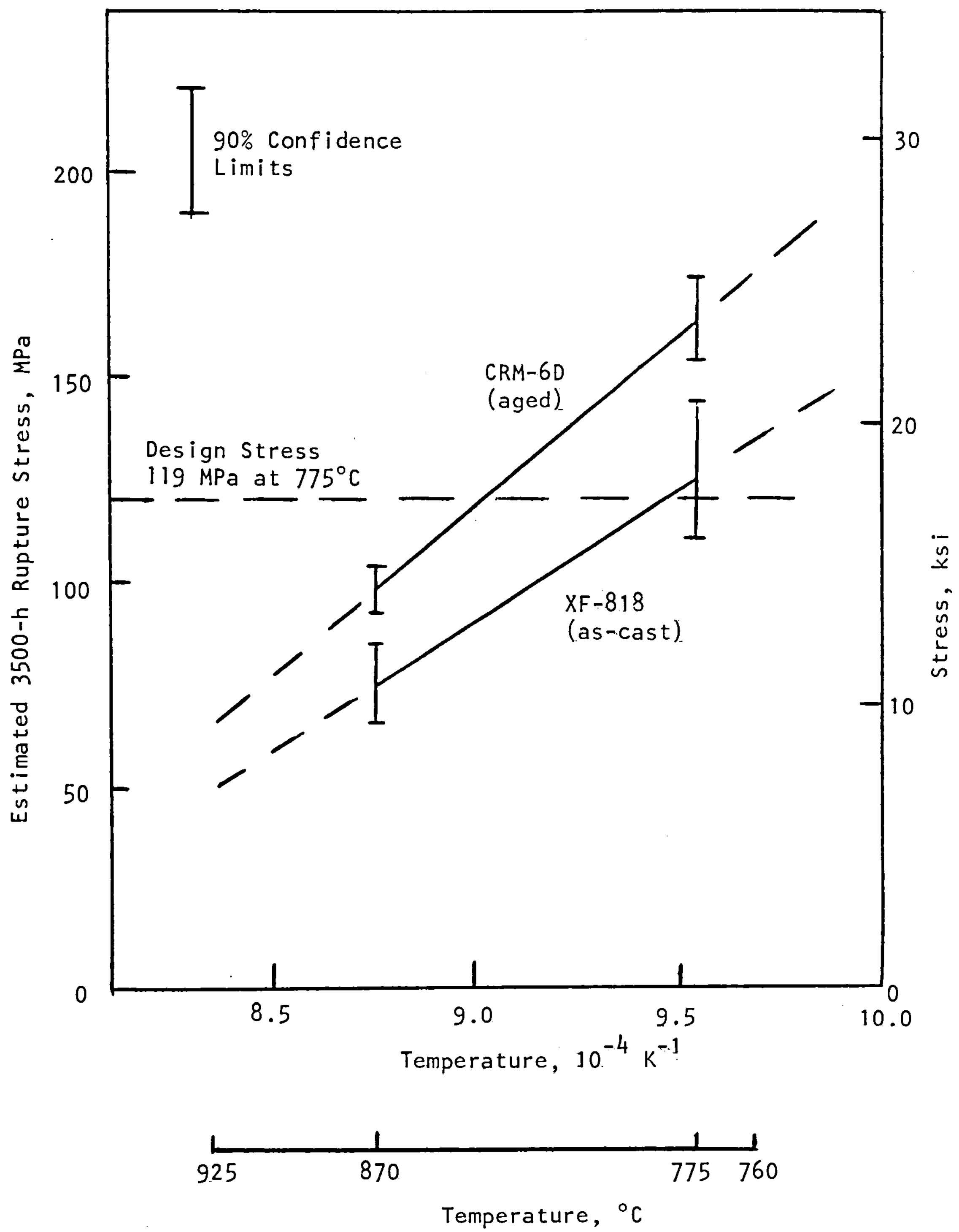

Figure 24. Estimated 3500-h rupture stress of Climax cast alloys as a function of temperature, tested in 15 MPa hydrogen.

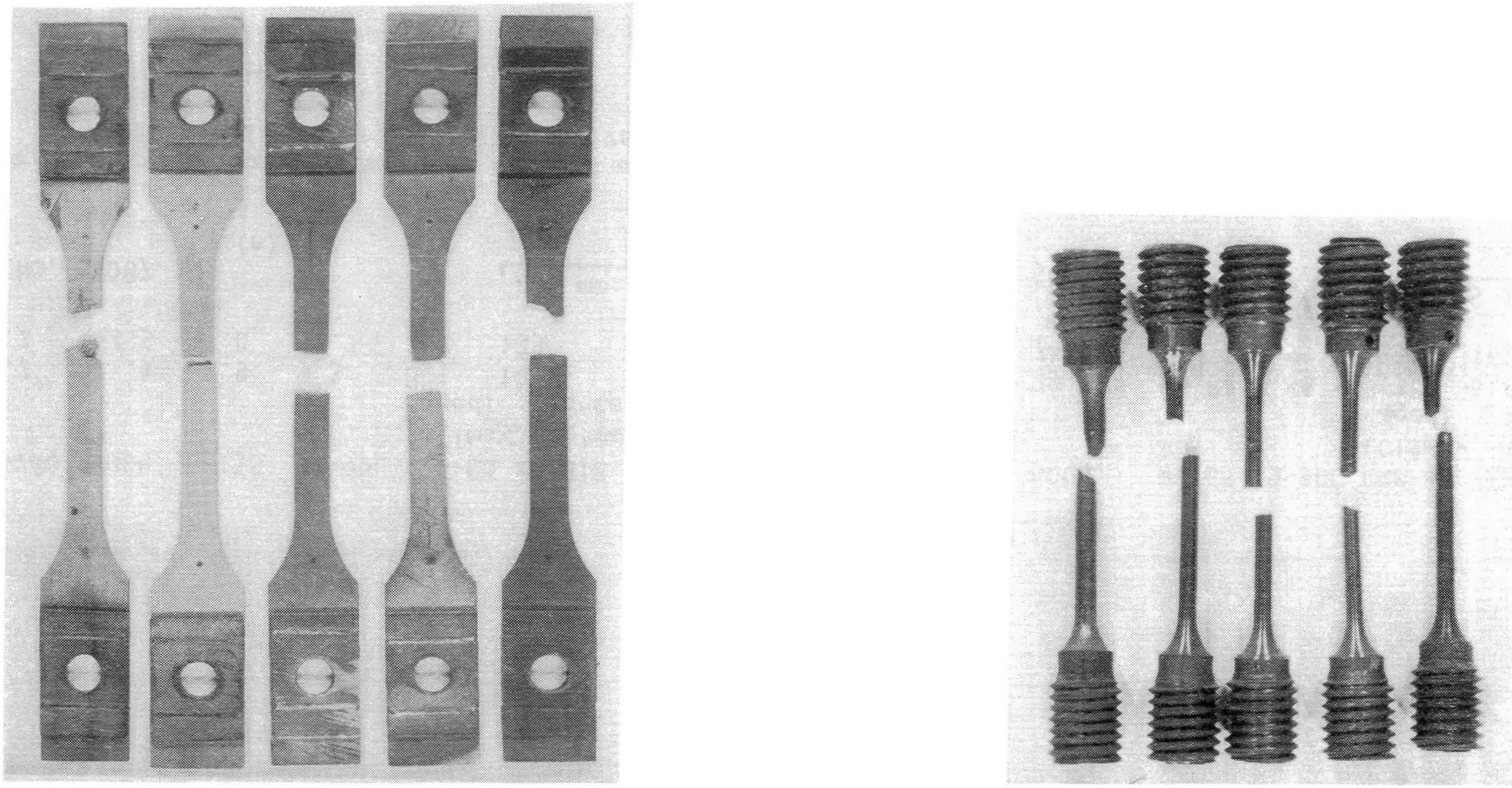

Temp., °C	815	760	705	705	760
Stress, MPa	93.4	163	306	237	109
Elong., %	9.4	28.5	8.0	15.0	9.3

Neg. No. 53768

25 mm

(a)

Temp., °C	815	705	705	705	760
Stress, MPa	176	395	440	396	216
Elong, %	10.3	6.0	8.4	5.0	10.4
R. A., %	30.6	6.2	9.0	11.9	36.6

Neg. No. 53769

25 mm

(b)

Figure 25. Appearance of fractured wrought and cast alloy specimens tested in 15 MPa hydrogen. (a) 19-9DL, (b) XF-818 (Climax, as-cast).

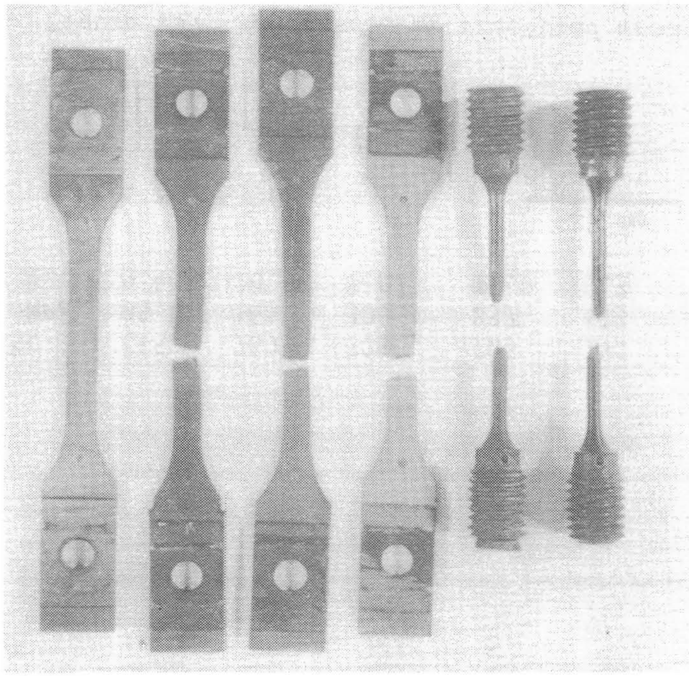

Alloy	A-286	800H	N-155	19-9DL	CRM-6D (Climax, aged)	XF-818 (Climax, as-cast)
Elong., %	2.7+	21.4	33.9	9.3	8.1	14.2
Stress, MPa	70.2	62.5	97.0	72.7	162	133

Neg. No. 54087

25 mm

(a)

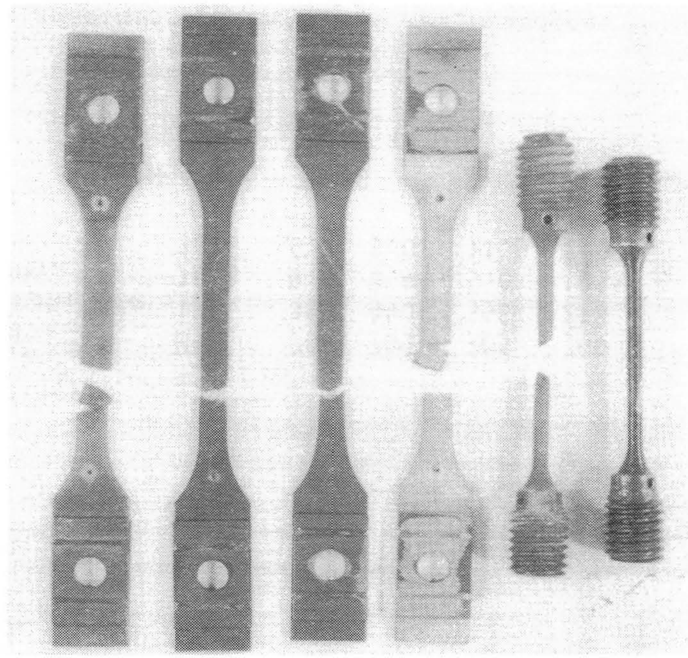

Alloy	A-286	800H	N-155	19-9DL	CRM-6D (Climax, aged)	XF-818 (Climax, as-cast)
Elong, %	8.14	29.1	25.8	7.86	7.38	6.62+
Stress, MPa	131	74.9	118	88.5	196	166

Neg. No. 54088

25 mm

(b)

Figure 26. Appearance of fractured wrought and cast alloy specimens tested in 15 MPa hydrogen. (a) 815°C, A-286 specimen did not fail; (b) 760°C, XF-8]8 (Climax, as-cast) specimen did not fail.

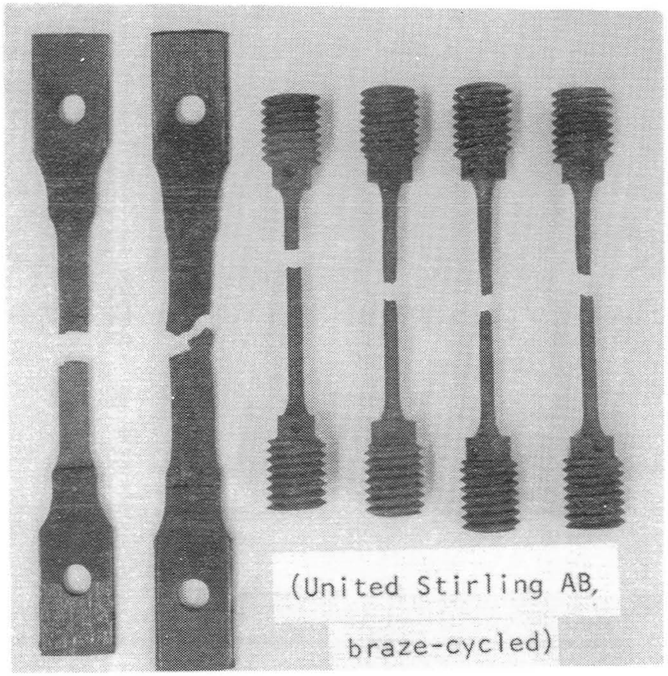

Alloy	CG-27	12RN72	SA-F11	HS-31	CRM-6D	XF-818
Elong., %	6.5	20.9	6.3	30.6	39.2	33.3
Stress, MPa	140	50.0	145	157	87.0	106

25 mm

Neg. No. 55515

(a)

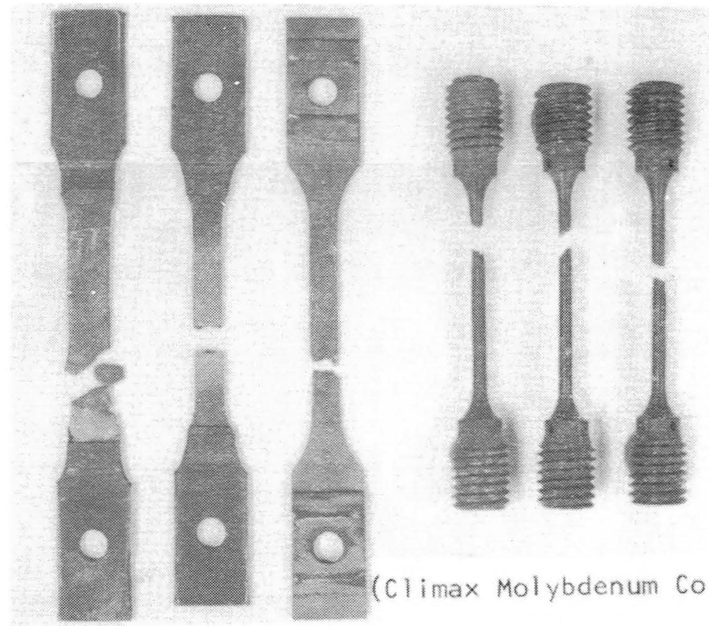

Alloy	12RN72	CG-27	800H	CRM-6D (aged)	XF-818 (as-cast)	XF-818 (as-cast)
Elong., %	15.4	2.6	13.8	22.6	10.7	8.5
Stress, MPa	85.0	275	95.0	220	195	210

25 mm

Neg. No. 55698

(b)

Figure 27. Appearance of fractured wrought and cast alloy specimens tested in 15 MPa hydrogen. (a) 815°C, (b) 760°C)

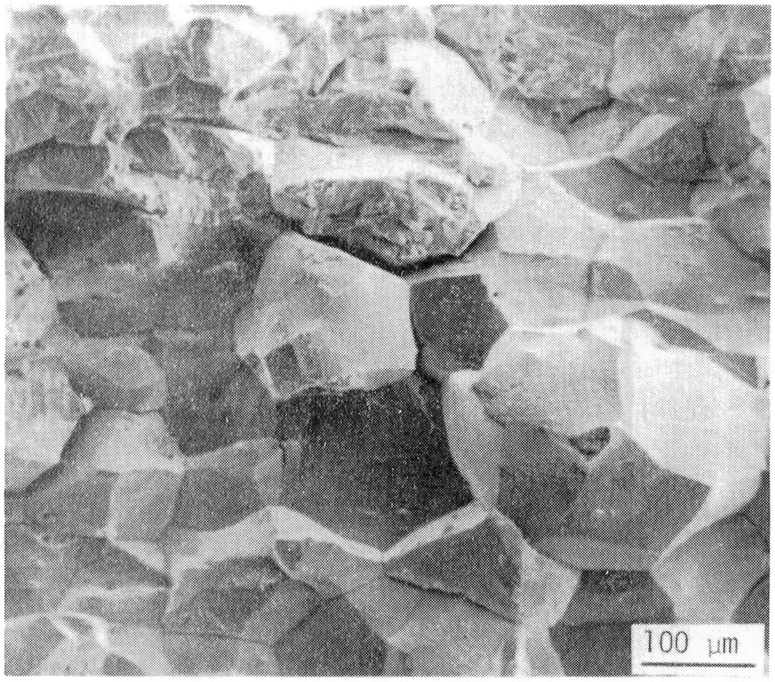

SEM No. 8375A

(a)

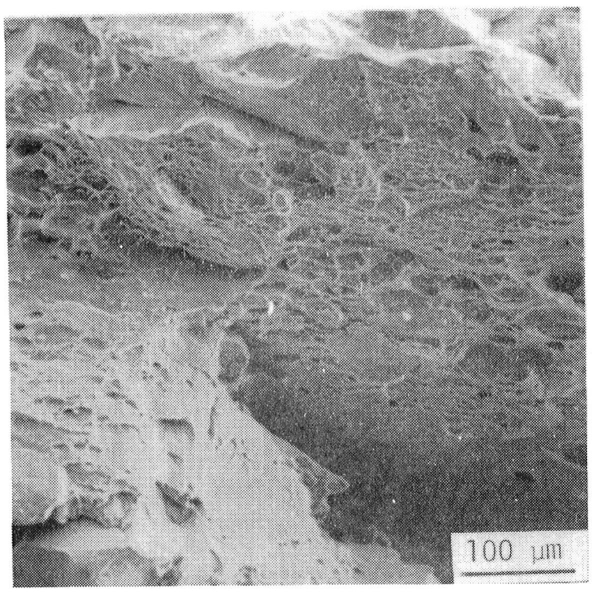

SEM No. 8377B

(b)

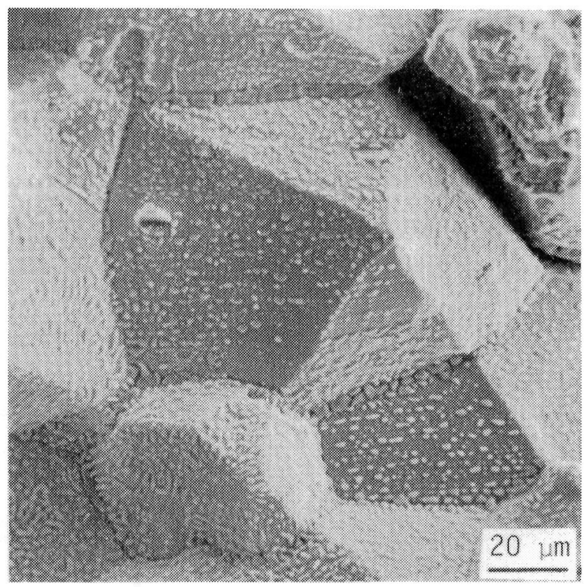

SEM No. 8375B

(c)

Figure 28. SEM microfractographs of A-286 tested in 15 MPa H_2 at 705°C. (a) Intergranular fracture; (b) ductile dimple fracture near the surface; (c) intergranular fracture with second phases on grain surfaces.

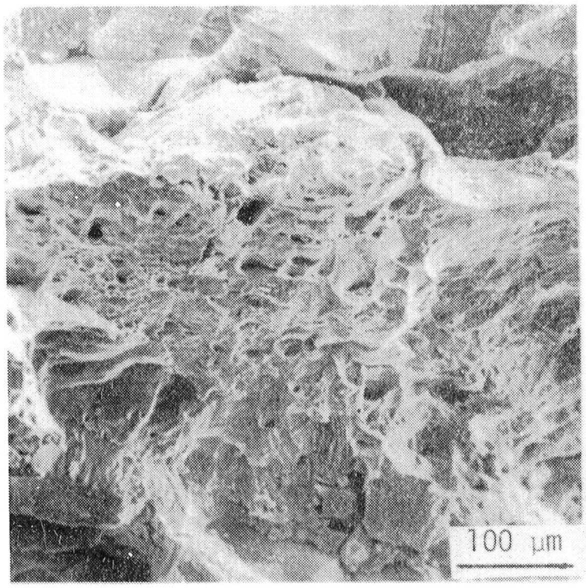

SEM No. 8373

(a)

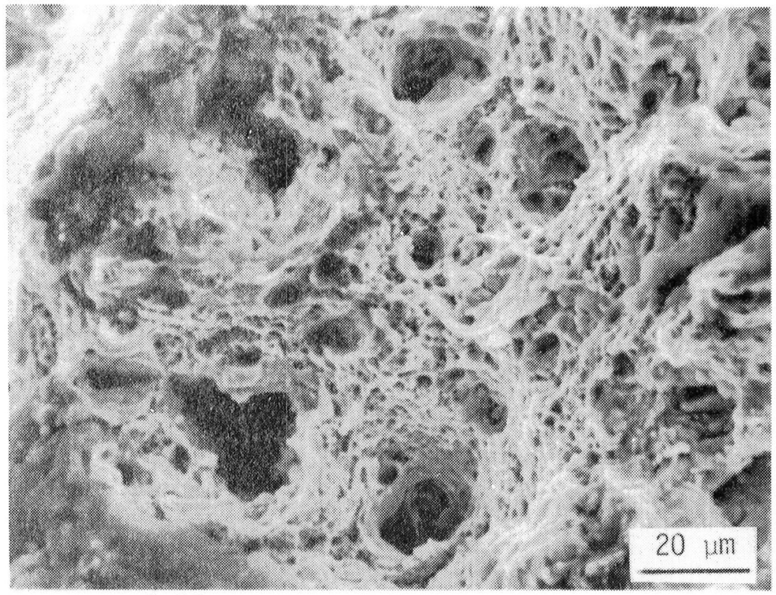

SEM No. 8366

(b)

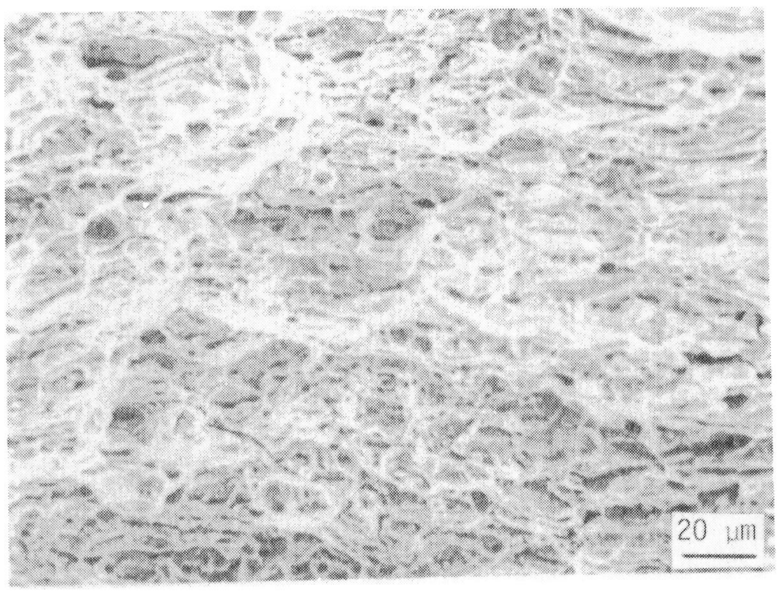

SEM No. 8362

(c)

Figure 29. SEM microfractographs of wrought alloys tested in 15 MPa H_2. (a) 800H, 760°C; (b) N-155, 760°C; (c) 19-9DL, 705°C. Extensive dimple rupture on all surfaces.

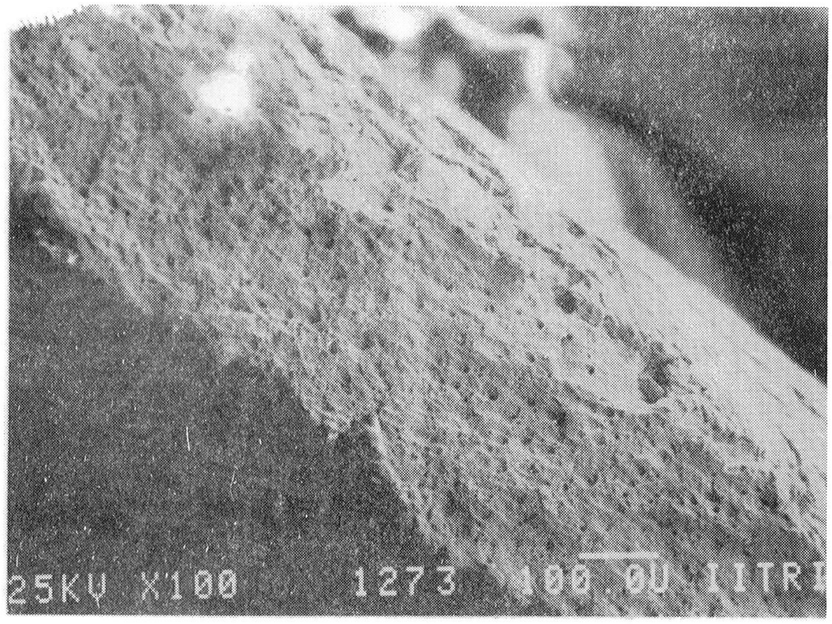

SEM No. 1273

(a)

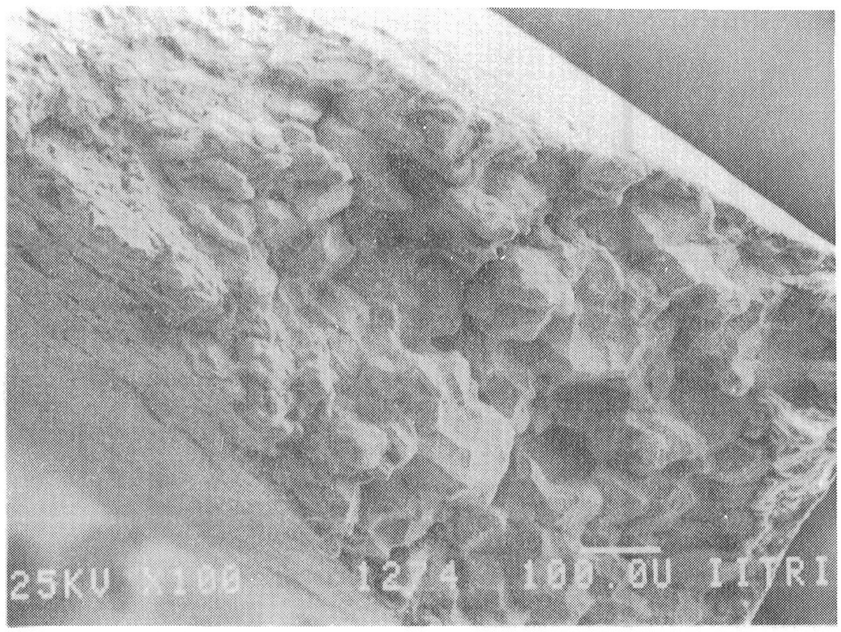

SEM No. 1274

(b)

Figure 30. SEM microfractographs of 12RN72 tested in 15 MPa H_2 at 760°C. (a) Dimple rupture; (b) decohesive separation of grains in an adjoining area; (c) details of dimples; (d) second-phase particles on decohesively ruptured grains.

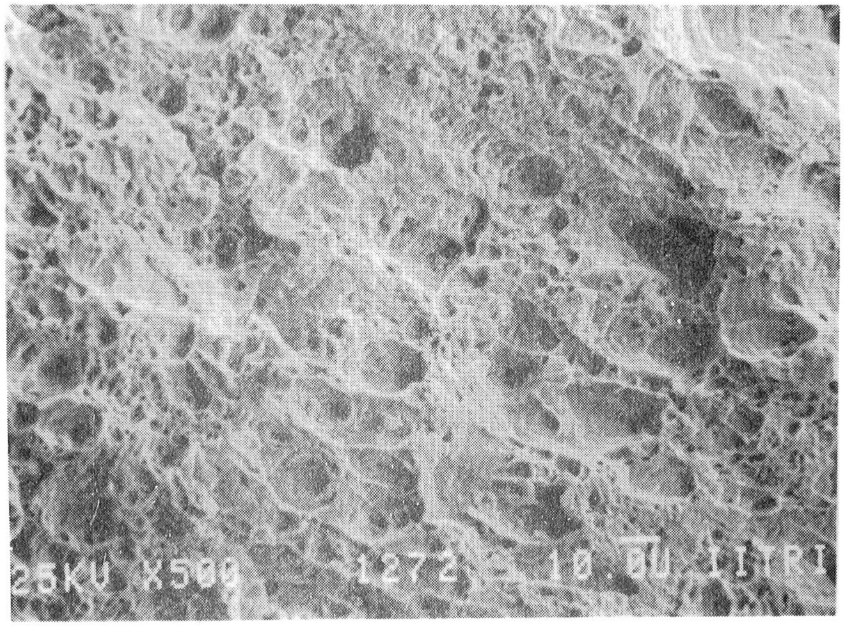

SEM No. 1272

(c)

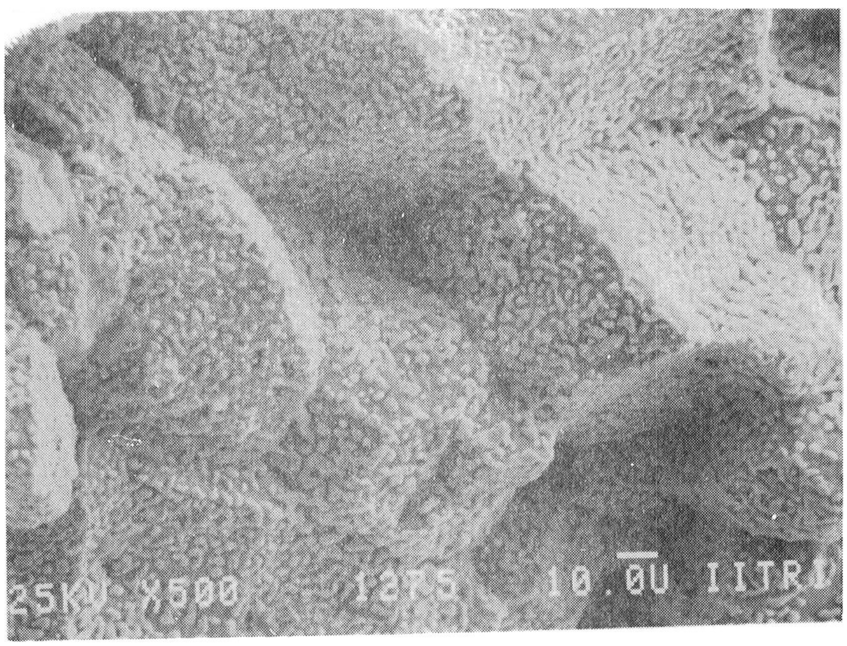

SEM No. 1275

(d)

Figure 30 (cont.)

SEM No. 1282

(a)

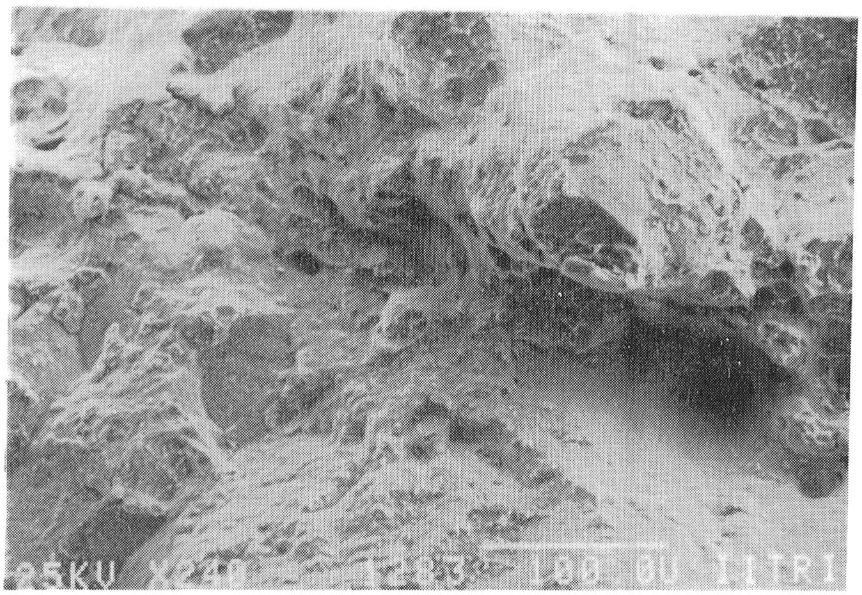

SEM No. 1283

(b)

Figure 31. SEM microfractographs of CG-27 tested in 15 MPa H_2 at 815°C. (a) Quasi-cleavage type fracture, (b) very few dimples in the structure.

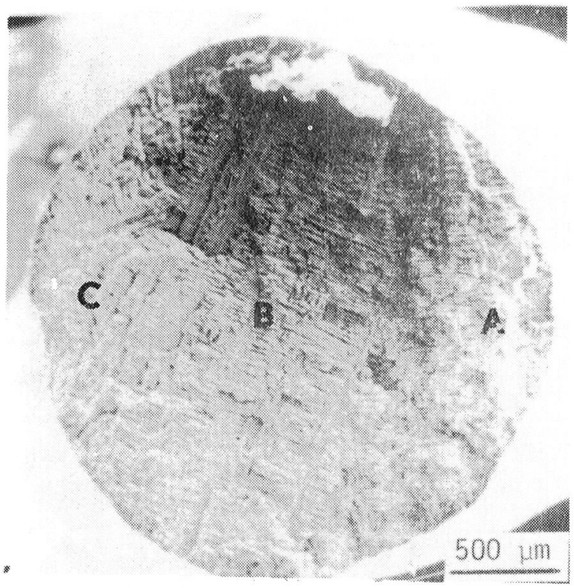

SEM No. 8356

(a) Climax (aged), 705°C, stress 395 MPa.

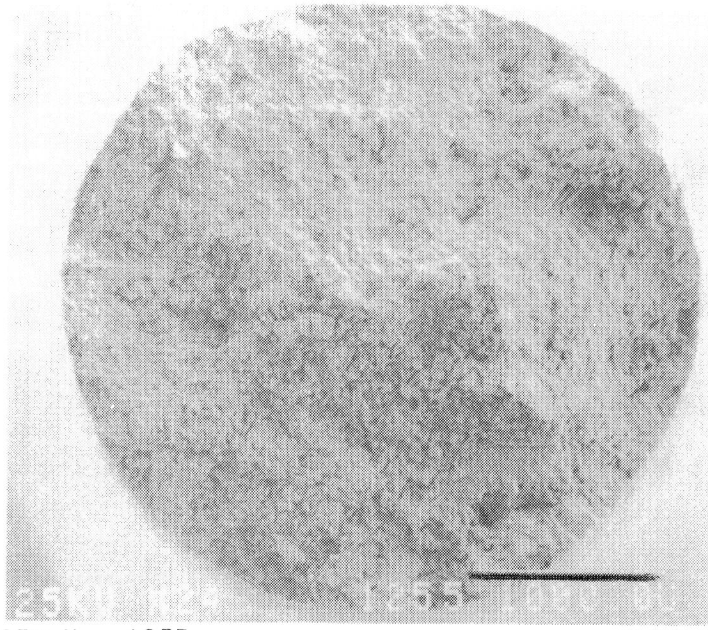

SEM No. 1255

(b) US/AB (braze-cycled), 760°C, stress 255 MPa.

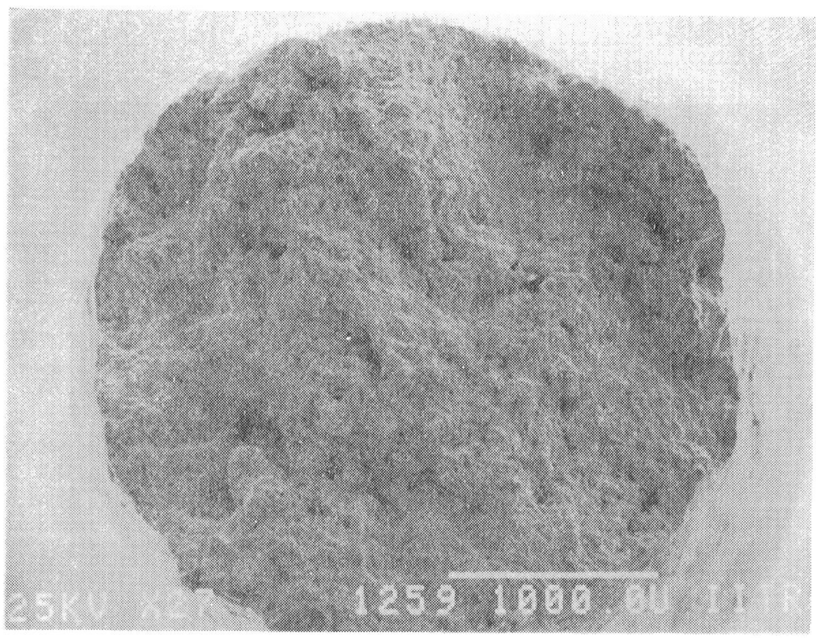

SEM No. 1259

(c) US/AB (braze-cycled), 815°C, stress 105 MPa.

Figure 32. SEM macro- and microfractographs of CRM-6D tested in 15 MPa H_2. Rough interdendritic and transdendritic fracture topographies are observed.

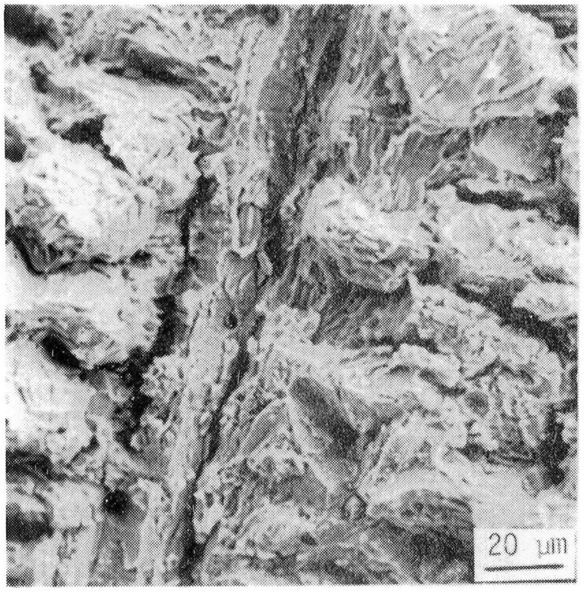

SEM No. 8357

(d) Climax (aged), 705°C, stress 395 MPa

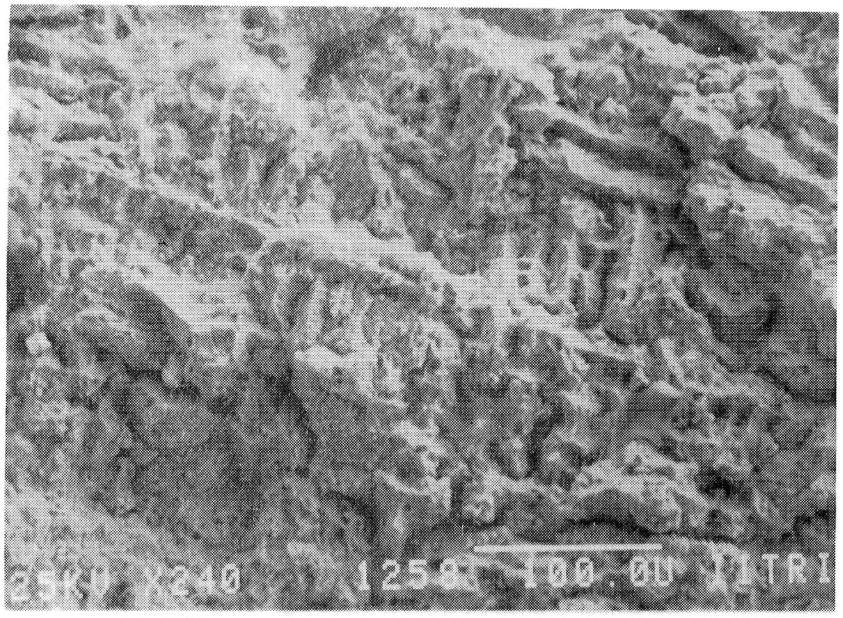

SEM No. 1258

(e) US/AB (braze-cycled), 760°C, stress 255 MPa.

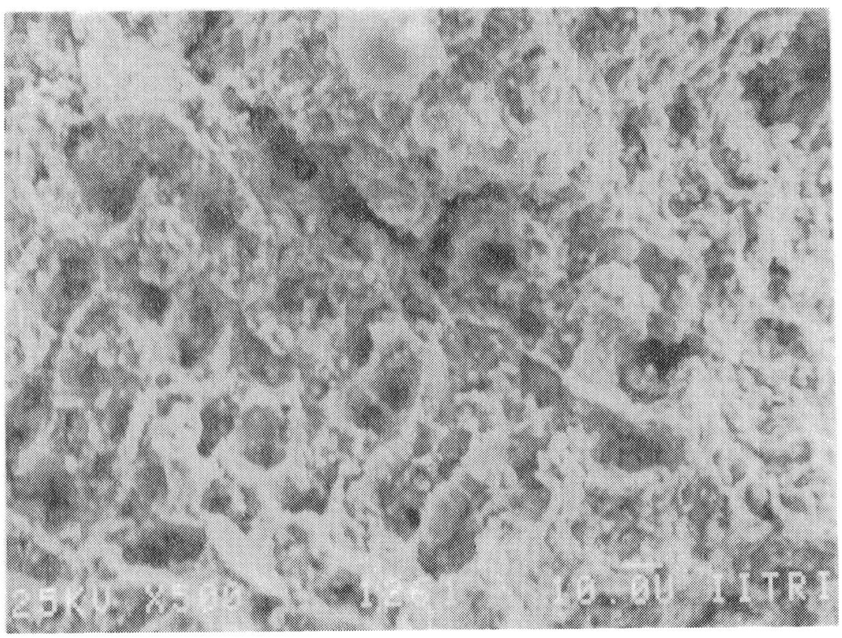

SEM No. 1261

(f) US/AB (braze-cycled), 815°C, stress 105 MPa.

Figure 32 (cont.)

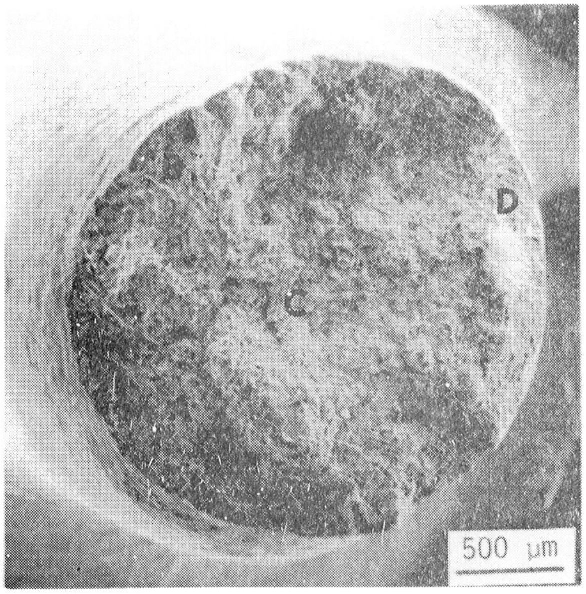

SEM No. 8352

(a) Climax (as-cast), stress 216 MPa.

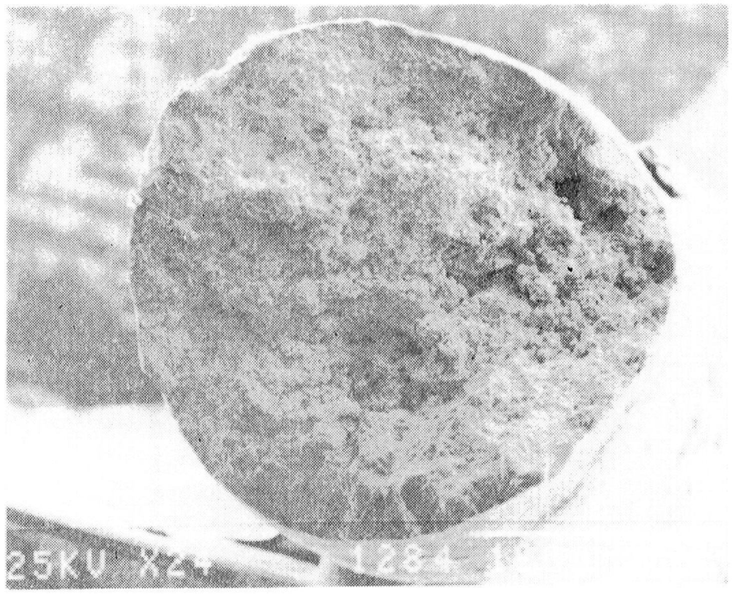

SEM No. 1284

(b) US/AB (braze-cycled), stress 185 MPa.

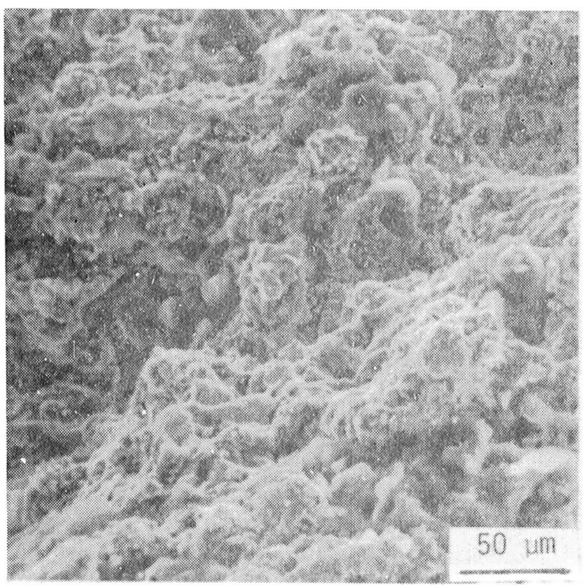

SEM No. 8355

(c) Climax (as-cast), stress 216 MPa.

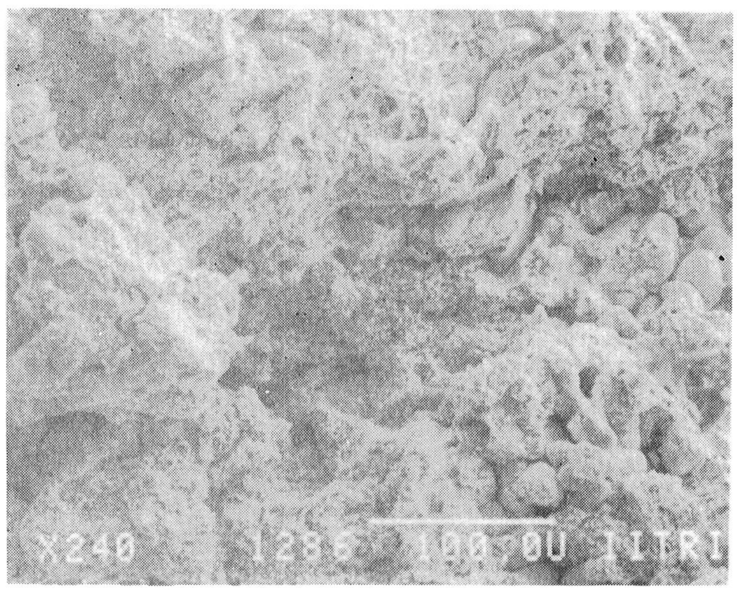

SEM No. 1286

(d) US/AB (braze-cycled), stress 185 MPa.

Figure 33. SEM macro- and microfractographs of XF-818 tested in 15 MPa H_2 at at 760°C. Inter- and transdendritic fracture with some fine dimples are to be noted.

SEM No. 1264

(a)

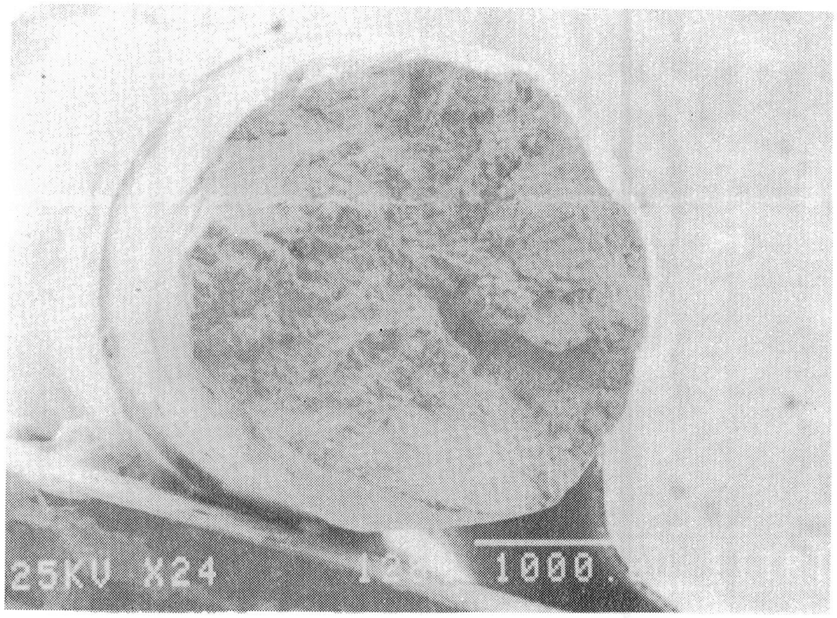

SEM No. 1288

(b)

Figure 34. SEM macro- and microfractographs of HS-31 (US/AB, braze-cycled), tested in 15 MPa H_2 at 760°C, 245 MPa (a,c); 815°C, 165 MPa (b,d). Ductile dimple rupture associated with dendritic fracture.

SEM No. 1268

(c)

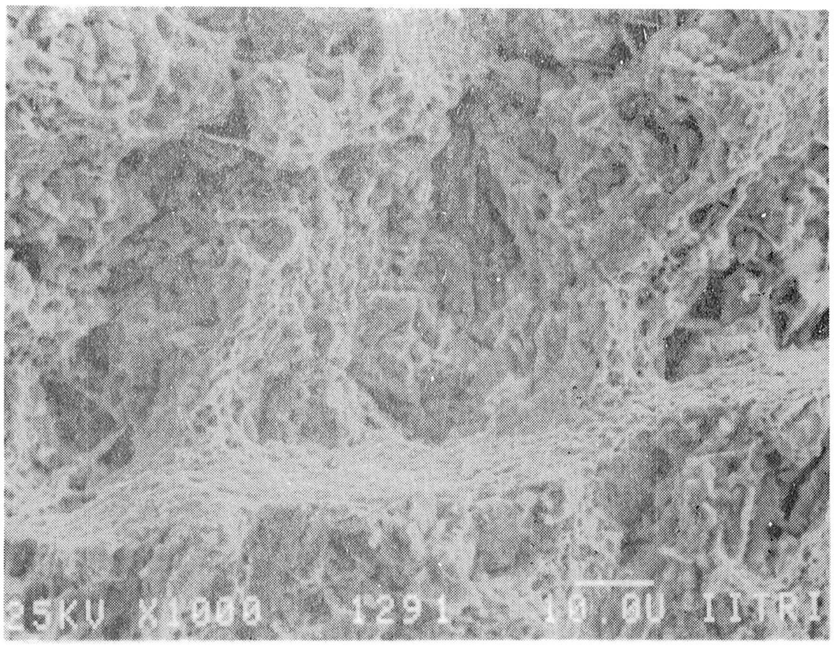

SEM No. 1291

(d)

Figure 34 (cont.)

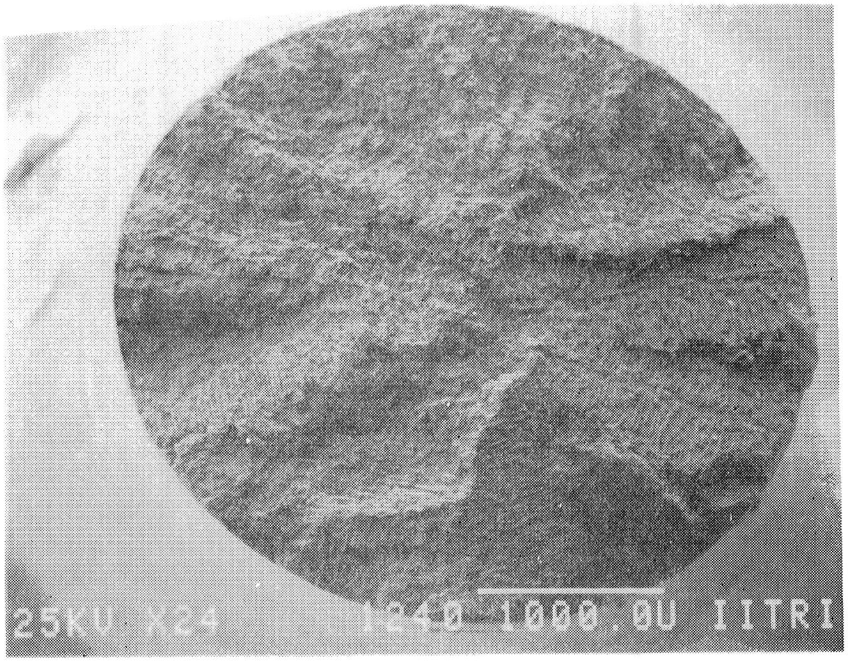

SEM No. 1240

(a)

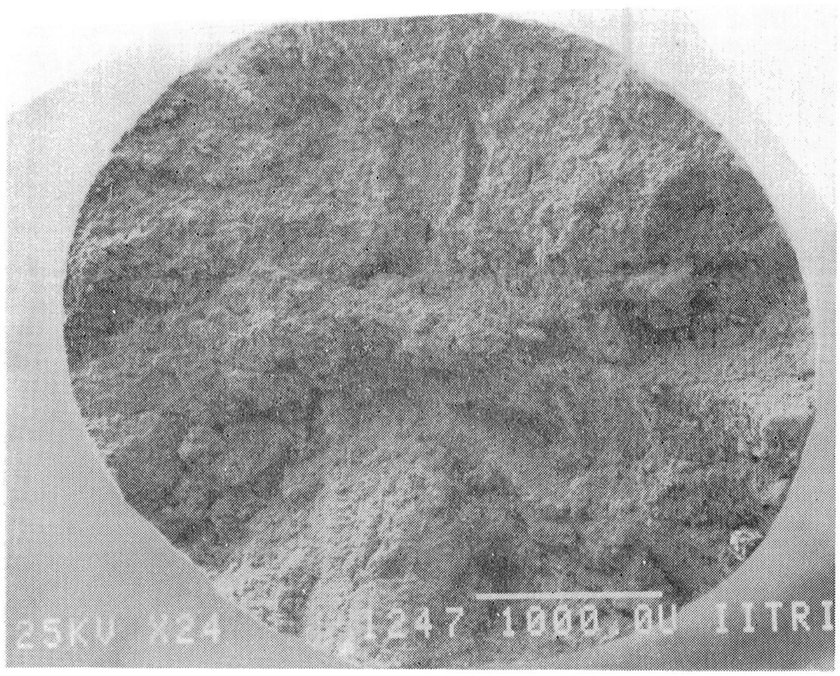

SEM No. 1247

(b)

Figure 35. SEM macro- and microfractographs of SA-F11 (US/AB, braze-cycled), tested in 15 MPa H_2 at 760°C, 230 MPa (a,c,d); 815°C, 160 MPa (b,e,f).

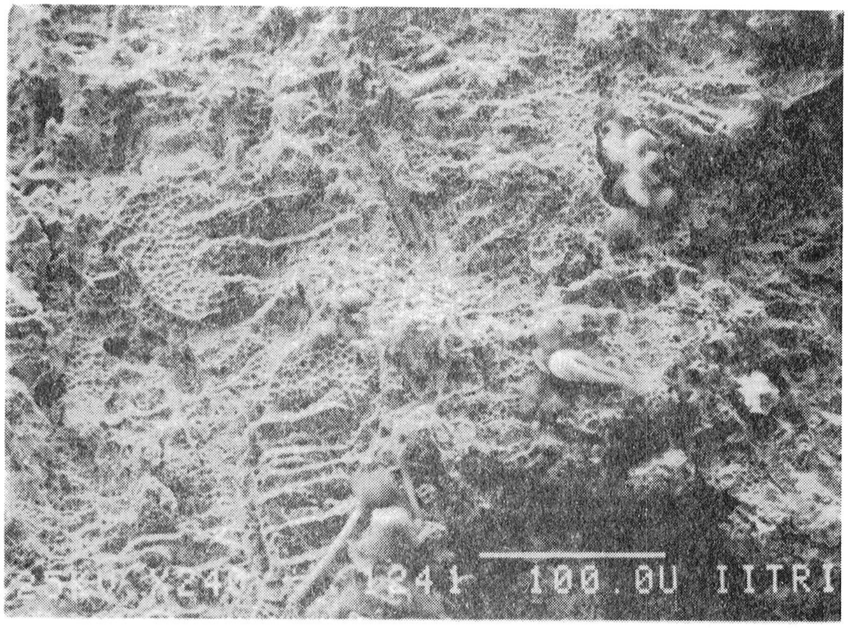

SEM No. 1241

(c)

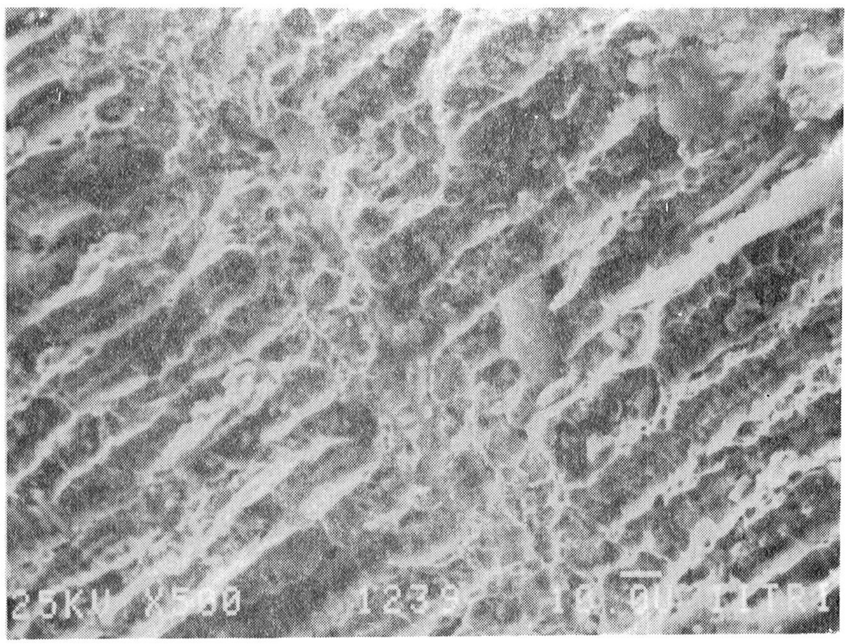

SEM No. 1239

(d)

Figure 35 (cont.)

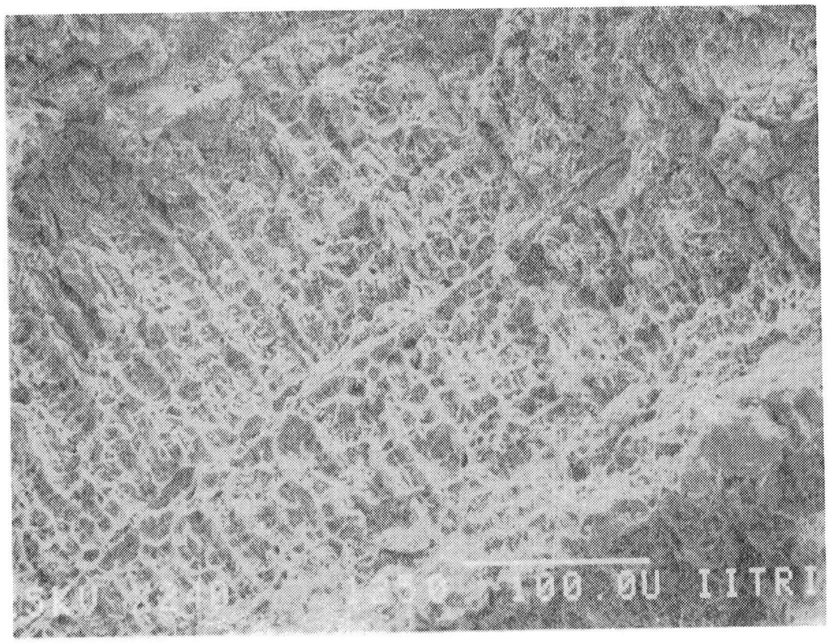

SEM No. 1250

(e)

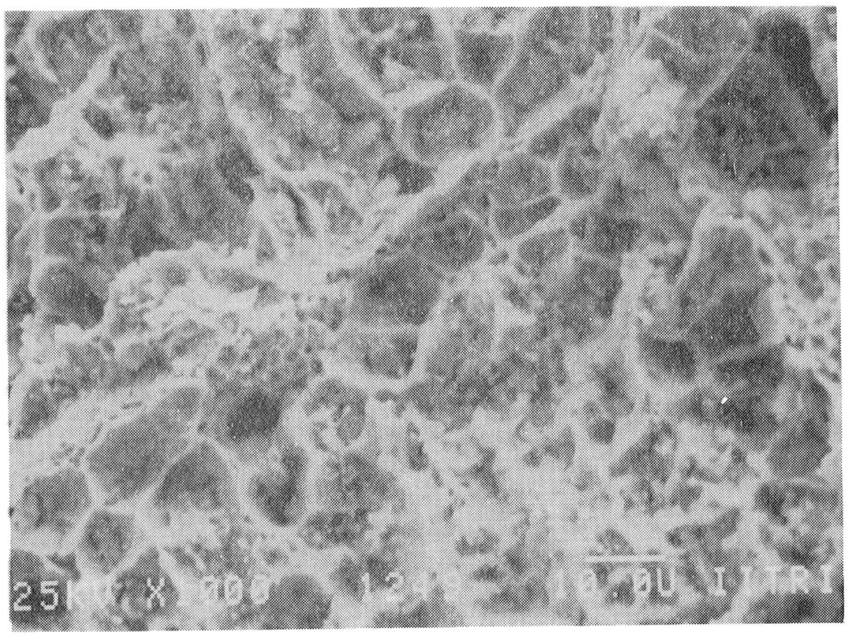

SEM No. 1249

(f)

Figure 35 (cont.)

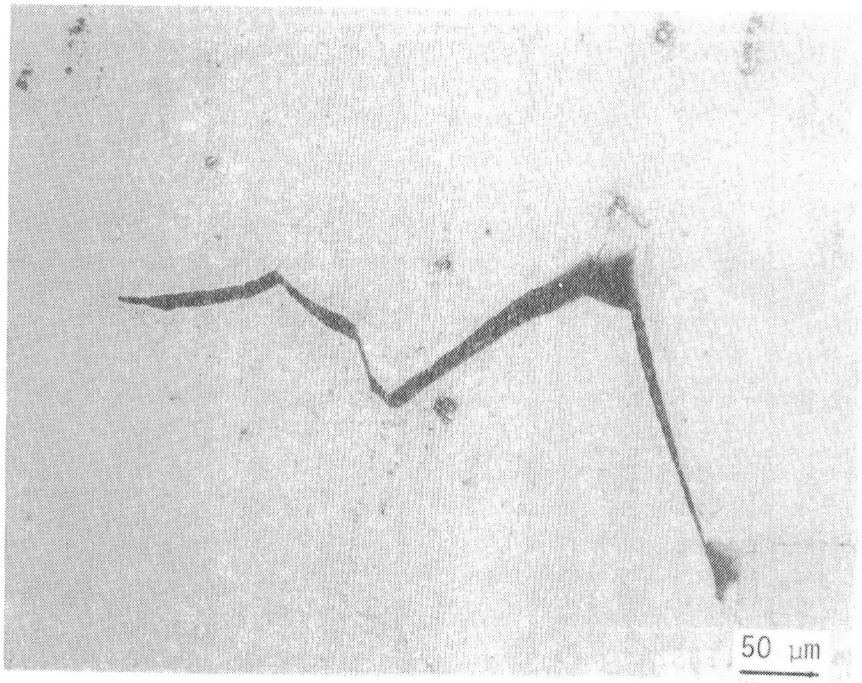

Neg. No. 55520

(a) A-286, 760°C, 131 MPa, elong. 8.1%

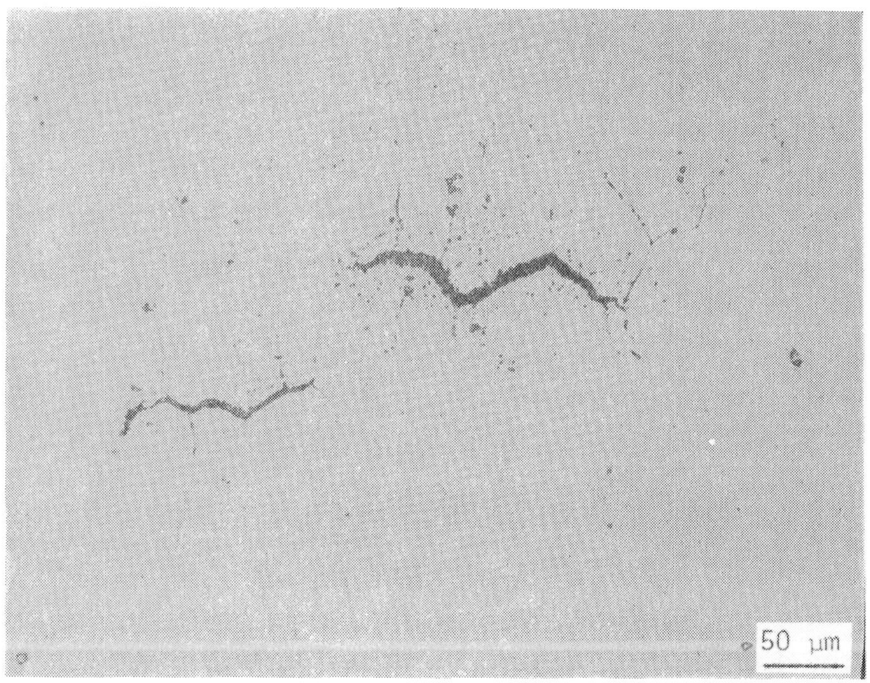

Neg. No. 55518

(b) 800H, 815°C, 62.5 MPa, elong. 21.4%

Figure 36. Photomicrographs of cross-sections of wrought alloys tested in 15 MPa H_2. Creep cavities and cracks between grains to be noted.

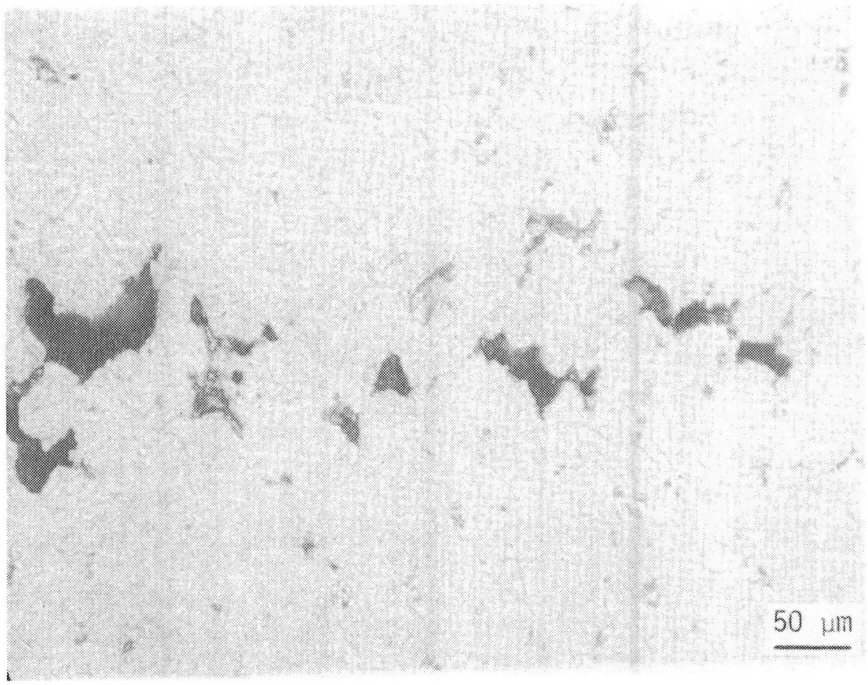

Neg. No. 55525

(c) N-155, 815°C, 97.0 MPa, elong. 33.9%

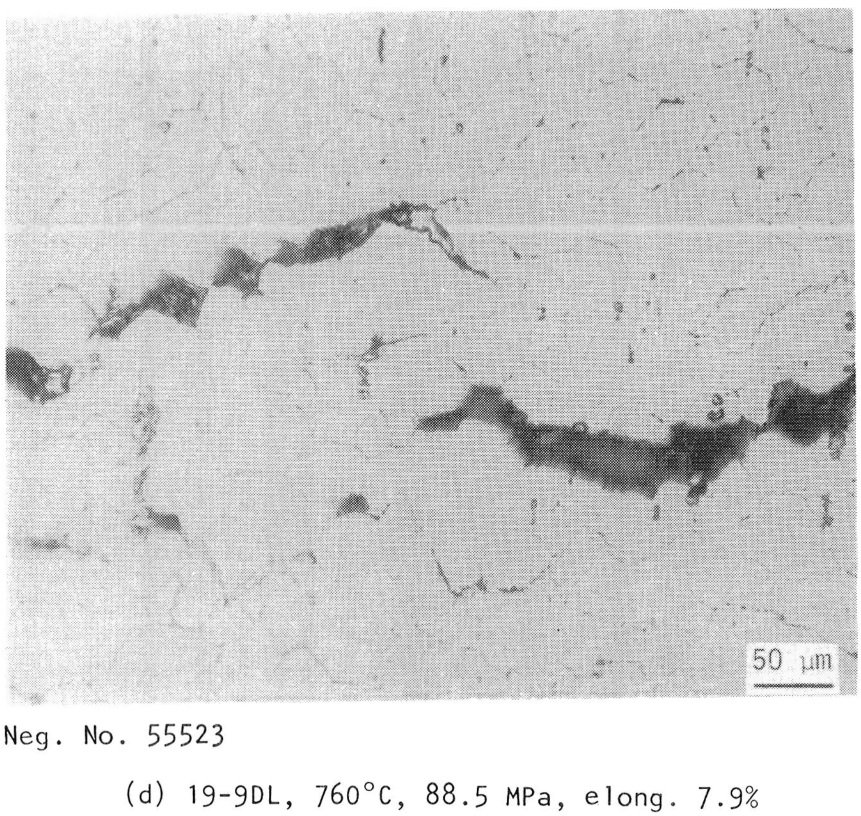

Neg. No. 55523

(d) 19-9DL, 760°C, 88.5 MPa, elong. 7.9%

Figure 36 (cont.)

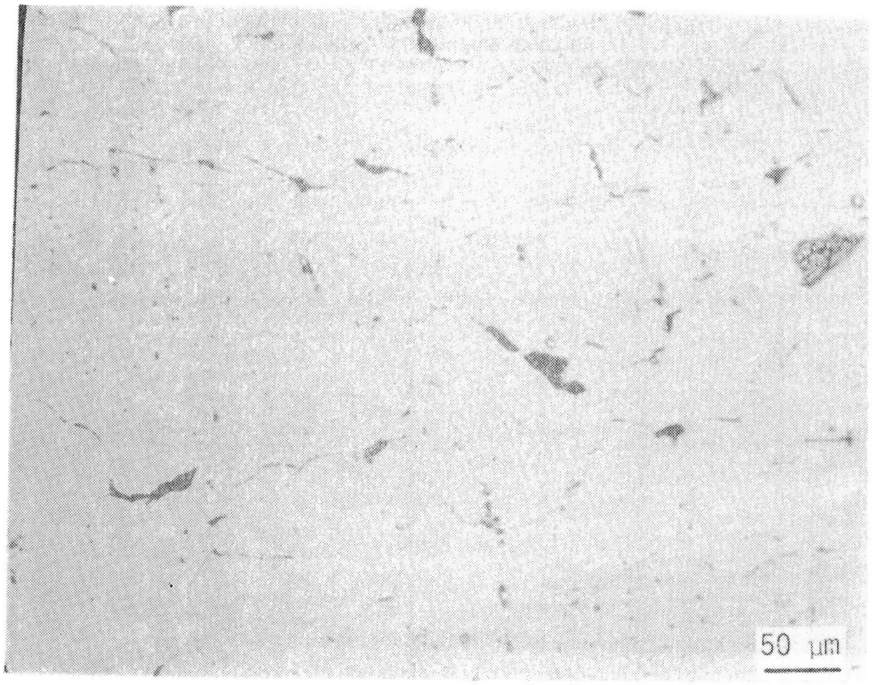

Neg. No. 55513

(a) 12RN72, 815°C, 57 MPa, elong. 24.7%

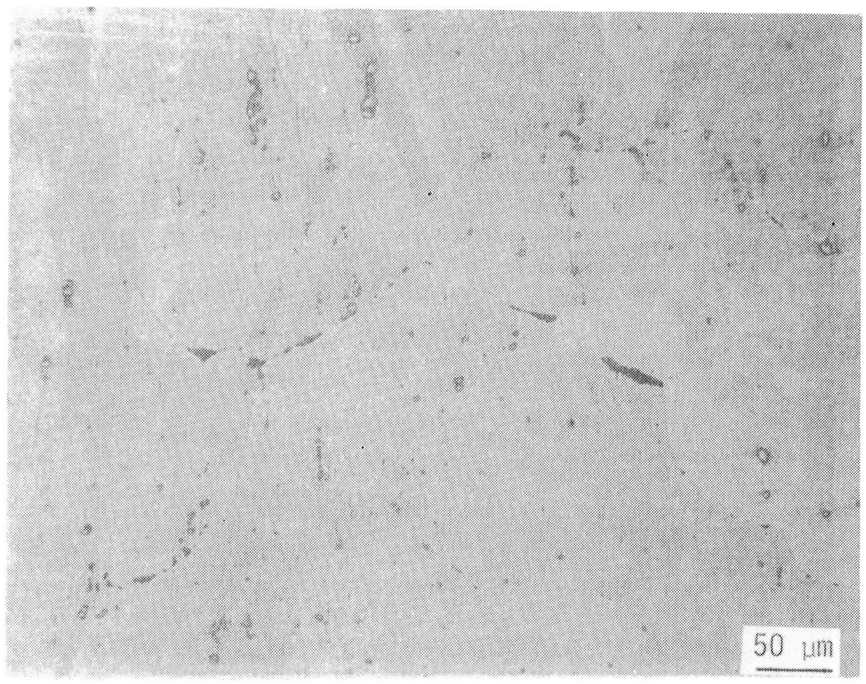

Neg. No. 55505

(b) CG-27, 815°C, 190 MPa, elong. 5.8%

Figure 37. Photomicrographs of cross-sections of wrought alloys tested in 15 MPa H_2 at 815°C showing resultant creep cavities between grains. (a) 12RN72, (b) CG-27.

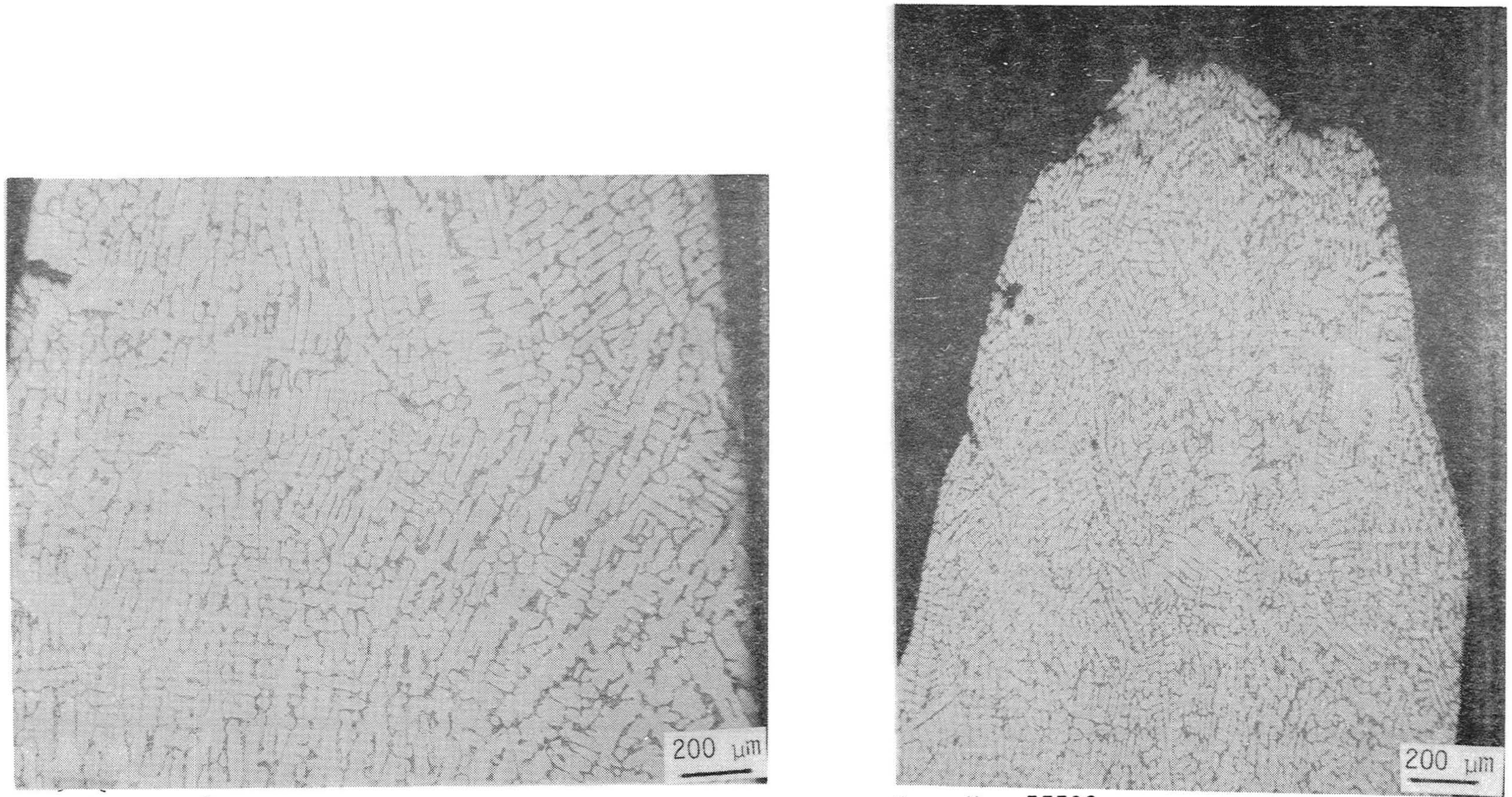

Neg. No. 55528

(a) CRM-6D (Climax, aged), 815°C, 151 MPa, elong. 7.0%

Neg. No. 55503

(b) CRM-6D (US/AB, braze-cycled), 815°C, 105 MPa, elong. 27.3%

Figure 38. Photomicrographs of cross-sections of cast alloys tested in 15 MPa H_2 at 815°C. Cast structures show little evidence of creep cavity development. Stress axis is vertical.

Neg. No. 55532

(c) XF-818 (Climax, as-cast), 875°C, 118 MPa, elong. 16.2%

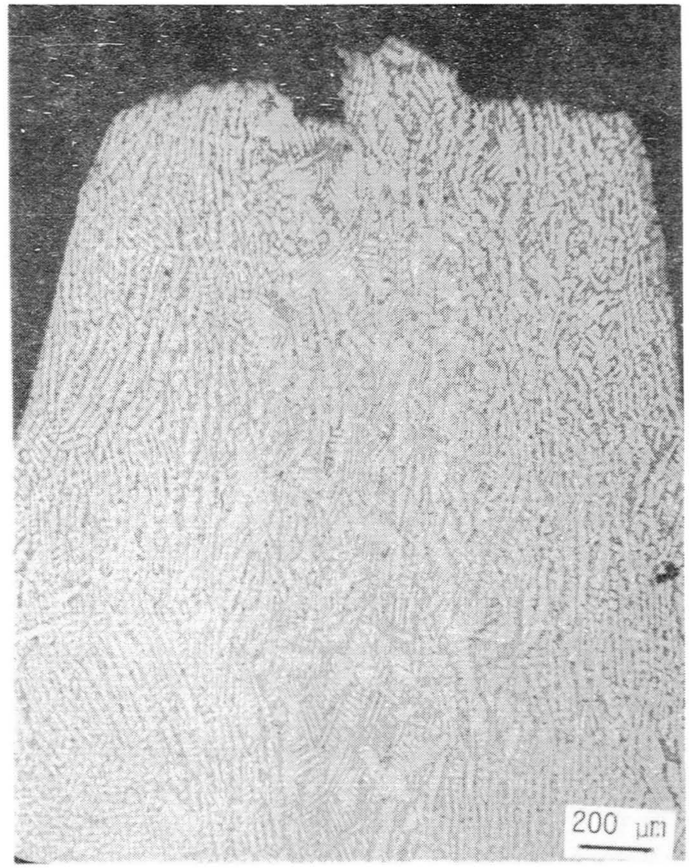

Neg. No. 55509

(d) XF-818 (US/AB, braze-cycled), 815°C, 120 MPa, elong. 19.0%

Figure 38 (cont.)

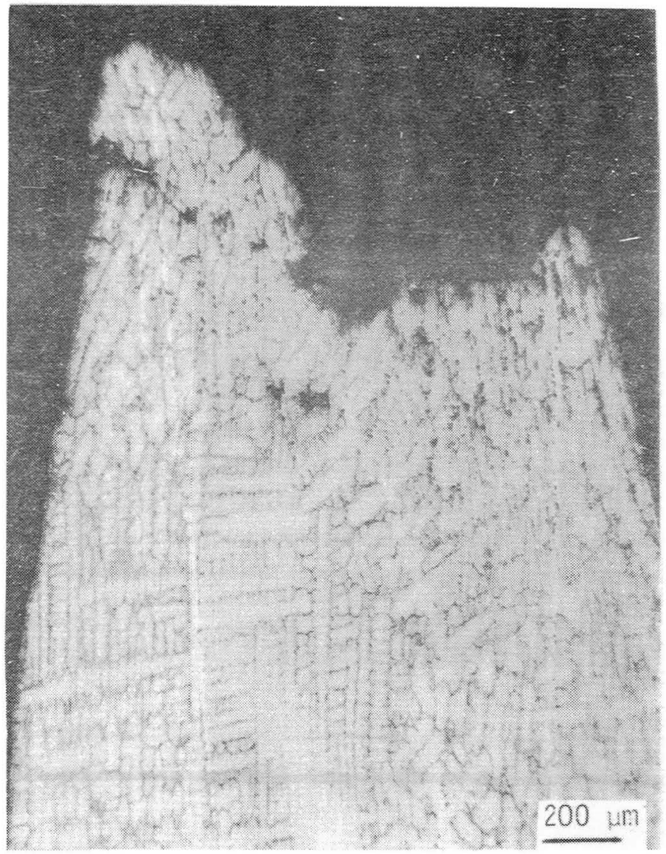

Neg. No. 55491

(a) HS-31 (US/AB, braze-cycled), 760°C, 242 MPa, elong. 23.2%

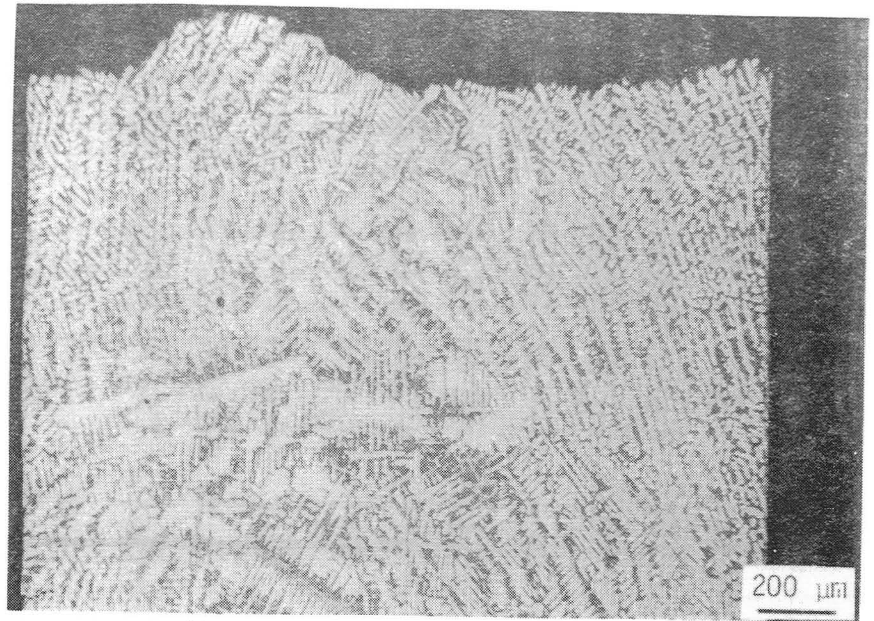

Neg. No. 55495

(b) SA-F11 (US/AB, braze-cycled), 760°C, 230 MPa, elong. 5.0%

Figure 39. Photomicrographs of cross-sections of cast alloys tested in 15 MPa H_2 at 760°C. (a) Significant cavities near fracture indicative of high rupture elongation; (b) very little cavity, indicating low ductility; (c,d) high magnifications reveal fine cavities. Stress axis is vertical.

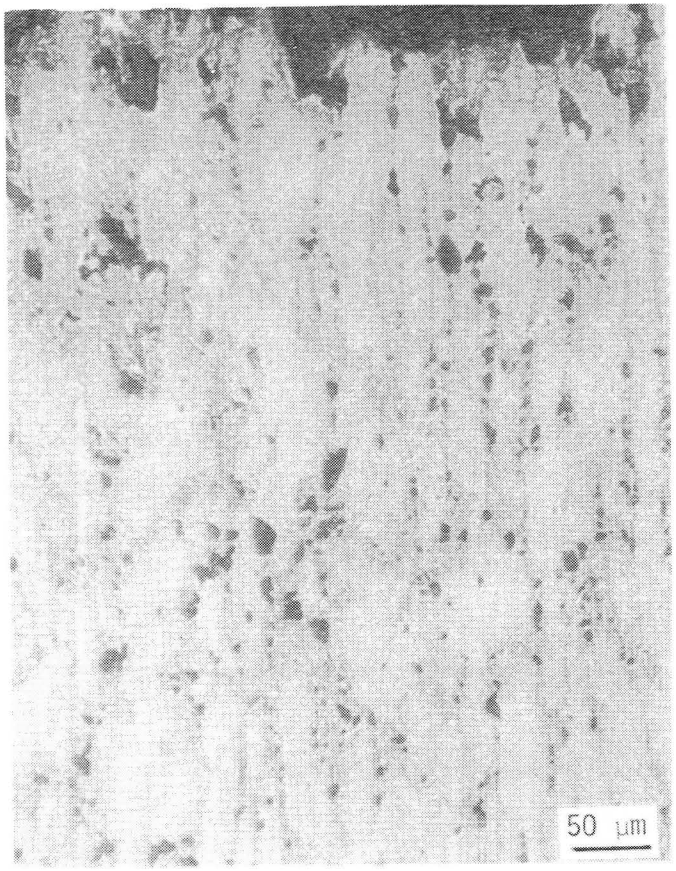

Neg. No. 55492

(c) HS-31 (US/AB, braze-cycled), 760°C, 242 MPa, elong. 23.3%

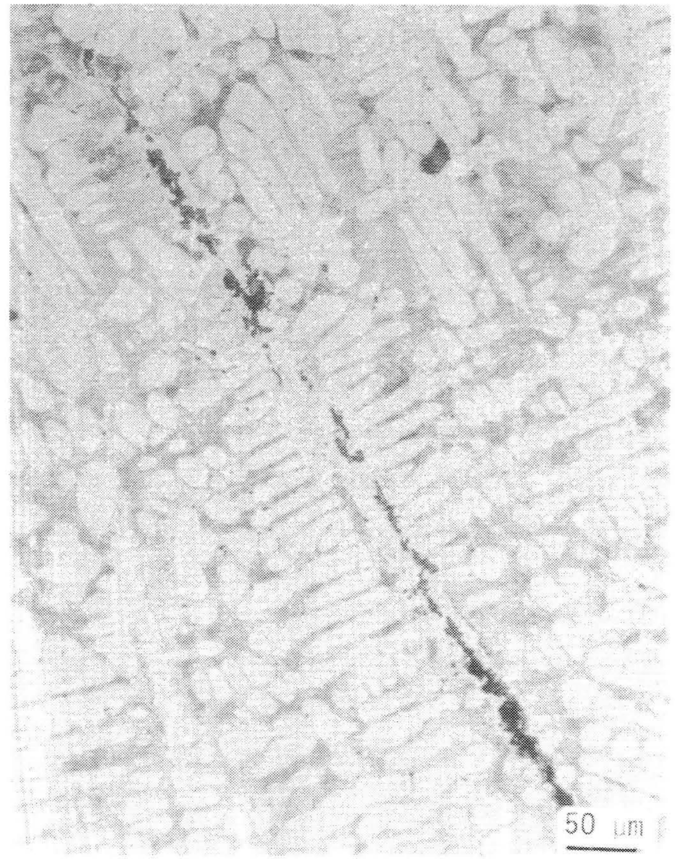

Neg. No. 55502

(d) SA-F11 (US/AB, braze-cycled), 815°C, 180 MPa, elong. 8.6%

Figure 39 (cont.)

June 1984

FINAL REPORT DISTRIBUTION LIST

NASA-Lewis Research Center
21000 Brookpark Road
Cleveland, OH 44135
Attn:

R. H. Titran	M. S. 49-1 (10 copies)
J. R. Stephens	M. S. 49-1
Materials Division - CF	M. S. 49-1
S. R. Schuon	M. S. 49-1
H. R. Gray	M. S. 49-3
H. B. Probst	M. S. 49-3
C. M. Scheuermann	M. S. 49-1
TU Office	M. S. 3-19
T. P. Burke	M. S. 501-11
W. E. B. Mason	M. S. 500-211
D. G. Beremand	M. S. 500-215
W. A. Tomazic	M. S. 500-215
F. J. Kutina, Jr.	M. S. 500-210
J. G. Slaby	M. S. 500-215
A. Long	M. S. 500-305
N. T. Musial	M. S. 500-113
R. J. Sovie	M. S. 500-203
W. K. Tabata	M. S. 500-215
Report Control Office	M. S. 5-5
Library	M. S. 60-3 (2 copies)
W. K. Tabata	M. S. 500-215

NASA Headquarters
Washington, DC 20546
Attn:

RJP J. F. Slomski
RJP E. E. Van Landingham
RTS-6 J. Mullin

NASA Jet Propulsion Laboratory
4800 Oak Grove Drive
Pasadena, CA 91103
Attn:

F. W. Hoehn	M. S. 125-224
R. C. Heft	M. S. 510-250
G. W. Meisenholder	M. S. 502-307
V. Truscello	M. S. 502-419
H. E. Cotrill, Jr.	M. S. 157-208
J. F. Mondt	M. S. 169-515
G. Stapfer	M. S. 169-515

NASA Scientific & Technical Information Facility (50 copies)
Attn: Accessioning Dept.
P. O. Box 8757
Balt/Wash. International Airport, MD 21240

STIRLING ENGINE DISTRIBUTION LIST
Department of Energy

Department of Energy
Attn: R. T. Alpaugh
MS CE-131
Forrestal Building
Washington, DC 20585

Department of Energy
Attn: Karl Bastress
MS CE-142
1000 Independence Ave., S. W.
Washington, DC 20585

Department of Energy
Attn: John J. Brogan
MS CE-14
Forrestal Building
Washington, DC 20585

Department of Energy
Attn: Dr. Robert J. Gottschall
ER-151
GTN J-309
Washington, DC 20545

Department of Energy
Attn: Marvin Gunn
MS CE-142
1000 Independence Ave., S.W.
Washington, DC 20585

Department of Energy
Attn: E. Lister
Div. of Coal Utilization
GTN E-178
Washington, DC 20545

Department of Energy
Attn: Robert B. Morrow
GTN B-107
Washington, DC 20545

Department of Energy
Attn: John W. Neal
Division of Coal Utilization
GTN E-178
Washington, DC 20545

Department of Energy
Attn: Patrick L. Sutton
MS 5-G030
Forrestal Building
Washington, DC 20585

DOE Technical Information Center
(198 copies)
Building 1916-T-1
Oak Ridge Turnpike at Athens Road
Oak Ridge, TN 37830
Attn: T. Laughlin

STIRLING ENGINE DISTRIBUTION LIST
Other Government Agencies

Argonne National Laboratory
Attn: Dr. Kenneth Uherka
Components Tech. Div., Bldg. 330
9700 South Cass Avenue
Argonne, IL 60439

Kenneth Bradford
P. O. Box 99909
Cleveland, OH 44199

Argonne National Laboratory
Attn: R. E. Holz
Bldg. H330
9700 South Cass Avenue
Argonne, IL 60439

Department of Transportation
Attn: H. Miller
Trans. Systems Center, Code TSC-404
Kendall Square
Cambridge, MA 02142

FINAL REPORT DISTRIBUTION LIST (cont.)

DARPA
Attn: Lt. Comdr. W. Wright
1400 Wilson Blvd.
Arlington, VA 22209

House of Representatives
Attn: Honorable Mary Rose Oakar
107 Cannon House Office Building
Washington, DC 20515

Naval R&D
Attn: R. Bloomquist
Code 2724
Annapolis, MD 21402

NUWES
Attn: Charles R. Gundersen
Code 7022
Keyport, WA 98345

Oak Ridge National Laboratory
Attn: F. A. Creswick
P. O. Box Y
Oak Ridge, TN 37830

Oak Ridge National Laboratory
Attn: C. D. West
P. O. Box Y
Bldg. 9201-3, MS-5
Oak Ridge, TN 37830

Solar Energy Research Institute
Attn: Joseph Finegold
1617 Cole Boulevard
Golden, CO 80401

U.S. Air Force Wright Aero. Labs.
Attn: Lt. Richard Honneywell
Energy Conversion Branch
Aero Propulsion Laboratory, POOC
Wright Patterson AFB, OH 45433

U.S. Air Force Wright Aero. Labs
Attn: Jerrell M. Turner
Energy Conversion Branch
Aero Propulsion Laboratory, POOC
Wright Patterson AFB, OH 45433

U.S. Air Force Wright Aero. Labs.
Attn: Valerie J. VanGriethuysen
Energy Conversion Branch
Aero Propulsion Laboratory, POOC
Wright Patterson AFB, OH 45433

U.S. Dept. of Army - Headquarters
Attn: Dr. Charles H. Church
DAMA-ARZ-E Pentagon
Washington, DC 20310

U.S. Army Materials and Mechanics
Research Center
Attn: Dr. W. J. Croft
Watertown, MA 02172

U.S. Army Mobility Equipment
R&D Command
Attn: Paul Arnold
DRDME-EM
Fort Belvoir, VA 22060

U.S. Army Mobility Equipment
R&D Command
Attn: Richard Belt
DRDME-EC
Fort Belvoir, VA 22060

U.S. Army Belvoir R&D Center
Attn: STRBE-EMP D. Vaughn
Fort Belvoir, VA 22060

E. E. Bailey
AFAPL/DO
Wright Patterson AFB, OH 45433

U.S. Bureau of Mines
Attn: J. Alton Burks
Pittsburgh Research Center
Cochrans Mills Road
P.O. Box 18070
Pittsburgh, PA 15236

STIRLING ENGINE DISTRIBUTION LIST
Universities

Bucknell University
Attn: Dr. Barry Maxwell
Mechanical Engineering Dept.
Lewisburgh, PA 17837

California Polytechnic State Univ.
Attn: Professor C. R. Russell
Mechanical Engineering Dept.
San Luis Obispo, CA 93407

Massachusetts Institute of Technology
Attn: Dr. L. H. Linden
Energy Laboratory
Cambridge, MA 02139

Rensselaer Polytechnic Institute
Attn: Prof. Fred Ling
Dept. of Mechanical Engineering
Troy, NY 12181

University of Virginia
Attn: Ira Dye
School of Engineering &
Applied Science
Thornton Hall
Charlottesville, VA 22901

University of Washington
Attn: Maurice A. White
Joint Center for Graduate Study
100 Sprout Road
Richland, WA 99352

Virginia Technology
Attn: Dr. R. Sisson
Dept. of Materials Engineering
Blacksburg, VA 24061

Western Michigan University
Attn: Richard P. Heintz
Dept. of Transportation Technology
Kalamazoo, MI 49008

California Polytechnic State Univ.
Attn: Raymond G. Gordon
Mechanical Engineering Dept.
San Luis Obispo, CA 93407

Case Western Research University
Attn: Professor A. Dybbs
Dept. of Mechanical & Aerospace Engg.
Cleveland, OH 44106

Massachusetts Institute of Technology
Attn: Prof. Joseph L. Smith, Jr.
Mechanical Engineering Dept.
San Luis Obispo, CA 93407

University of Calgary
Attn: Prof. G. Walker
Dept. of Mechanical Engineering
Calgary, Alberta T2NIN4
Canada

University of Washington
Attn: R. P. Johnston
Joint Center for Graduate Study
100 Sprout Road
Richland, WA 99352

University of Wisconsin - R. F.
Attn: Dr. J. R. Senft
River Falls, WI 54022

Western Michigan University
Attn: Harley D. Behm
Dept. of Transportation Techology
Kalamazoo, MI 49008

FINAL REPORT DISTRIBUTION LIST (cont.)

STIRLING ENGINE DISTRIBUTION LIST
Philips Licensees

Ford Aerospace & Communications Corp.
Attn: Robert L. Pons
Aeronutronic Division
Newport Beach, CA 92663

Philips Laboratories
Attn: Alex Daniels
345 Scarborough Road
Briarcliff Manor, NY 10510

Stirling Thermal Motors, Inc.
Attn: Dr. R. J. Meijer, Pres.
2841 Boardwalk
Ann Arbor, MI 48104

United Stirling
Attn: Bengt Hallare
211 The Strand
Alexandria, VA 22314

United Stirling
Attn: Worth Percival
211 The Strand
Alexandria, VA 22314

United Stirling Research Labs
Attn: Erik Skog
S-201-10 Malmo 1
SWEDEN

STIRLING ENGINE DISTRIBUTION LIST
Industrial Companies & Foundations

Advanced Mechanical Technology, Inc.
Attn: Dr. Walter D. Syniuta, Pres.
141 California Street
Newton, MA 02158

Aeroject Energy Conversion Company
Attn: Mark I. Rudnicki
P.O. Box 13222
Sacremento, CA 95813

Aeroject Liquid Rocket Company
Attn: Lawrence C. Hoffman
Dept. 9860, Bldg. 2001
P. O. Box 13222
Sacremento, CA 95813

Aerospace Corporation
Attn: Wolfgang Roessler
2350 East El Segundo Blvd.
El Segundo, CA 90245

AiResearch Casting Company
Attn: Michael Woulds
2525 West 190 Street
Torrance, CA 90509

Avco-Lycoming Corporation
Attn: Frank Riddell
Vice Pres., Advanced Prod. Planning
652 Oliver Street
Williamsport, PA 17701

Arthur D. Little, Inc.
Attn: Prafulla C. Mahata
Acorn Park
Cambridge, MA 02140

Climax Molybdenum Co. of Michigan
Attn: Dr. William Hagel
3475 Plymouth Road
Ann Arbor, MI 48106

Chrysler Corporation
Attn: J. D. Withrow
Vice President, Engineering
P. O. Box 1118
Detroit, MI 48281

Consultant
Paul Huber
500 S. Highland
Dearborn, MI 48124

Davy McKee Corporation
Attn: David R. Cormier
6200 Oaktree Blvd.
Cleveland, OH 44131

Dayton T. Brown, Inc.
Attn: John Herlihy, P.E.
Engineering & Test Division
Church Street
Bohemia, L. I., NY 11716

Detroit Diesel Allison
Attn: H. E Barrett
Industrial Gas Turbines, MS T-15
P. O. Box 894
Indianpolis, IN 46206

Detroit Diesel Allison
Attn: Harold E. Helms
Division of G.M.C.
P. O. Box 894-T15
Indianapolis, IN 46206

Dynasim Company
Attn: Richard P Heintz
428 W. South
Kalamazoo, MI 49007

Eaton Corporation
Attn: Dr. Lamont Eltinge
Director of Research
P. O. Box 766
Southfield, MI 48037

Energy Research & Dev. Foundation
Attn: R. T. Brinsmade
600 New Hampshire Ave., Suite 450
Washington, DC 20037

Energy Research & Generation, Inc.
Attn: Dr. Glen Benson
Director of R, D & E
Lowell & 57 Street
Oakland, CA 94608

Fairchild Space & Electronic Co.
Attn: A. Schock
Germantown, MD 20767

Flow Industries, Inc.
Attn: Dr. John H. Olsen
P. O. Box 5040
21414-68th Avenue, South
Kent, WA 98031

Ford Motor Company
Attn: Ernest Kitzner
Rm. S-2100 Scientific Research Lab.
P. O. Box 2053
Dearborn, MI 48121

Foster-Miller Associates
Attn: B. Poulin
350 Second Avenue
Waltham, MA 02154

Foster-Miller Associates
Attn: Dr. William M. Toscano
350 Second Avenue
Waltham, MA 02154

Gas Research Institute
Attn: M. Klinch
8600 W. Bryn Mawr Ave.
Chicago, IL 60631

General Electric Company
Attn: William Auxer
Space Division
P. O. Box 8661
Philadelphia, PA 19101

General Electric Company
Attn: B. J. Tharpe
Space Division
P. O. Box 8661
Philadelphia, PA 19101

General Electric Company
Attn: R. Meier
P. O. Box 527
King of Prussia, PA 19406

General Motors Research Laboratory
Attn: F. Earl Heffner
Engine Research Department
Warren, MI 48090

Grumman Aerospace Corporation
Attn: Clifford A. Hoelzer
Head, Propulsion Systems
M.S. C32-05
Bethpage, NY 11714

Martini Engineering
Attn: Dr. W. R. Martini
2303 Harris
Richland, WA 99352

Mechanical Technology Inc.
Attn: Bruce Goldwater
968 Albany-Shaker Road
Latham, NY 12110

Mechanical Technology Inc.
Attn: Dr. B. Sternlicht
968 Albany-Shaker Road
Latham, NY 12110

METEX Corporation
Attn: George Ward
Industrial Products Division
Thermal & Mechanical Group
970 New Durham Road
Edison, NJ 08817

Rasor Associates, Inc.
Attn: Dr. Edward J. Britt
Direct Energy Conversion Dept.
253 Humboldt Court
Sunnyvale, CA 94086

Space Conditioning Research
Institute of Gas Technology
Attn: Jaroslav Wurn
3424 South State Street
Chicago, IL 60616

Sunpower, Inc.
Attn: W. Beale
6 Byard Street
Athens, OH 45701

Teledyne Continental Motors
Attn: T. Schwallie
General Products Division
76 Getty Street
Muskegon, MI 49442

International Harvester
Attn: Paul N. Blumberg
Science & Technology Laboratory
16 W. 260 83rd Street
Hinsdale, IL 60521

Mechanical Technology Inc.
Attn: William Sumigray
968 Albany-Shaker Road
Latham, NY 12110

Mechanical Technology Inc.
Attn: Michael Cronin
968 Albany-Shaker Road
Latham, NY 12110

Mechanical Technology Inc.
Attn: George Dochat
968 Albany-Shaker Road
Latham, NY 12110

Motor Vehicle Man. Assn.
of the United States, Inc.
Attn: Christian Van Schayk
300 New Center Bldg.
Detroit, MI 48202

Sigma Research Incorporated
Attn: E. D. Waters
2950 George Washington Way
Richland, WA 99352

Stirling Power Systems Corp.
Attn: William Houtman
7101 Jackson Road
Ann Arbor, MI 48103

TCA Stirling Engine Research
and Development Corporation
Attn: Dr. Ted Finkelstein
P. O. Box 643
Beverly Hills, CA 90213

Teledyne Energy Systems
Attn: G. Linkous
110 W. Timonium Road
Timonium, MD 21093

Thermal Electron Corporation
Attn: Parinal S. Patel
R & D Center
101 First Avenue
Waltham, MA 02154

United Aircraft Products, Inc.
Attn: John F. Unger
Manager, Advanced Technology
Box 1335
Dayton, OH 45401

Vadetec Corporation
Attn: Yves Kemper
Chief Executive Officer
2681 Industrial Road
Troy, MI 48084

United Technologies Research Center
Attn: Frank Lemkey
East Hartford, CT 06108

Valmont Industries
Attn: William Eaton
Valley, NE 68064

Varian Associates
Attn: Chris Flegel
MS G-028
611 Hansen Way
Palo Alto, CA 94303

Wasson Associates
P. O. Box 26800
San Jose, CA 95159

Westinghouse Electric Corporation
Attn: Library/R. Holman
Advanced Energy Systems Division
P. O. Box 10864
Pittsburgh, PA 15236